Design of a Magnetic Coupling for Caravan and Trailer Signal Lights

Wireless Power and Data Transfer

Prepared by:

Azhar Ebrahim

EBRAZH001

Department of Electrical Engineering
University of Cape Town

Prepared for:

Dr Willem Schonken

DEPARTMENT OF ELECTRICAL ENGINEERING
University of Cape Town

November 2021

Submitted to the Department of Electrical Engineering at the University of Cape Town in partial fulfilment of the academic requirements for a Bachelor of Science degree in Mechatronics Engineering.

Abstract

This project covers an application of wireless power transfer, namely inductive coupling. The project aims to design a magnetic coupling system for caravan and trailer signal lights. The current implementation relies on the physical contact of conductors, through a cable and special sockets on the vehicle and the trailer. This connection is problematic as dust and oil interrupt the connection.

Many circuits are designed and integrated into the system, including oscillators, filters, amplifiers, filters, and rectifiers. These are all crucial to data transfer. Moreover, inductive coils are designed for wireless power transfer. The individual elements of the system work well both in simulation and practically. The resulting combination of the circuitry and the coils, however, does prove to be troublesome. This is especially due to the lack of physical component availability.

Acknowledgements

I extend my sincere appreciation to all the following individuals who assisted me in my research project.

Firstly, I would like to express my heartfelt gratitude to my supervisor, Dr. Schonken for his support, guidance, and motivation. The lessons that I have learned from him encouraged me and made me more confident. His meticulous input, insight, and experience also assisted me in researching and completing my thesis to the best of my ability.

My mom and sister for their prayers, sacrifices, and unwavering support. Their faith in me has encouraged me to reach my full potential. They have instilled important values in me from a young age for which I will always be grateful.

My peers, Crystal, Salmaan, Muneeb, Kavir, Taqi, Reesen, and Trivaan who have been a pillar of strength throughout my studies. I am thankful for their moral and emotional support.

Also, to my other friends who steered me in the right direction and had confidence in me. I will always have fond memories of the experiences we shared as a group and our UCT days.
I am also thankful to all my lecturers who provided me with the necessary skills and knowledge to achieve my goals.

Lastly, to the University of Cape Town, where most of my components were sourced from and who gave me access to their labs.

Plagiarism declaration

1. I know that plagiarism is wrong. Plagiarism is to use another's work and pretend that it is one's own.
2. I have used the IEEE convention for citation and referencing. Each contribution to, and quotation in, this final year project report from the work(s) of other people, has been attributed and has been cited and referenced.
3. This final year project report is my work.
4. I have not allowed, and will not allow, anyone, to copy my work with the intention of passing it off as their work or part thereof.

Word count: 15500

Name: **Azhar Ebrahim**

Signature: **A.Ebrahim** **Date:** 07 November 2021

Table of Contents

Abstract ..... **i**
Acknowledgements ..... **ii**
Plagiarism declaration ..... **iii**
Table of Contents ..... **iv**
List of Figures ..... **vi**
List of Tables **1**
Nomenclature **2**
1. Introduction **3**
1.1 Introduction 3
1.2 Motivation 4
1.3 Problem statement 4
1.4 Objectives 4
1.5 Thesis contributions 4
1.6 Terms of reference 4
1.7 Scope and limitations 5
1.8 Thesis outline 5
2. Literature Review **6**
2.1 Introduction 6
2.2 Oscillators 6
2.3 Amplifiers 9
2.4 Magnetic Induction 12
2.5 Filters 21
2.6 Rectifiers and Regulators 26
2.7 Conclusion 27
3. Methodology **28**
3.1 Overview 28
3.2 Method for Oscillators 28
3.3 Method for Amplifiers 28
3.4 Method for Magnetic Coupling 28
3.5 Method for Filters 28
3.6 Method for Rectifiers and regulators 29
3.7 Testing 29
4. Design of the systems **30**
4.1 Background to the design and current implementation 30
4.2 Design of the Oscillators 34
4.2.1 Simulation Design 34
4.2.2 Hardware Design 38
4.3 Design of the Amplifiers 40
4.3.1 Software Design 40
4.3.2 Hardware Design 41
4.4 Design of the Magnetic Coupling Coils 43
4.4.1 Software set-up and Design 44
4.4.2 Hardware Design 48
4.5 Design of the Filters 52
4.5.1 Simulation Design 52
4.5.2 Hardware Design 56
4.6 Design of the Rectifiers and Regulators 57

4.6.1 Simulation Design 57
4.6.2 Hardware Design 58
4.7 Complete Design and Integration into the Test Rig 60
5. Results 62
5.1 Results of the Oscillator designs 62
5.2 Results of the Amplifier designs 67
5.3 Results of the Magnetic Coupling Coil designs 72
5.4 Results of the Filter designs 82
5.5 Results of the Rectifier designs 88
5.6 Results of the Combined system 92
6. Conclusion 93
6.1 Conclusions 93
6.2 Future work 93
Appendices 98

List of Figures

Figure 1.1 Example of a trailer to be investigated 3
Figure 2.1 Literature Review Structure 6
Figure 2.2 Structure of a Sine wave oscillator [2] 7
Figure 2.3 Colpitts Oscillator [2] 8
Figure 2.4 Hartley Oscillator [2] 9
Figure 2.5 Example of Common emitter configuration [4] 10
Figure 2.6 Example of Common base configuration [4] 10
Figure 2.7 Operation of an ideal op-amp [5] 11
Figure 2.8 Non-inverting op-amp configuration [6] 11
Figure 2.9 Depiction of Ampere's Law with field lines [7] 12
Figure 2.10 General Transformer structure [8] 13
Figure *2.11 The feature definitions of the different coplanar coils [10]* 14
Figure 2.12 Simulated magnetic flux density for Type A(a), B(b), C(c), D(d), E(e) coils [10] 15
Figure 2.13 Simulation results for self-inductance [10] 16
Figure 2.14 Simulation results for mutual inductance [10] 16
Figure 2.15 Spiral coil with misalignment [11] 17
Figure 2.16 Influence of relative position on mutual inductance [11] 17
Figure 2.17 Magnetic field strength of the spiral air core coil inductance in the z-axis; (a) a distance at 25 mm (b) a distance at 50 mm (b) a distance at 75 mm (b) a distance at 100 mm [12] 18
Figure 2.18 Magnetic field strength of the spiral ferrite core coil inductance in the z-axis; (a) a distance at 25 mm (b) a distance at 50 mm (b) a distance at 75 mm (b) a distance at 100 mm [12] 19
Figure 2.19 Power transfer efficiency vs distance [14] 20
Figure 2.20 Implementation of wireless charging [17] [18] 21
Figure 2.21 MIMO wireless power transfer of RFID tag [21] 21
Figure 2.22 Frequency response of a low pass filter [22] 22
Figure 2.23 Frequency response of a high pass filter [22] 23
Figure 2.24 Frequency response of a bandpass filter [22] 23
Figure 2.25 RC passive low pass and high pass filter circuits [22] 24
Figure 2.26 Active low pass and high pass filter circuits [27] 24
Figure 2.27 Bessel, Butterworth, Chebyshev, and Elliptic filter responses [28] 24
Figure 2.28 Conversion process from AC to DC Voltage [29] 26
Figure 2.29 Bridge full-wave rectifier [30] 27
Figure 4.1 Socket on the vehicle-side (on the left) and socket on the trailer (on the right) 30
Figure 4.2 7-pin connector layout 30
Figure 4.3 Trailer lamps from Takealot.com[31] 31
Figure 4.4 V-Diagram 32
Figure 4.5 OPM 32
Figure 4.6 System 33
Figure 4.7 Colpitts Oscillator design in LT Spice 34
Figure 4.8 Tank Circuit design in LT Spice 35
Figure 4.9 Voltage divider biasing of BJT circuit done on KiCad 36
Figure 4.10 DC load-line and Operating point (Q) [33] 36
Figure 4.11 Pin Diagram of 2N2222 [34] 39
Figure 4.12 Oscillator Circuit on a breadboard 39
Figure 4.13 Non-inverting amplifier circuit in LT Spice 41
Figure 4.14 Pin-Out diagram of the LM358P [35] 42

Figure 4.15 Physical Implementation of the Amplifier 42
Figure 4.16 Schematics of the coils, (a) helix coil, (b) spiral coil, (c) square helix coil [37] 43
Figure 4.17 Efficiency vs distance between transmitter and receiver coils of the different structures [37] ... 44
Figure 4.18 Properties menu in Ansys Maxwell 45
Figure 4.19 Spiral transmitter and receiver coils developed in Ansys Maxwell 45
Figure 4.20 Materials of the coil and box 45
Figure 4.21 Current excitations of the coils in Ansys Maxwell 46
Figure 4.22 Mesh definition in Ansys Maxwell 46
Figure 4.23 Refinement of passes in Ansys Maxwell 47
Figure 4.24 LT spice Simulation of the coils 48
Figure 4.25 Early iteration of the physical coil 48
Figure 4.26 Final coils (20 turns) built with the materials used 49
Figure 4.27 Matlab function to determine the length of the wire 50
Figure 4.28 Design 50
Figure 4.29 3-D printed housing 51
Figure 4.30 Active third-order Butterworth bandpass filter simulated on LT Spice 52
Figure 4.31 Python program used to calculate the component values for passive RC filters 53
Figure 4.32 Second-order passive bandpass filter simulated on LT Spice 53
Figure 4.33 Third-order passive RC bandpass filter simulated on LT Spice 53
Figure 4.34 Fourth-order passive bandpass filter simulated on LT Spice 54
Figure 4.35 Chebyshev microwave filter simulated on LT Spice 54
Figure 4.36 Python program used to calculate component values for microwave filters 55
Figure 4.37 Microwave filter design in LT Spice with a 1.92MHz peak frequency 55
Figure 4.38 Hardware circuit setup of the first microwave filter 56
Figure 4.39 Rectifier circuit in LT Spice 57
Figure 4.40 Layout of the regulator[41] 58
Figure 4.41 Layout of the diode [40] 58
Figure 4.42 Diodes(IN5404) soldered together with the capacitor on the output 59
Figure 4.43 The physical regulator(7812CT) in its casing 59
Figure 4.44 Physically attaching the system [42] 60
Figure 4.45 Prototype of the system for one signal line 61
Figure 4.46 Schematic on LT spice 61
Figure 5.1 Oscillator Circuits which are simulated on LT Spice 62
Figure 5.2 Output of the 2MHz Oscillator 62
Figure 5.3 Zoomed-in output of the 2MHZ Oscillator to see the start of oscillations 63
Figure 5.4 Further zoomed-in output of the 2MHz Oscillator 63
Figure 5.5 The outputs of the different oscillator circuits 64
Figure 5.6 Output of the physical oscillator on the oscilloscope 65
Figure 5.7 Crystal Oscillator circuit 65
Figure 5.8 Output of the Crystal Oscillator 66
Figure 5.9 Non-Inverting amplifier circuits which are simulated 67
Figure 5.10 Output of the amplifier with the op-amp set to (Slew=100Meg) 68
Figure 5.11 Output of the amplifier with the op-amp set to (Slew=1000Meg) 68
Figure 5.12 Outputs of the amplified signals on LT Spice 69
Figure 5.13 Output of the physical amplifier at 2MHz (full wave) 70
Figure 5.14 Output of the physical amplifier at 2MHz (half-wave) 71
Figure 5.15 Visual representation of an arbitrary simulation set-up in Ansys Maxwell 72
Figure 5.16 Simulation with coil ratio of 40:20 72
Figure 5.17 Simulation with coil ratio of 20:20 (Chosen design) 72
Figure 5.18 Simulation with coil ratio of 40:40 72

Figure 5.19 Top view of the Magnetic Flux Density magnitude plot 73
Figure 5.20 Side view of the Magnetic Flux Density vector plot 73
Figure 5.21 Angled view of the Magnetic Flux Density vector plot 74
Figure 5.22 Cross-sectional view of the Magnetic Flux Density vector and magnitude plot 74
Figure 5.23 Angled view of the Magnetic Field Intensity magnitude plot 75
Figure 5.24 Angled view of the Magnetic Field Intensity vector plot 75
Figure 5.25 Cross-sectional view of the Magnetic Field Intensity vector and magnitude plot 76
Figure 5.26 Coupling circuit simulated in LT Spice 76
Figure 5.27 Input and output signal of the coupling circuit 77
Figure 5.28 Physical set-up of the coupling circuit 77
Figure 5.29 Voltage source signal at 2MHz on an oscilloscope 78
Figure 5.30 Voltage output signal at 2MHz on an oscilloscope 79
Figure 5.31 Voltage source at 6MHz signal on an oscilloscope 80
Figure 5.32 Voltage output at 6Mhz signal on an oscilloscope 80
Figure 5.33 Voltage output at 6Mhz signal on an oscilloscope (coils "squashed") 81
Figure 5.34 Microwave filter circuits which are simulated on LT Spice 82
Figure 5.35 Third-order active filter frequency response simulated on LT Spice 82
Figure 5.36 Comparison of RC passive higher-order filters simulated on LT Spice 83
Figure 5.37 Close up of the fourth-order RC passive filter's output simulated on LT Spice 83
Figure 5.38 Frequency response of the Chebyshev microwave filter simulated on LT Spice 84
Figure 5.39 Frequency responses of the five microwave bandpass filters simulated on LT Spice 84
Figure 5.40 Frequency response of microwave filter with altered inductor values simulated on LT Spice ... 84
Figure 5.41 Input and output of microwave filter at 2MHz 85
Figure 5.42 Input and output of microwave filter at 3MHz 85
Figure 5.43 Input and output of microwave filter at 4MHz 86
Figure 5.44 Input and output of microwave filter at 5MHz 86
Figure 5.45 Input and output of microwave filter at 6MHz 87
Figure 5.46 Identical rectifier circuits to be simulated 88
Figure 5.47 Output of the rectifier with ideal diodes 88
Figure 5.48 Output of the rectifier with 1N194 diodes 89
Figure 5.49 Oscilloscope output of the rectifier for the 2MHz signal 89
Figure 5.50 Oscilloscope output of the rectifier for the 6MHz signal 90
Figure 5.51 Effect of smoothing capacitor on the 2MHz signal 90
Figure 5.52Effect of smoothing capacitor on the 6MHz signal 91

List of Tables

Table 4.1 User and System Requirements 31
Table 4.2 Capacitor and Inductor values for different frequencies 35
Table 4.3 Datasheet specifications 37
Table 4.4 Resistor Values for different Gains 40
Table 4.5 Different coils simulated 47
Table 4.6 Theoretical frequencies of Oscillation 55
Table 4.7 Element values and parameters for different peak frequencies 55
Table 5.1 Output frequencies and voltages in LT spice 64

Nomenclature

Acronym	Term
AC	Alternating current
DC	Direct Current
RFID	Radio Frequency Identification
MIMO	Multiple Input, Multiple Output
Op-amp	Operational amplifier
B Field	Magnetic Flux Density field
H Field	Magnetic Field Intensity field
R	Resistance
C	Capacitance
L	Inductance

1. Introduction

1.1 Introduction

If you want to find the secrets of the universe think in terms of energy, frequency, and vibration.

-Nikola Tesla

Wireless energy transfer dates back to the 1800s, becoming particularly famous due to Nikola Tesla's demonstration, powering a field of lamps without the use of wires. It is based on Faraday's Law of Induction as well as Lenz's law. Today, many applications of wireless energy transfer are found ranging from wireless charging of phones to charging electric vehicles.

This project covers one such application of wireless energy transfer, namely inductive coupling. The project aims to design a magnetic coupling system for caravan and trailer signal lights. Indicator and brake lights for caravans and trailers are connected to the towing vehicle with a special socket, which relies on the physical contact of conductors. This connection is prone to interruption due to dust and oil accumulation on the conductors. In this project, a contactless alternative using magnetic induction to transfer information and energy is designed. An image of an example trailer to be investigated is shown in Figure 1.1.

Figure 1.1 Example of a trailer to be investigated

1.2 Motivation

A solution to the beforementioned problem will be useful as the problem has been prevalent for many years. The current wired implementation is costly, especially due to the need for it to be replaced. Furthermore, the inefficiency of the current implementation is dangerous as the lack of indicator lights and brake lights can cause accidents on the road. Therefore, the financial and social impact that the project can achieve provides a good motive for research into the topic. A successful implementation will make roads safer and save consumers money.

1.3 Problem statement

Existing technology is available to remedy the current problem. The technology involves using Bluetooth as well as antennas to transmit radio frequencies to the trailer lights. However, this technology is usually expensive and separate light kits are used as opposed to the built-in trailer lights. This is therefore expensive and not aesthetically appealing.

1.4 Objectives

The primary objective of the following project is to design, simulate and implement the magnetic coupling between two wire coils (inductors). The shape, orientation, size, and design are determined based on the required inductance ratios and mutual inductance coupling factors.

The input of the designed system stems from the car battery as the source. For inductive coupling, this DC voltage needs to be converted to an AC voltage. Therefore the primary loop (transmitter coil) is connected to the source through an oscillator circuit. Furthermore, the signal from the oscillator circuit is amplified with a common amplifier before reaching the primary coil. The frequency of oscillations is dependant on the selected signal to differentiate them. Thus, oscillator circuits and amplifiers are to be explored.

The output of the secondary coil is fed into various band-pass filters. This will differentiate each signal and power the corresponding light. Moreover, the signals are to be rectified for operation. Therefore, filter design and rectification are crucial.

1.5 Thesis contributions

The main contribution of this thesis is to provide a novel methodology of solving the problems caused by physical connections between cars and trailer lights. This will be attempted using theories of magnetic induction and wireless power transfer.

1.6 Terms of reference

The main objective as stated before is to transfer power wirelessly from the vehicle to the trailer/caravan. Therefore, this is the main requirement. Next, an important requirement is to differentiate signals to power individual lights. A more straightforward requirement to meet, but a necessary one is to convert the signals from DC to AC, and vice versa. This is a lower level requirement but is still essential for the system to work. These top-level requirements are further broken down in the remainder of the report. The requirements come as a result of meetings with the project supervisor as well as insight and research.

Wireless power transfer is achieved through magnetic induction, this being later discussed in the literature review. Differentiating signals is complex and requires circuitry on both ends of the magnetic coupling to perform properly. Therefore, the use of oscillators and filters is investigated. For the conversion of signals,

once more the oscillators are useful. This is paired up with regulators and rectifiers on the secondary side of the system to revert to the original signal.

The performance of the functionalities is first tested in simulation software, namely LT Spice and Ansys Maxwell. For hardware implementation, all parts of the system are tested on signal generators and oscilloscopes found in the lab.

1.7 Scope and limitations

Time is a constraint for the project. The project spans the second semester of the 2021 academic year. A 14-week duration meant that efficiency was important and there was not much room for error. Furthermore, the research coincides with three other engineering courses which are to be done simultaneously.

Next, the research has a monetary ceiling. The project is capped at R1500. This means many of the components have to be constructed instead of bought, such as copper coils and filters. This affects efficiency greatly as tolerances are higher

Moreover, the software to be used (Ansys Maxwell), is computationally taxing. It uses up a lot of ram and memory and needs to be run on a good processor. All simulations and designs shown in the report are run on a 16Gb ram laptop with an I5 processor. This is not ideal and means simulations take long to run and are less accurate.

Lastly, the covid-19 impact cannot be ignored. Meetings with the research supervisor are more difficult as they are contactless. Also, contacting people with regards to part collection and orders proves more difficult.

1.8 Thesis outline

The project has the following sequential order:

- *Chapter 2*
  The Literature review. This will cover induction theories, filter design, and adaptations of wireless energy transfer.

- *Chapter 3*
  The Methodology. Here the design approach is summarised along with the software used.

- *Chapters 4*
  The Design. The design of the system is implemented based on the relevant theory and methodology. Each sub-chapter corresponds to a different sub-system.

- *Chapter 5*
  The Results. When the design is finalised, the system is simulated/built and the results are highlighted.

- *Chapter 6*
  Using the results, conclusions are drawn indicating the level of success of the project.

2. Literature Review

2.1 Introduction

The following literature review covers the five main topics that will be essential to designing the system. Relevant theories and techniques are discussed as well as current implementations in the industry. Moreover, relevant history and research into the topics will be discussed.

The topics are covered in order of occurrence in the system. Therefore, the review starts with oscillator circuit theory followed by amplifiers. Next, the review looks at magnetic induction (in green for emphasis), before looking into filters. Finally, the review deals with rectifiers. A simple tree diagram of the structure of the review is shown in Figure 2.1 depicting this.

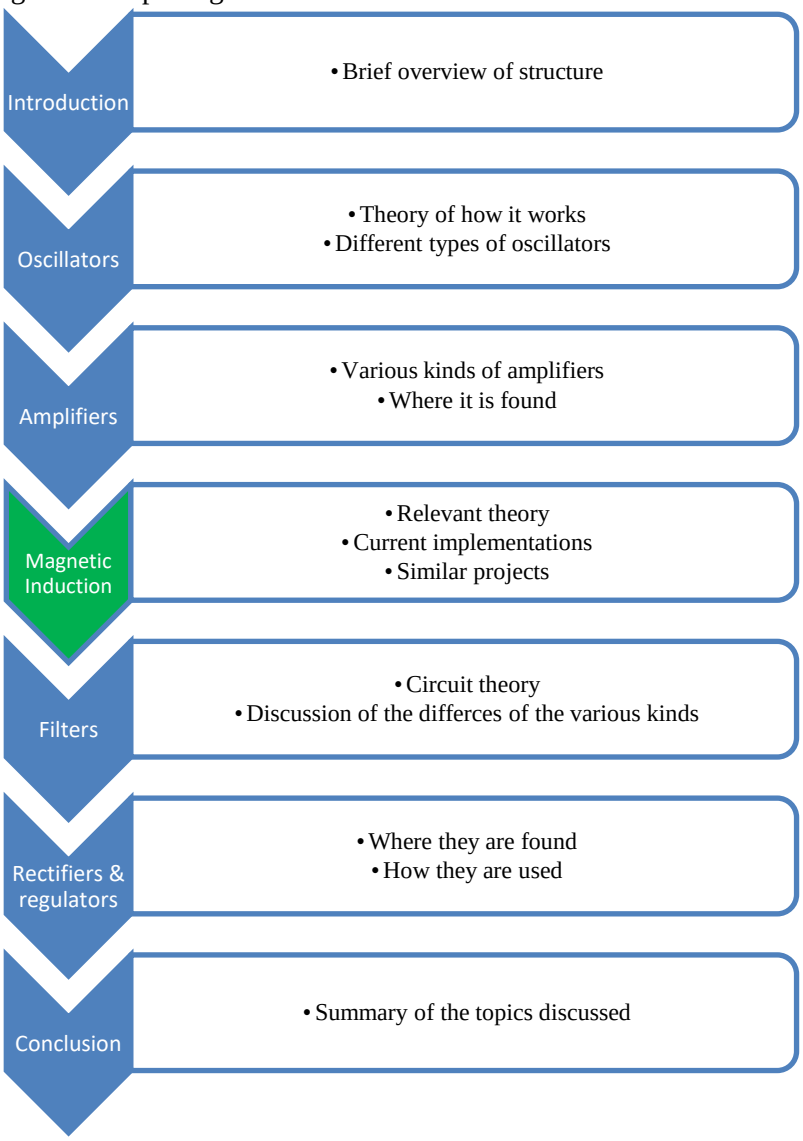

Figure 2.1 Literature Review Structure

2.2 Oscillators

The first part of the system involves converting a DC voltage into an AC sinusoidal voltage. This is due to the principle of magnetic induction, requiring an AC voltage, which will be discussed later. This can be achieved by using a microcontroller in conjunction with PWM (Pulse Width Modulation) signals. However, this would

be both financially straining and time-consuming as microcontroller are relatively expensive and can be complex. Therefore, the implementation is done using an oscillator circuit.

Oscillators are electronic circuits that convert Direct Current to Alternating current. They produce periodic signals such as sine waves which is critical for the project. The two main types of oscillators are harmonic oscillators and relaxation oscillators. The harmonic (feedback) oscillators produce sinusoidal outputs as opposed to the relaxation oscillates, therefore the former will be analysed. [1]

Feedback Oscillators consist of an amplifier circuit (forward path) and a feedback circuit (filter). This is shown in Figure 2.2. They are further classified by the filter they use in the feedback circuit, either RC (resistor and capacitor) or LC (inductor and capacitor).

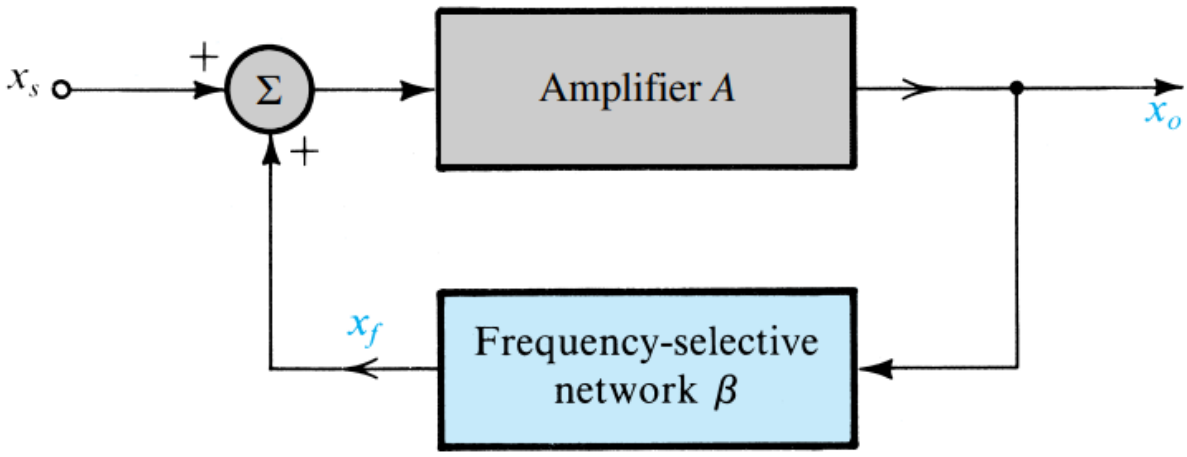

Figure 2.2 Structure of a Sine wave oscillator [2]

RC oscillators such as the Wien Bridge Oscillator and phase shift oscillator are generally used to generate low-frequency waves. The system designed makes use of high-frequency signals, therefore LC oscillators are more preferable. The two most common LC Oscillators are the Colpitts Oscillator and the Hartley Oscillator. Their circuit diagrams are shown in Figure 2.3 and Figure 2.4 below. The Colpitts Oscillator contains two capacitors in the feedback circuit, whereas the Hartley Oscillator contains two inductors in the feedback circuit.

These oscillators use an LC circuit in feedback to provide phase shift and to act as resonant filters. Equation 2.1 represents the frequency of oscillation, f_r, for a Colpitts Oscillator with Equation 2.2 representing that of the Hartley Oscillator. Equation 2.1.1 and 2.2.1 gives series capacitance and inductor totals.

$$f_r \cong \frac{1}{2\pi\sqrt{LC_T}} \tag{2.1}$$

Where C_T is the total capacitance given by:

$$C_T = \frac{C1C2}{C1 + C2} \tag{2.1.1}$$

$$f_r \cong \frac{1}{2\pi\sqrt{L_T C}} \tag{2.2}$$

Where L_T is the total inductance given by:

$$L_T = L1 + L2 \tag{2.2.1}$$

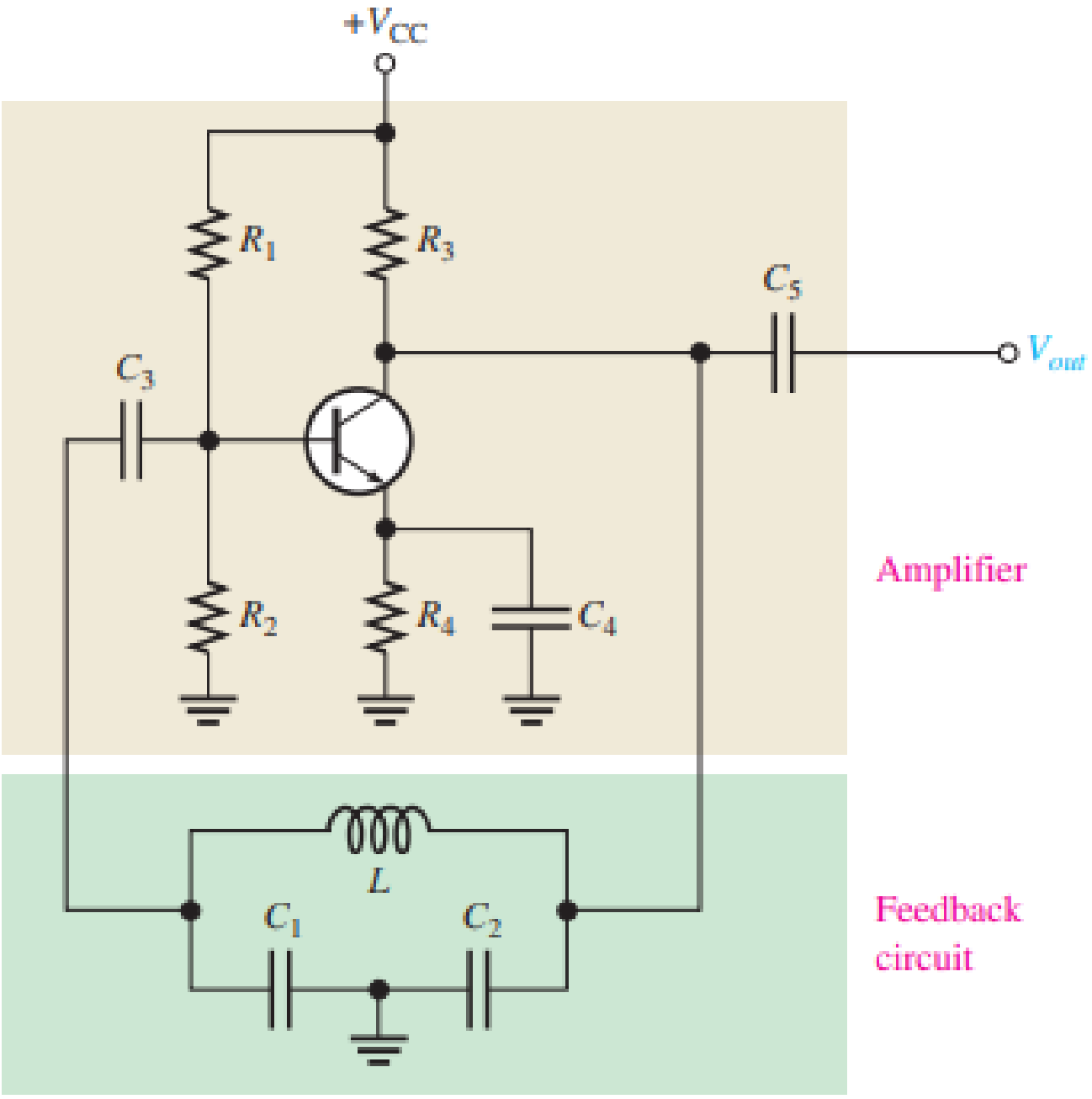

Figure 2.3 Colpitts Oscillator [2]

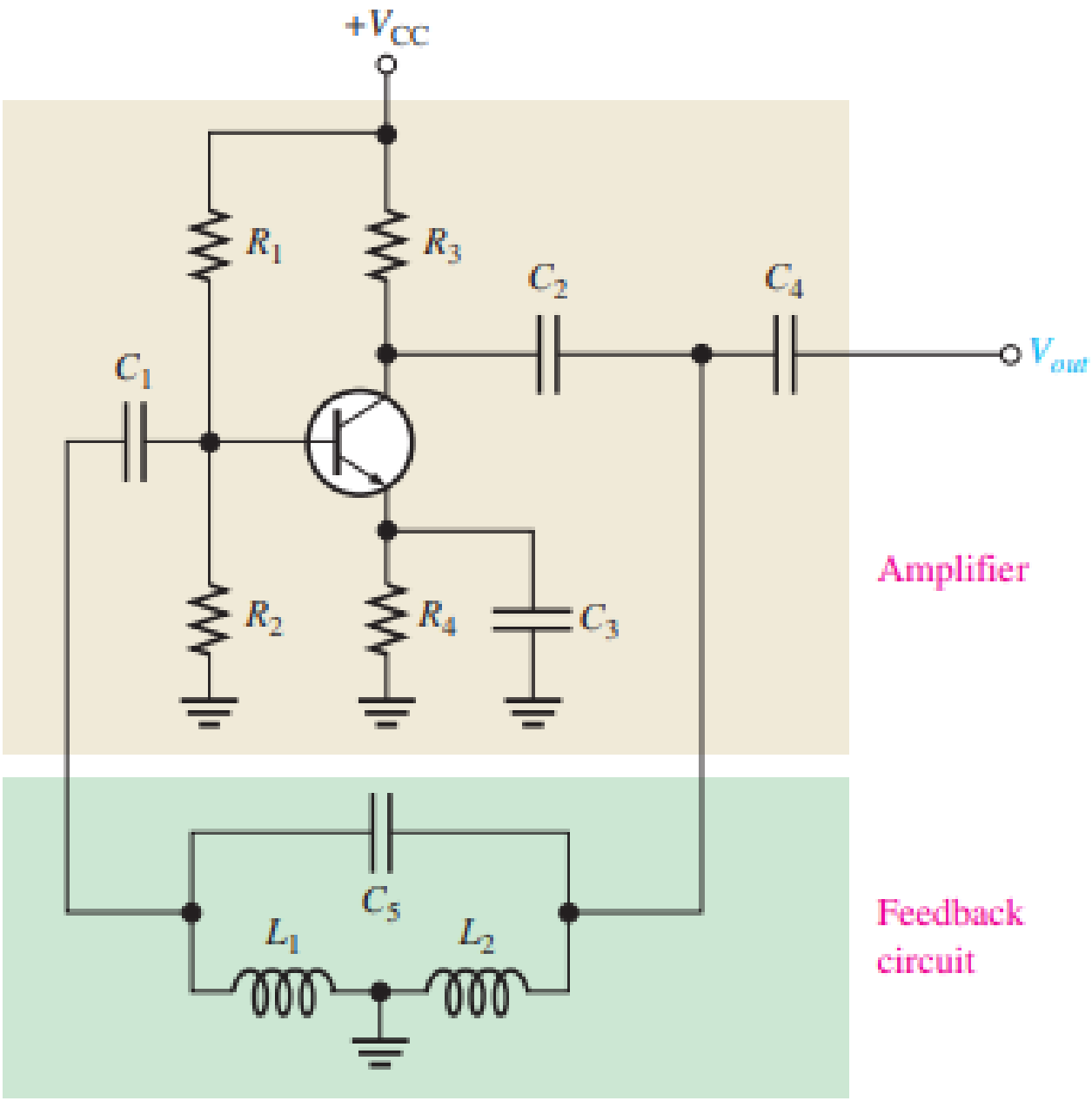

Figure 2.4 Hartley Oscillator [2]

2.3 Amplifiers

Using the oscillators in the previous step causes a voltage drop. Therefore, an amplifier is needed to amplify the voltage to the original voltage. Two main options are discussed namely a voltage amplifier using a transistor (BJT) and the other using an operational amplifier.

The common emitter configuration or common base configuration of a transistor is used to achieve voltage amplification. An example of the common-emitter configuration is shown in Figure 2.5. The input of this configuration is at the base with the output found at the collector. The capacitors are used to block DC voltages. It can be seen that in this type of configuration the output voltage is an amplified version of the input shifted by 180 degrees (sign change). [3]

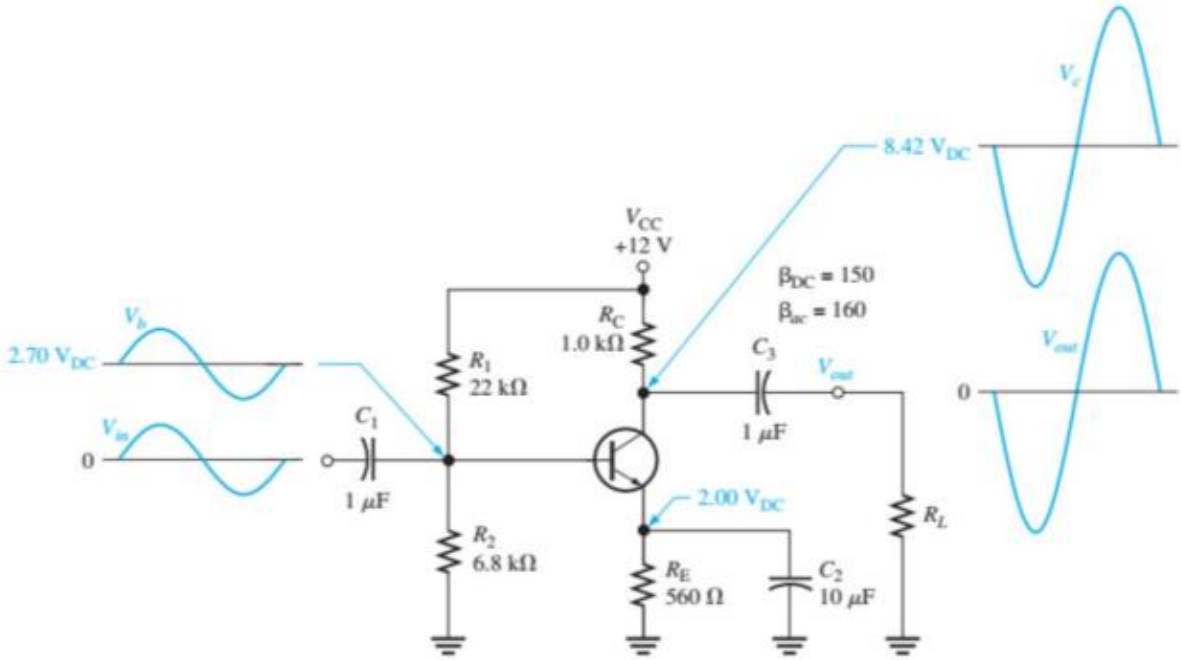

Figure 2.5 Example of Common emitter configuration [4]

Contrary, in Figure 2.6 we see the common base configuration. The input of this configuration is at the emitter with the output found at the collector. They are non-inverting voltage amplifiers that are suitable for high-frequency signals. Furthermore, they act as current buffers. [3]

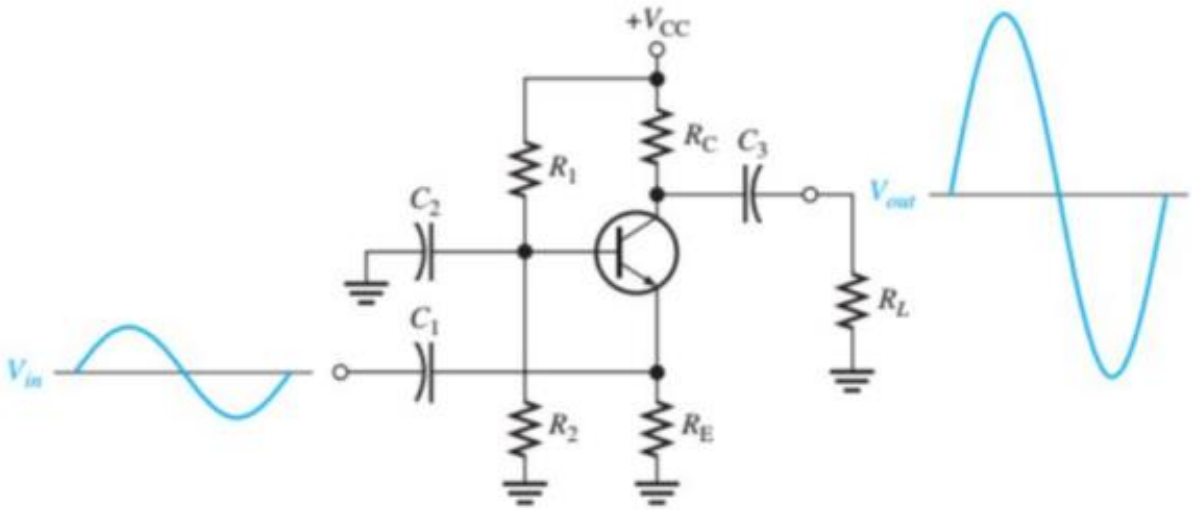

Figure 2.6 Example of Common base configuration [4]

The next type of amplifier as beforementioned is the operational amplifier. It is considered a high-gain voltage amplifier [5]. Although made up of many components it is considered a single circuit element due to its simple operation. Therefore, it may seem easier and more aesthetically pleasing to use as opposed to the BJT configurations. Figure 2.7 below depicts the operation of an ideal op-amp.

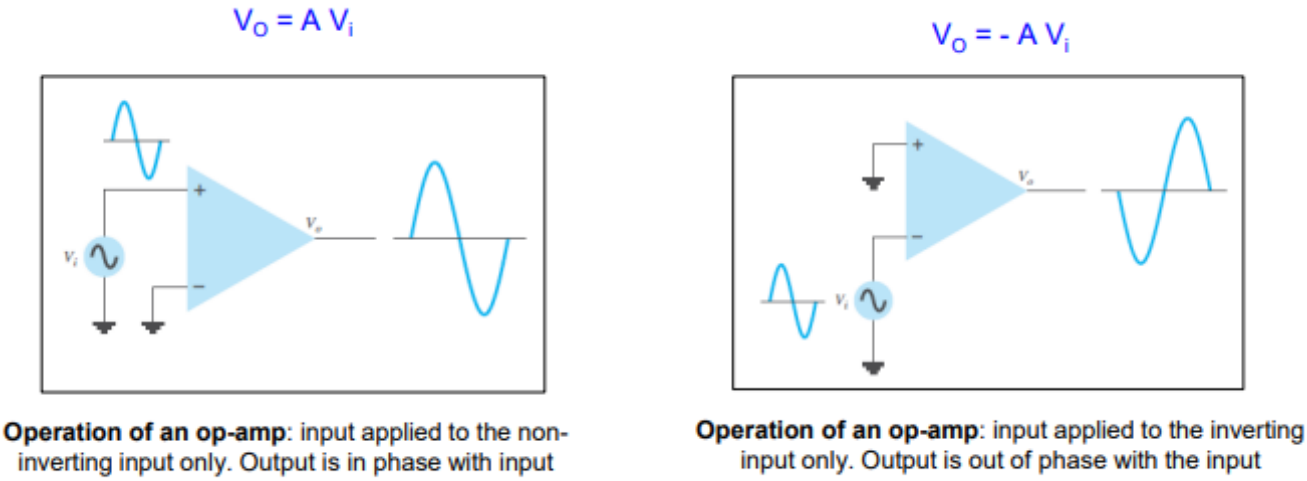

Figure 2.7 Operation of an ideal op-amp [5]

The two most common configurations of the op-amp circuitry for voltage gain are the inverting and non-inverting op-amps. The project will value the latter more as it is not concerned with inverting the input voltage. The gain of the configuration is determined by the ratio of the resistors found in the circuitry. Equation 2.3 indicates the formula for the gain with Figure 2.8 representing the circuitry of the non-inverting op-amp. [6]

$$A_{(cl)} = 1 + \frac{R_f}{R_i} \tag{2.3}$$

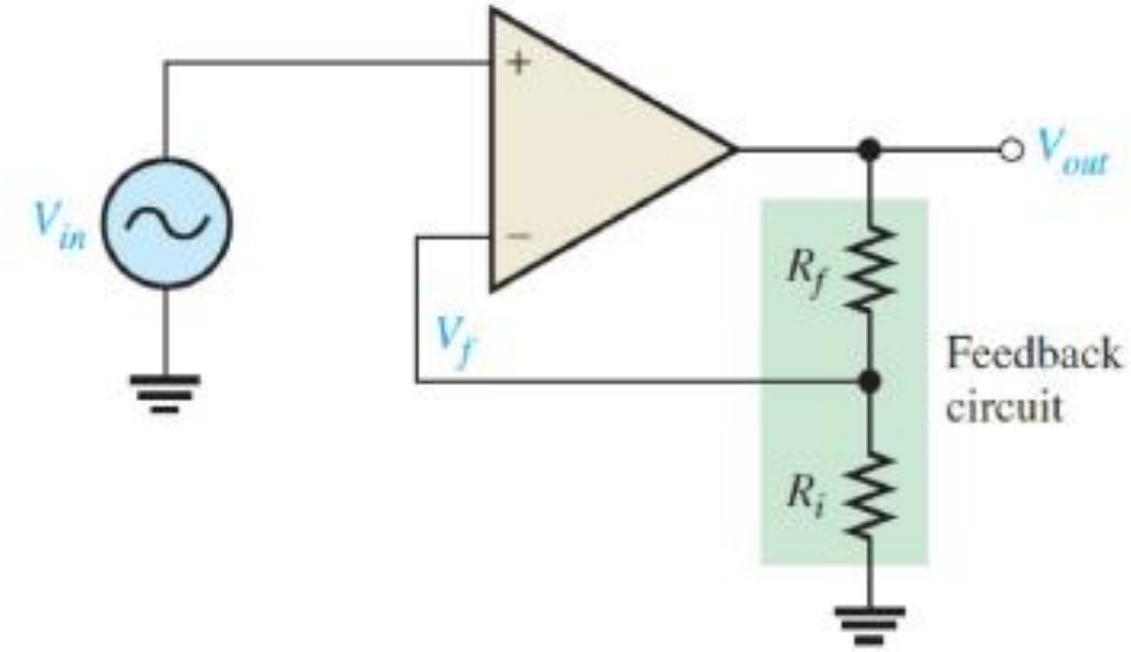

Figure 2.8 Non-inverting op-amp configuration [6]

2.4 Magnetic Induction

Electromagnetic induction involves power transmission from one coil of wire to another coil, by means of a magnetic field. The primary coil is called the transmitter while the secondary coil is called the receiver. Together these coils form a transformer. Ampere's Law, governed by Equation 2.4, states that an alternating current (AC) applied to to the transmitter coil will create an oscillating magnetic field. A visual representation of this is shown in Figure 2.9. [7]

$$\oint \vec{B}.dI = \mu_0 I_{encl} \tag{2.4}$$

Where $\vec{B}$ is the magnetic field density, dI the changing current, μ_0 the permeability of the medium, and I_{encl} the enclosed current.

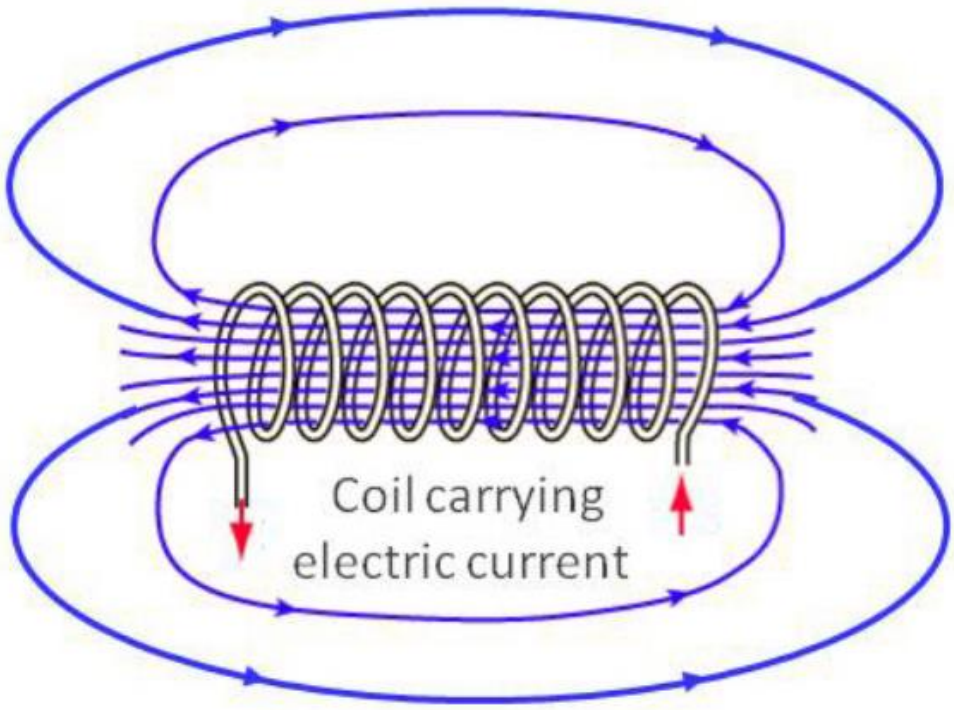

Figure 2.9 Depiction of Ampere's Law with field lines [7]

This magnetic field then passes through the receiver coil. By Faraday's Induction Law, an alternating emf, ε_{ind}, governed by equation 2.5, is induced subsequently inducing an alternating current. This alternating current is then used to drive a load, at times being rectified first. In the equation, $d\emptyset_B$ is the changing flux.

$$\varepsilon_{ind} = \frac{-d\emptyset_B}{dt} \tag{2.5}$$

The two coils can be modelled as a transformer, as in Figure 2.10, with air being the permeable core. Assuming an ideal transformer, the relationship between the primary coil voltage (V_1) and secondary coil voltage (V_2) is given in Equation 2.6 below. The relationship is, therefore, dependant on the turns ratio (where N is the number of turns) of the two coils and therefore the inductance of them. [8]

$$\frac{V_1}{V_2} = \frac{E_1}{E_2} = \frac{N_1}{N_2} \tag{2.6}$$

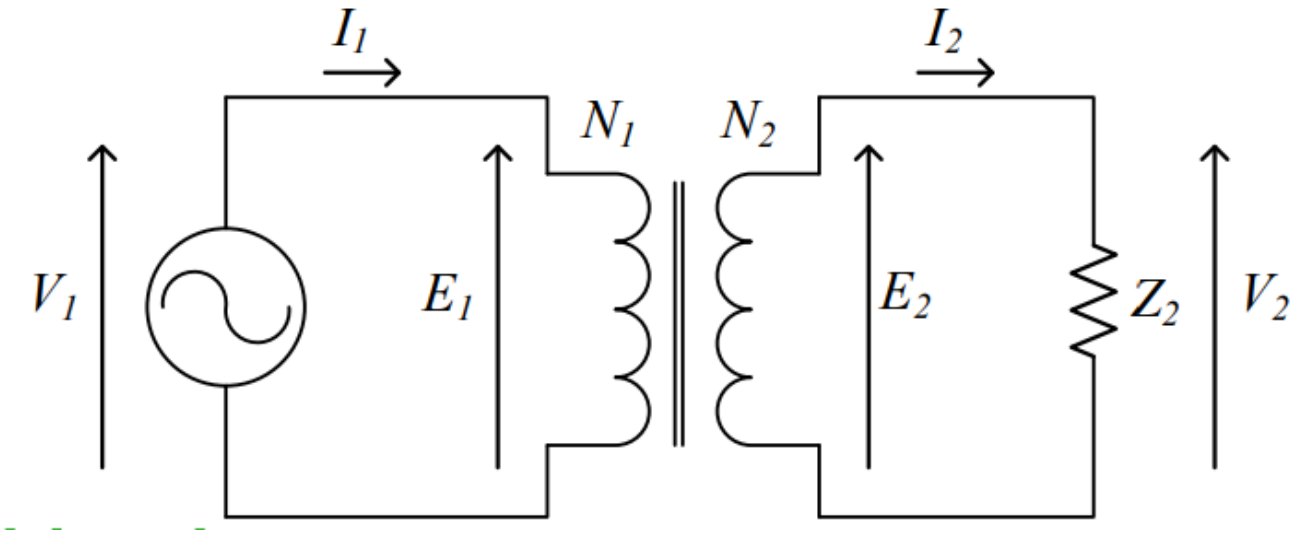

Figure 2.10 General Transformer structure [8]

However, an ideal transformer is impossible in practice. Many non-ideal effects are found in transformers as follows:

- Finite winding resistance
- Presence of leakage flux
- Core not infinitely permeable
- Hysteresis losses
- Eddy current losses

The power that is transferred increases with an increase in frequency and mutual induction. The mutual inductance is dependant on the geometry of the coils, the material of the coils, and the distance between the coils. Therefore, to optimise the efficiency of the power transfer the mutual inductance is optimised. A key measure of the power transfer efficiency is the coupling factor k. This is a value between 0 and 1 where a value closer to the upper limit indicates better efficiency. The equation for the coupling factor is given in Equation 2.7, where M is the mutual inductance and L the self-inductance. Furthermore, this factor is an indication of the amount of magnetic flux of the transmitter coil that passes through the receiver coil.

$$k = \frac{M}{\sqrt{L_1 L_2}} \tag{2.7}$$

As beforementioned, the following affects the mutual inductance and coupling factor:

Geometry of coils

The shape and orientation of coils have a significant impact on the self-inductance as well as the mutual inductance of the coils. Most of the research that has been done with regards to the geometry of coils has been around spiral planar coils. The reason for this has not been explicitly stated in many papers and it can be concluded that this is a gap in the field of research. Generally, it is stated that spiral planar coils are less space-consuming and are more aesthetically appealing. This is a fair subjective conclusion. Furthermore, research done at the Hangzhou Dianzi University on coplanar coils [9] concluded that the mutual inductance coefficient is much higher when the turns of coils are concentrated along the radius of the coil (spiral) as opposed to being distributed at the outer circumference (as seen in solenoids).

A paper by the Department of Automatic Control Engineering at the Feng Chia University [10], further looked into the effects of five different structures of the coil, namely, square, square-like, rounded rectangular, circle like and circular. These structures are defined in Figure 2.11 with an appropriate depiction.

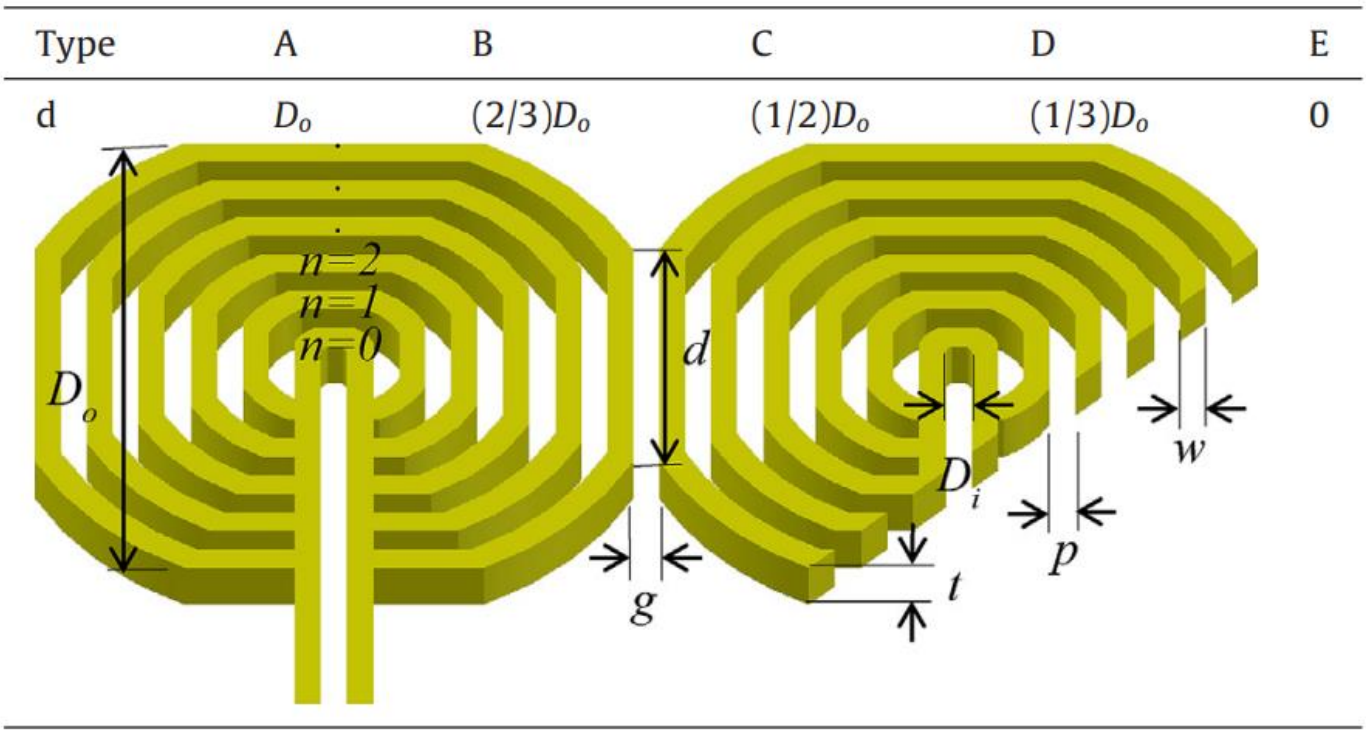

Fi*gure 2.11 The feature definitions of the different coplanar coils [10]*

Simulations were done in COMSOL, where the structure was simulated as a nickel film (electrical conductivity of 13.8e-6 S/m and relative permeability of 1240). The dimensions of t, g, p, w, and Di were set to 10 µm. Furthermore, the coil was excited with a current of 0.2A. The results of the magnetic flux density for the different structures with 10 turns are shown in Figure 2.12 below. It is evident that an increase in the parallel length of the coils subsequently increases the effect of the magnetic inductance as seen in Type A, where there is a large distribution in the field. Note that the maximum of the scale bars in the figure is set to 0.45mT.

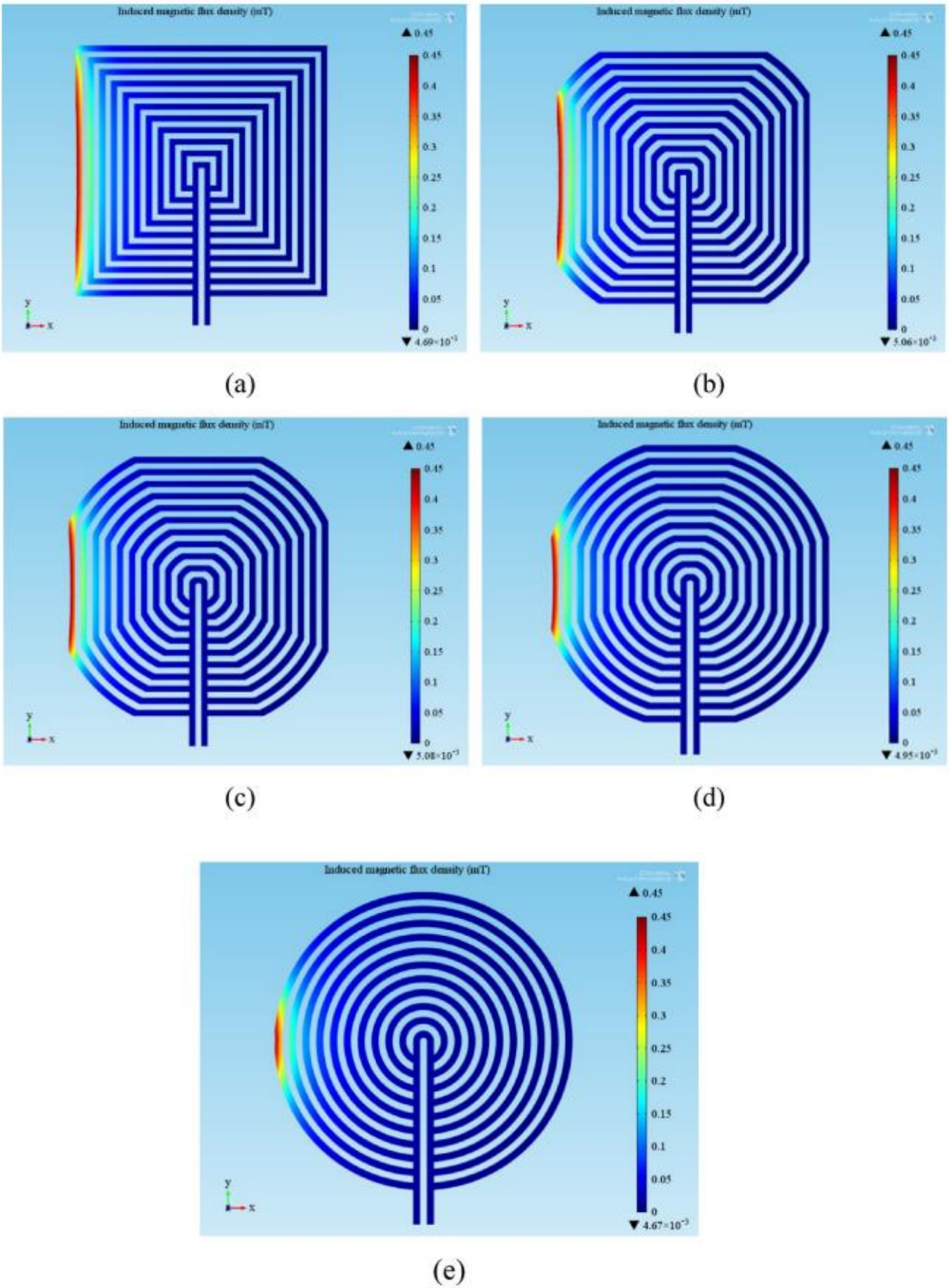

Figure 2.12 Simulated magnetic flux density for Type A(a), B(b), C(c), D(d), E(e) coils [10]

Furthermore, the paper goes on to calculate the mutual inductance and self-inductance of the different types of coils, for both 20 and 10 Turns. The results of these simulations are seen in Figure 2.13 and Figure 2.14 below. Again, it can be seen that type A is the most favourable with type E the least favourable.

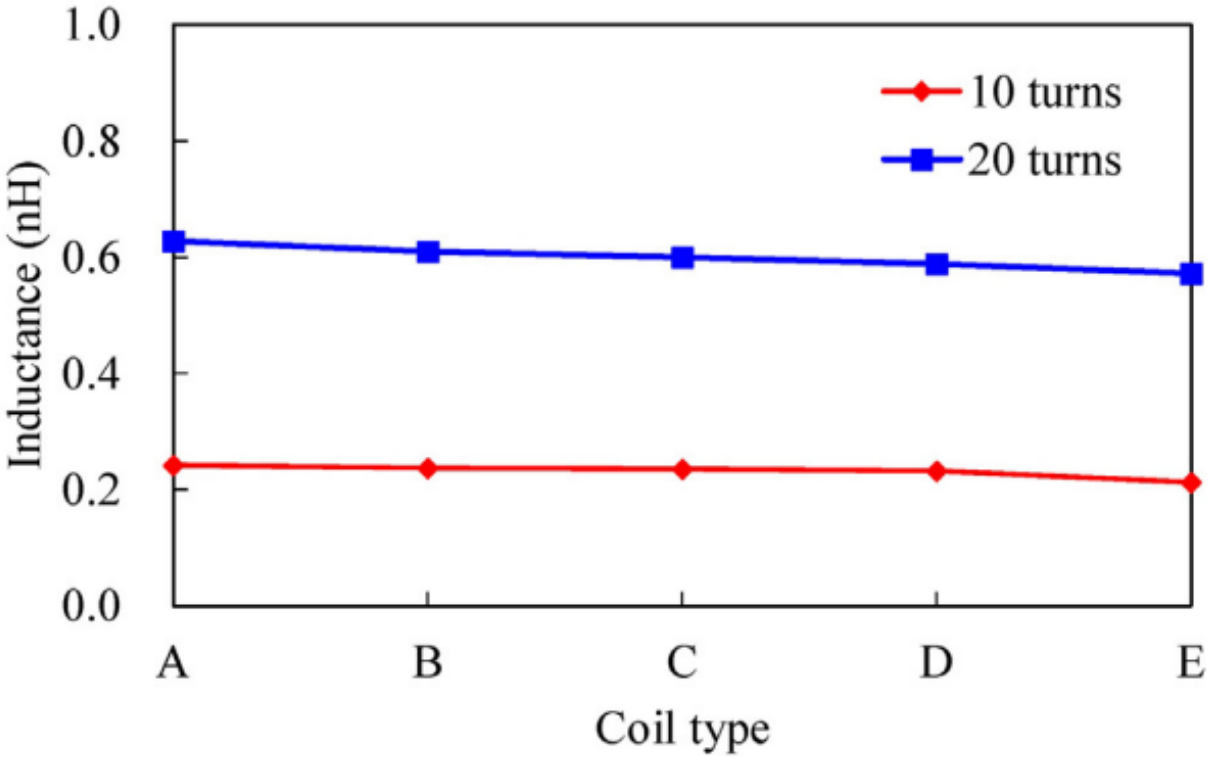

Figure 2.13 Simulation results for self-inductance [10]

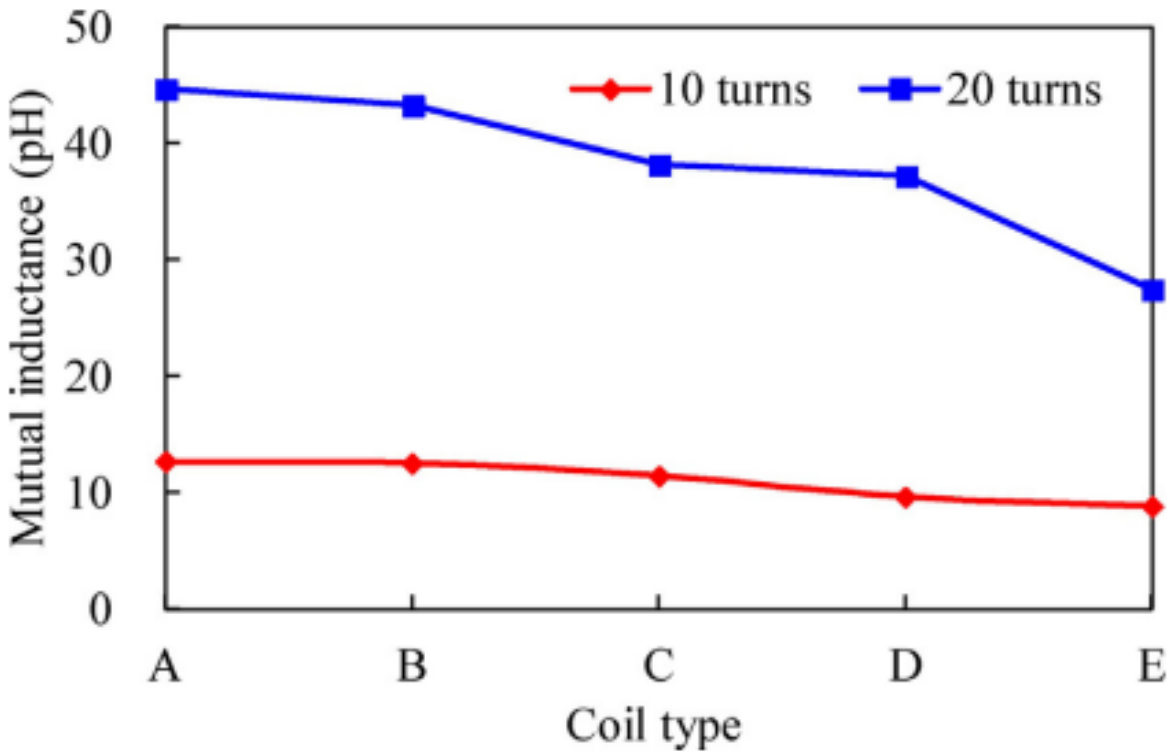

Figure 2.14 Simulation results for mutual inductance [10]

Lastly, the coupling coefficient and mutual inductance of laterally misaligned coils, shown in Figure 2.15, and non-parallel coils are significantly lower than coaxial coils. This is no surprise as the magnetic field would not align and pass through efficiently. A paper by the Hefei University of technology [11] confirms this. The results of the effect of position on the mutual inductance are shown in Figure 2.16.

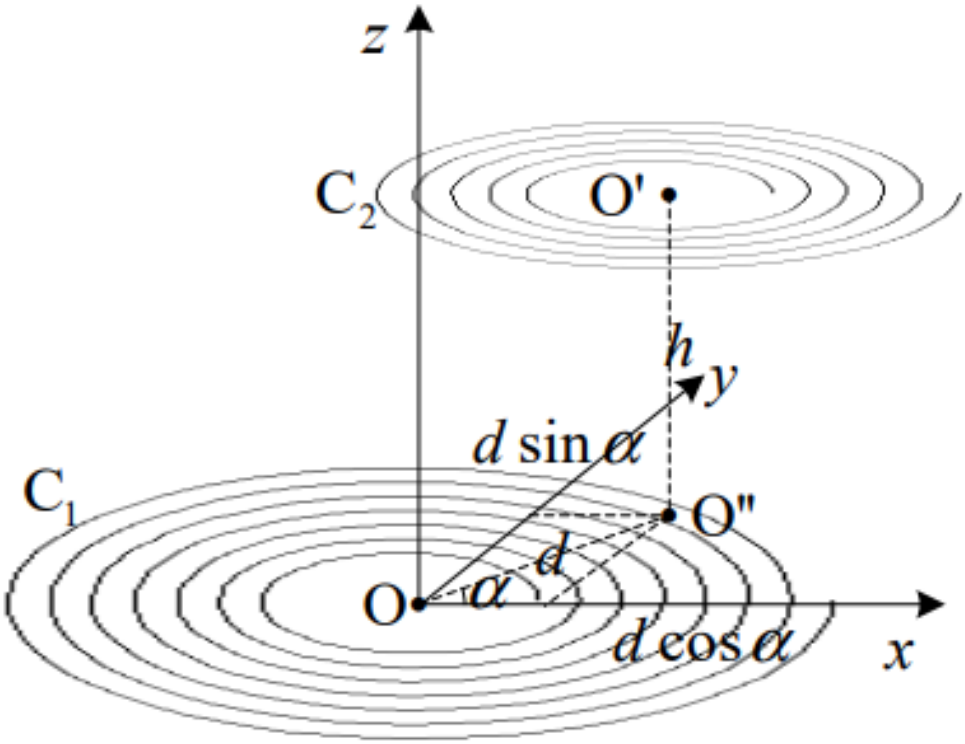

Figure 2.15 Spiral coil with misalignment [11]

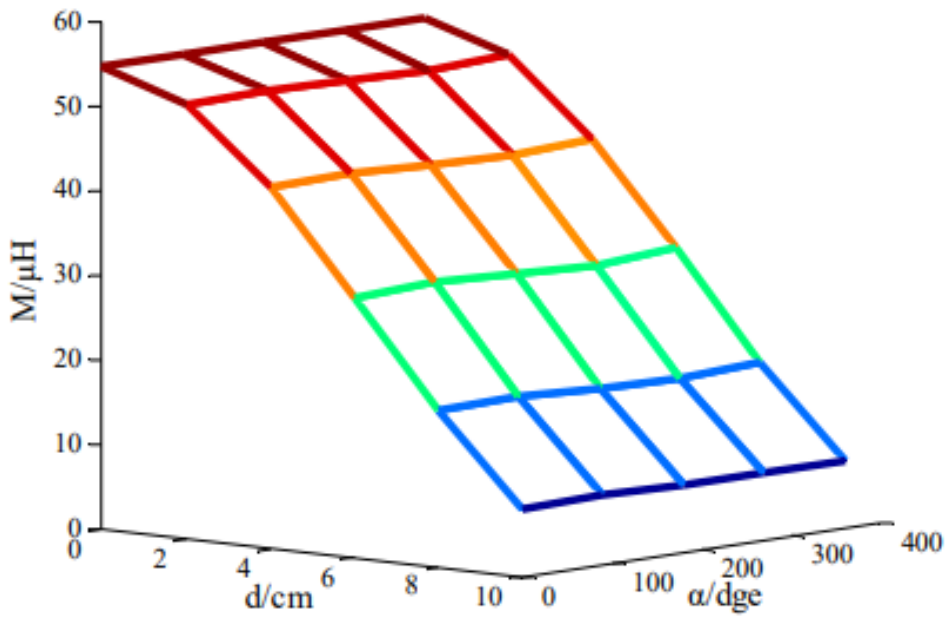

Figure 2.16 Influence of relative position on mutual inductance [11]

Material of coils and permeable core

A key factor that affects magnetic coupling is the ferromagnetic core which is found between the coils. An investigation done by the Suranaree University of technology [12], indicates undoubtedly that using a ferrite core increases the coupling factor. The comparison was done between an air coil and a ferrite core and the results of their magnetic field intensity are shown in Figure 2.17 and Figure 2.18 below. The result is as expected considering most transformer designs contain a ferromagnetic material for better coupling.[8]

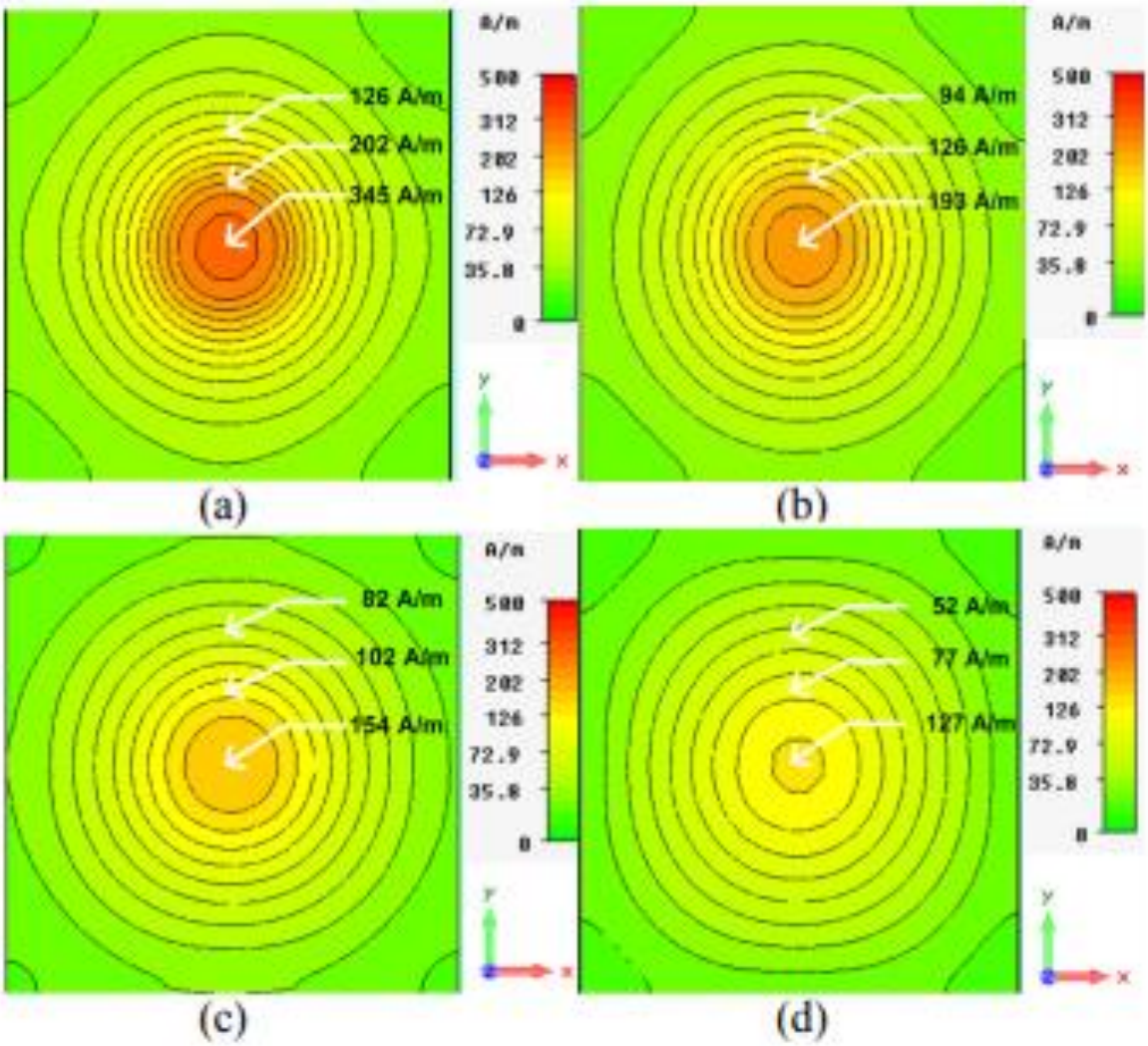

Figure 2.17 Magnetic field strength of the spiral air core coil inductance in the z-axis; (a) a distance at 25 mm (b) a distance at 50 mm (b) a distance at 75 mm (b) a distance at 100 mm [12]

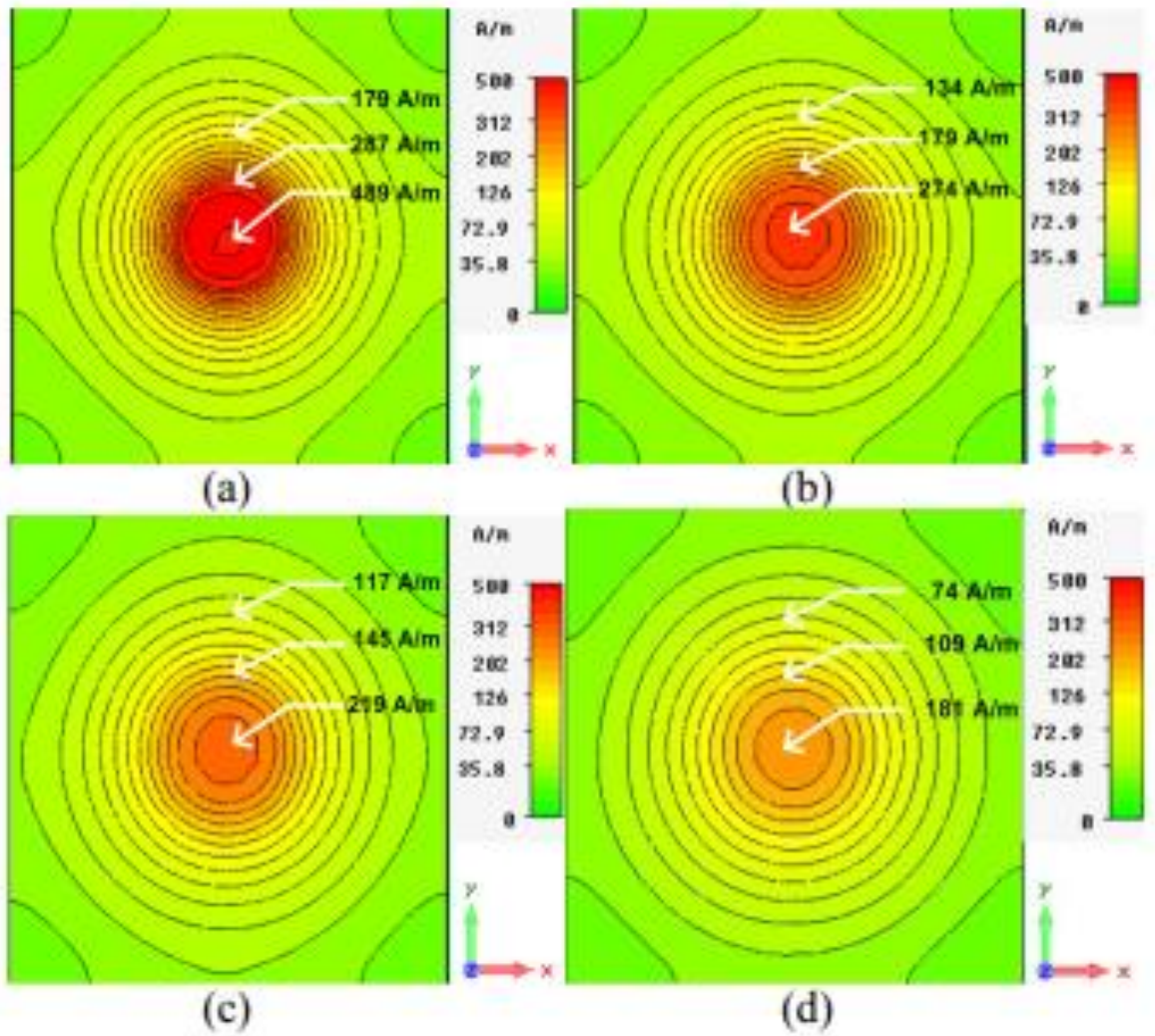

Figure 2.18 Magnetic field strength of the spiral ferrite core coil inductance in the z-axis; (a) a distance at 25 mm (b) a distance at 50 mm (b) a distance at 75 mm (b) a distance at 100 mm [12]

The material from which the coils are made has a significant impact on its inductance. The most common material, copper, has a conductivity of 5.96e7 S/m. Although there are alternatives with better conductivity, copper is well priced as is seen on the market. Equation 2.8 [13] below shows us that the permeability of the material, μ_e, used is directly proportional to the inductance, L. In the equation, l is the length, A the area, and N the turns.

$$L = \frac{\mu_e \mu_0 N^2 A}{l} \tag{2.8}$$

Distance between coils

Research done by the University of Malaysia Perlis [14], shows that the mutual inductance between two coils decays exponentially with an increase in the distance of separation between them. Although tests were done on one specific type of coil, with a fixed geometry, it is safe to assume that this would be the case for all types of coils. Figure 2.19 provides a visual representation of this. This is justified by the Biot-Savart law, stating that magnetic field strength is inversely proportional to distance.[7] This is further confirmed by the research in [9] and a study by the Urmia University [15] where we see the same effect.

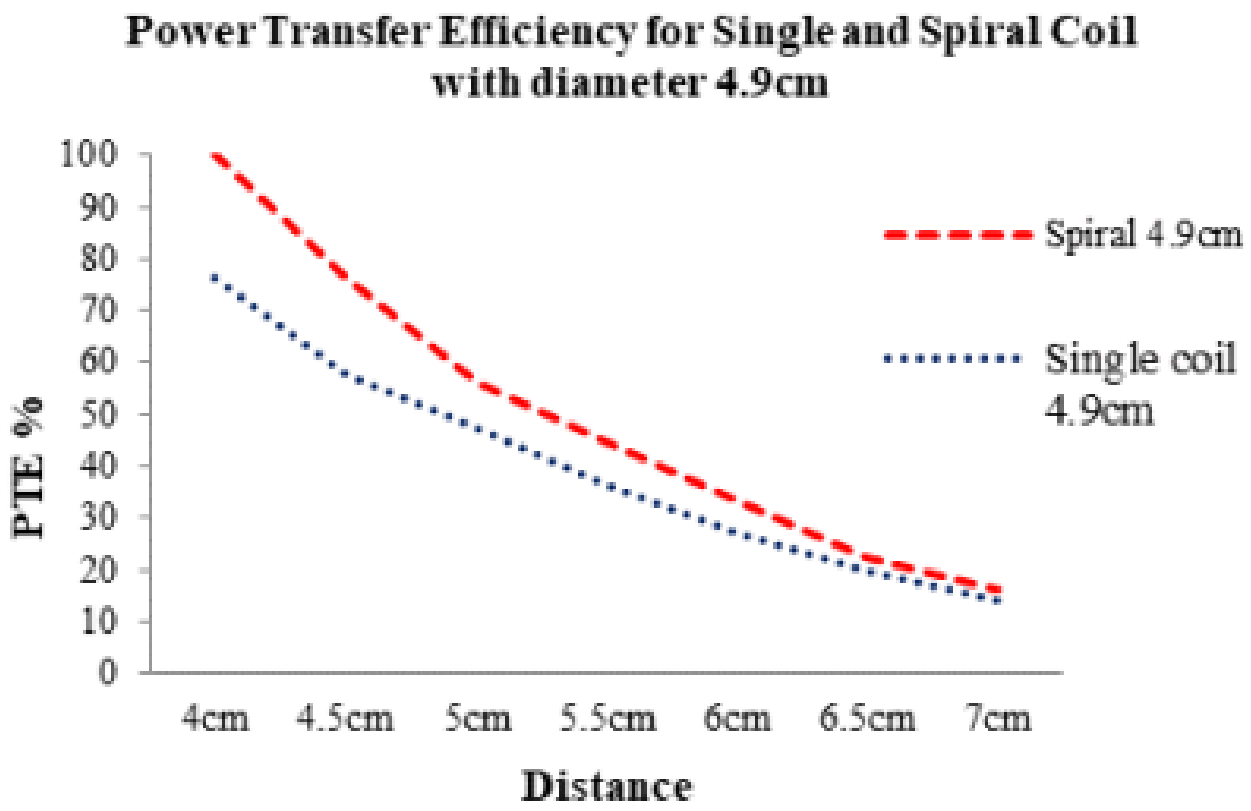

Figure 2.19 Power transfer efficiency vs distance [14]

Frequency

Another type of coupling is resonant magnetic coupling, where the coupling takes place solely at the resonance frequency. However, the coupling this project is concerned with is non-resonant magnetic coupling. Therefore, the coupling does not take place at one resonant frequency, and the effect of frequency needs to be investigated. Not much prior research has been done on this, therefore, the project aims to fill this gap.

Applications of Wireless Power Transfer (WPT)

Today WPT is used in many applications, most commonly in wireless cellphone chargers, shown in Figure 2.20, [16][17][18] and the charging of electric vehicles [19][20]. In a paper by L. Olvitz, a wireless charging system for a cellphone, with a power capability of 0.5W at 250mm is achieved. [17] With the ever-increasing availability of technology and lack of space for charging devices, this technology looks to bring a more space-efficient and aesthetically appealing environment. Lastly, the technology is gaining a lot of popularity in passive RFID tags. These are battery-less tags powered by RFID scanners shown in Figure 2.21. [21]

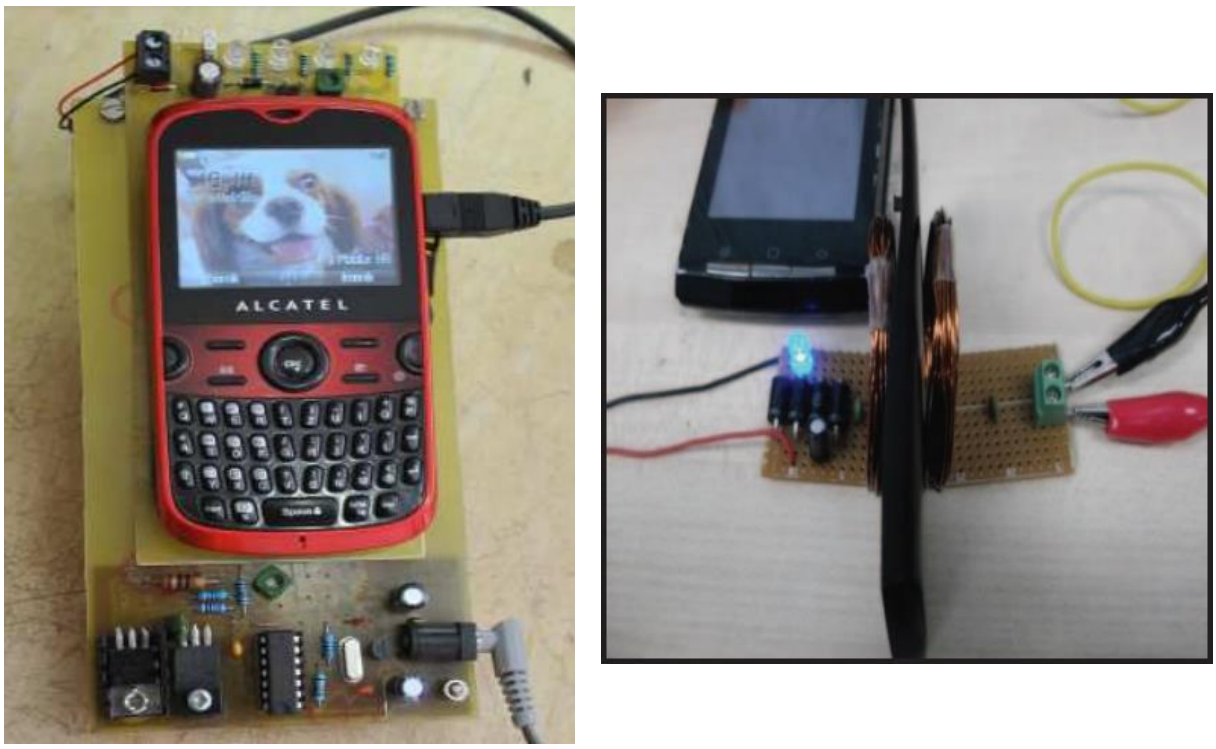

Figure 2.20 Implementation of wireless charging [17] [18]

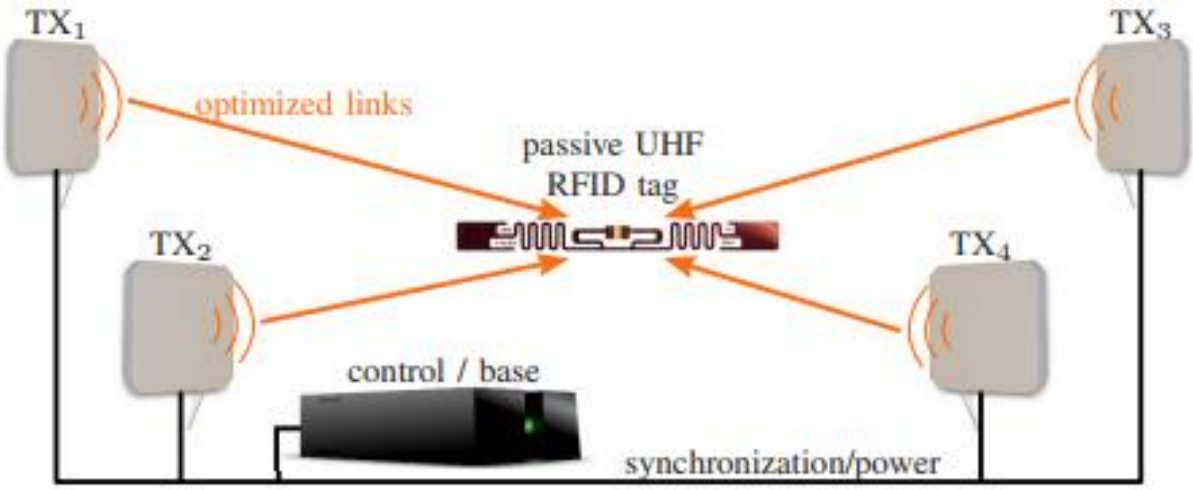

Figure 2.21 MIMO wireless power transfer of RFID tag [21]

Resonant inductive power transfer

Although not used in this project, resonant coupling has become popular in the engineering and technological world and is therefore worth a mention. This technology is similar to inductive coupling, however only operates at the set resonant frequency. Its weakness is that it is only efficient within the "several-metre" range. [16]

2.5 Filters

A filter circuit allows a selected range of desirable frequencies to pass through to the output without attenuation while attenuating undesirable frequencies. When it comes to electronics, filters have a wide range of applications such as radio communications, DC power supplies, audio electronics, analog-to-digital-conversion, etc. Filters are linear systems that alter the amplitude and phase of an input sinusoidal signal. The change in amplitude results in a gain that can be expressed as the ratio between the output signal and the input signal, and can also be referred to as the transfer function. The gain can be measured either linearly or in decibels (dB). The conversion between the

linear gain and the gain in decibels can be made using Equation 2.9, where $A_{(dB)}$ is the gain in decibels and $A_{(ratio)}$ is the linear gain.

$$A_{(dB)} = 20log_{10}(A_{ratio}) \tag{2.9}$$

The phase change results in a phase shift in the output signal, relative to the phase of the input signal [22]. The behavior of a filter is observed in the frequency domain by a bode plot, which plots the relationship between the gain and phase against frequency according to its transfer function [23]. Filters can be sub-categorized according to whether they are active or passive, high pass or low pass, their response type, or their order.

Low Pass vs High Pass

Filters can be designed to be low pass or high pass filters, and these can be cascaded to produce bandpass and stop pass filters. A low pass filter allows frequencies below a specified cut-off frequency, to pass through to the output while frequencies above the cut-off frequency are attenuated. The frequency response of a low pass filter is shown in Figure 2.22. A high pass filter allows frequencies above the cut-off frequency to pass through to the output while frequencies below the cut-off frequency are attenuated. The frequency response of a high pass filter is shown in Figure 2.23. The cut-off frequency for both low-pass and high-pass filters can be specified by the resistor and capacitor values according to Equation 2.10, where f_c is the cut-off frequency, R is the resistance and C is the capacitance.

$$f_c = \frac{1}{2\pi RC} \tag{2.10}$$

A bandpass filter allows frequencies within a particular range to pass through to the output while attenuating frequencies outside of that range. It is created by cascading a high-pass filter and a low-pass filter in series, where the pass frequencies range from the cut-off frequency of the high-pass filter to the cut-off frequency of the low-pass filter. This range of frequencies is also known as the bandwidth, and it can be adjusted to be wider or narrower by altering the values of the resistors and capacitors to change the cut-off frequencies. The range of frequencies that are suppressed is known as the stopband. Ideally, a filter would have a passband and a stopband only, but practically they also have a transition band, which is a sloped region between the passband and the stopband. The frequency response of a bandpass filter is shown in Figure 2.24. A band-stop filter suppresses frequencies within a specified range while allowing frequencies outside of that range to pass through to the output. It is created by connecting a low-pass filter and a high-pass filter in parallel [22].

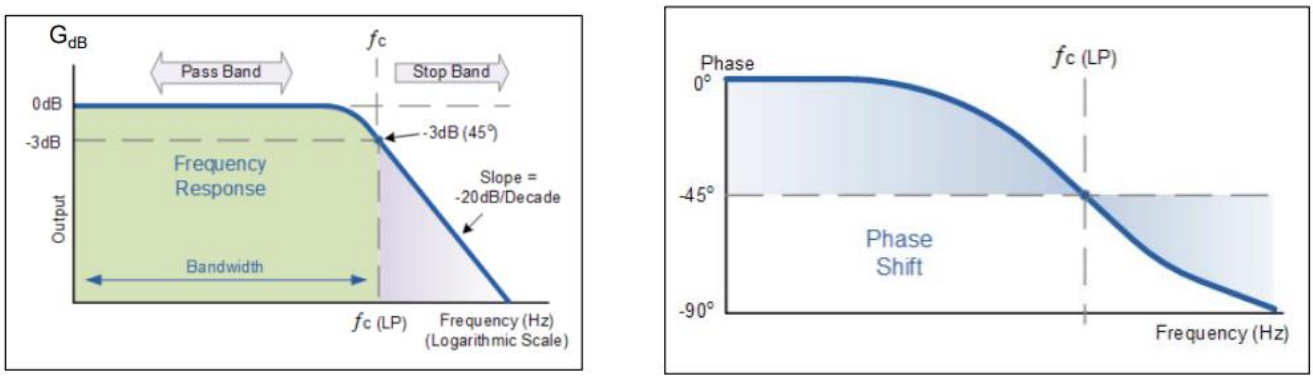

Figure 2.22 Frequency response of a low pass filter [22]

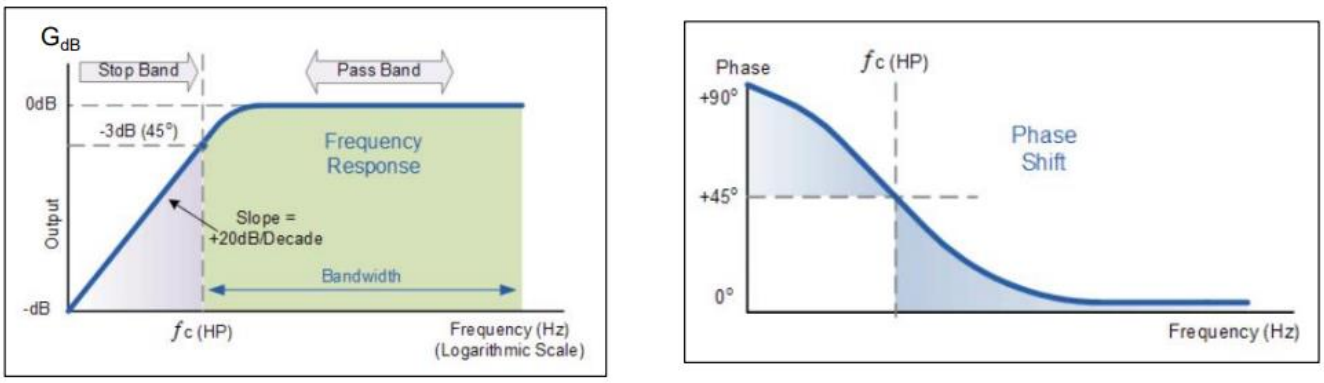

Figure 2.23 Frequency response of a high pass filter [22]

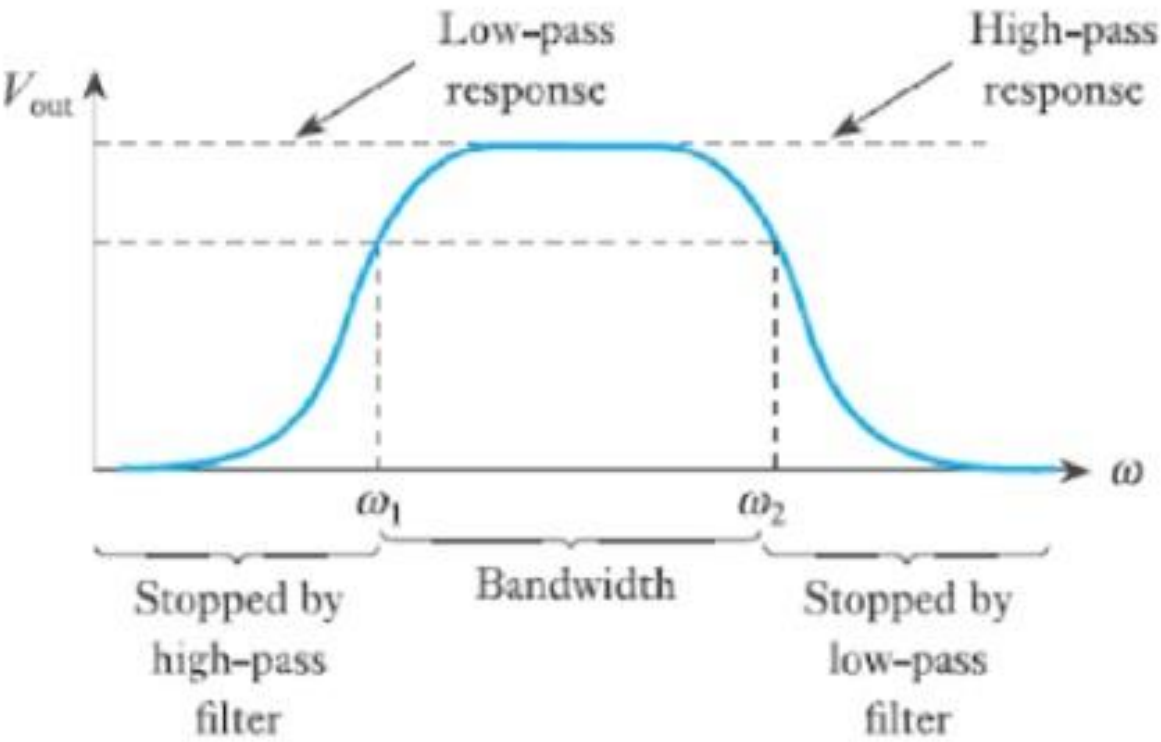

Figure 2.24 Frequency response of a bandpass filter [22]

Active Filters vs Passive Filters

Passive filters are designed using passive components such as resistors, capacitors, and inductors. These components can be used to design LC, LR, LRC, or RC filters. Passive filters can process all frequencies (including very high frequencies), as they do not have bandwidth limitations. However, they suffer from impedance dependency when they are cascaded [24]. Figure 2.25 shows an RC passive low pass filter circuit and an RC passive high pass filter circuit.

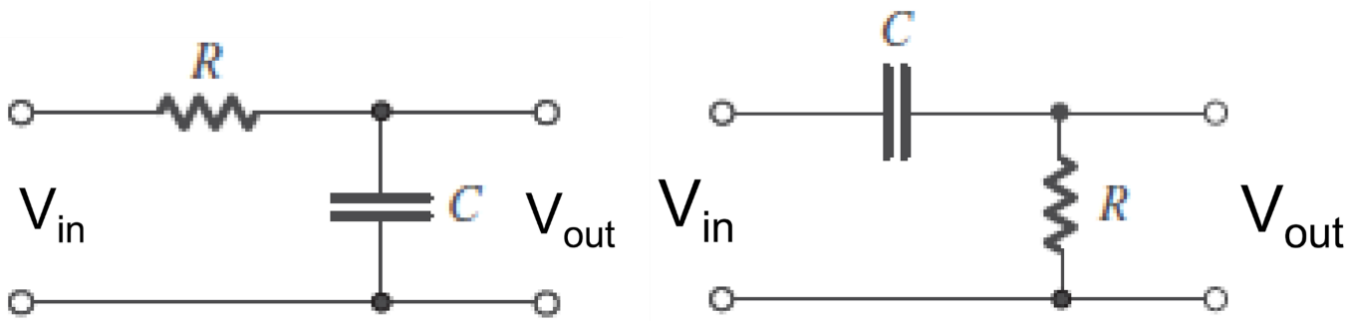

Figure 2.25 RC passive low pass and high pass filter circuits [22]

Active filters are designed using active components such as operational amplifiers and transistors, combined with passive components such as capacitors and resistors. Figure 2.26 shows the circuit setups of an active low pass filter and an active high pass filter. Active filters were designed with the intention of compensating for the problems associated with a passive filter design, however, they are more costly, and high pass active filters are not very practical because they amplify high-frequency noise components and are unstable. [22] There are four main types of active filters that are categorized according to their frequency response. They are Butterworth, Chebyshev, Bessel, and Elliptic and their differences can be seen in Figure 2.27 [25].

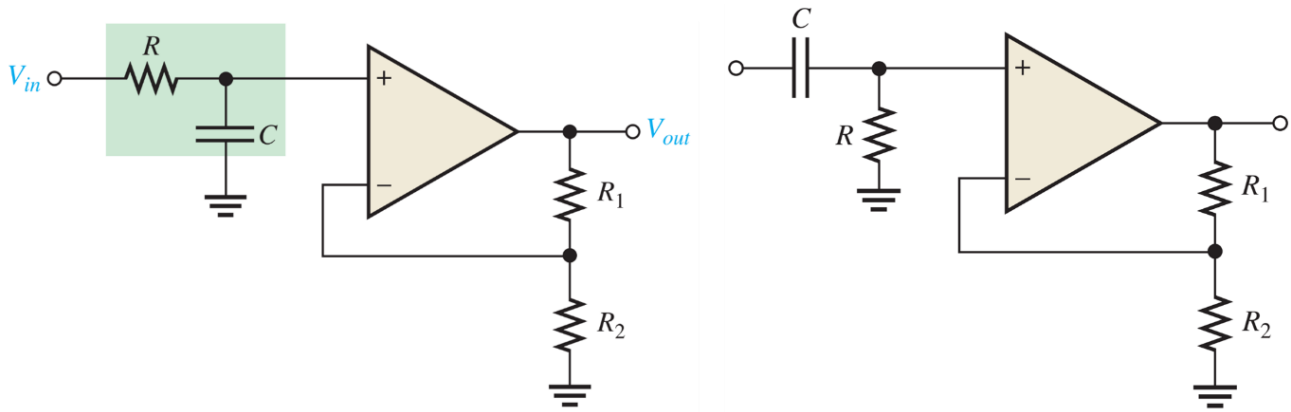

Figure 2.26 Active low pass and high pass filter circuits [27]

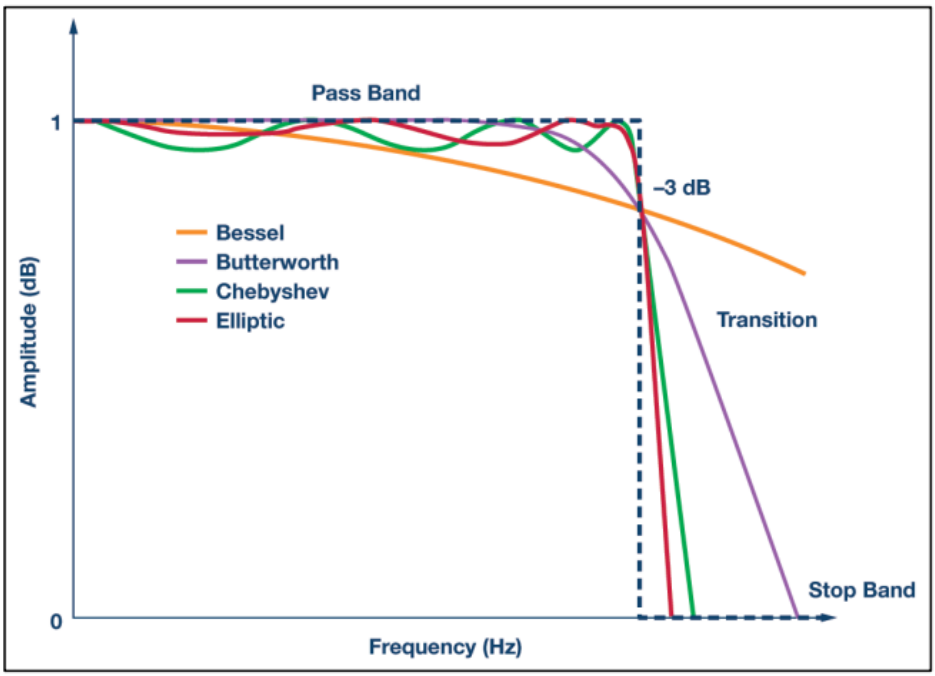

Figure 2.27 Bessel, Butterworth, Chebyshev, and Elliptic filter responses [28]

Order of Filters and Cascading Multiple Filters

The order of a filter is determined by its transfer function and influences the roll-off rate in the transition band. A first-order filter has a roll-off of -20dB/dec and the gain at the cut-off frequency is always 3dB less than the pass gain. The order of a filter can be increased by cascading multiple identical filters together, where the order corresponds to the number of filters cascaded [22]. Higher-order filters have steeper roll-off rates which increase proportionally with the order. In other words, a first-order filter has a roll-off rate of -20dB/dec, a second-order filter has a roll-off rate of -40dB/dec, and a third-order filter has a roll-off rate of 60dB/dec, etc. Higher-order filters are favourable as they filter out undesirable frequencies more effectively. The disadvantages of higher-order filters are that they narrow down the passband, they are more expensive as they require a greater number of components, and their design is more complex [23]. Cascading passive filters may result in loading effects if the impedance is not correctly defined, as mentioned previously. The combined transfer function is not the product of the individual filters transfer function and therefore the true gain of the filter is not realised. To compensate for this, the input impedance of each successive filter stage should be significantly higher than the output impedance of the previous stage. Active filters do not have this problem as operational amplifiers have a high input impedance and a low output impedance already built-in [25].

Microwave Filters

Microwave filters are built using resistors, capacitors, and inductors and are designed to operate under very high frequencies. In this case, the order of the filter is determined by the number of reactive elements (capacitors and inductors) used to build it. A microwave filter is designed using the insertion loss method, where the insertion loss represents the ratio of the power supplied by the source, to the power delivered to the load. This is shown in Equation 2.11, where P_{LR} is the power loss ratio, P_{inc} is the source power and P_{load} is the load power. The insertion loss in decibels is determined using Equation 2.12, where IL is the insertion loss and P_{LR} is the power loss ratio [26].

$$P_{LR} = \frac{P_{inc}}{P_{load}} \tag{2.11}$$

$$IL = 10\log(P_{LR}) \tag{2.12}$$

Practical Filter Responses

As mentioned previously, the different filter response types include Butterworth, Chebyshev, Bessel, and Elliptic. This project will focus specifically on Butterworth, or otherwise known as a Maximally flat response, and the Chebyshev response. A Maximally flat response provides a flat passband, which is a desirable characteristic of a frequency response. A Chebyshev provides a steep roll-off rate, however, there is also ripple in the passband [26].

Microwave Filter Design

Designing a microwave filter includes first designing a low pass prototype, and then scaling it to the specified frequency and impedance. The circuit element values are labelled as g_k and range from g_0 to g_{N+1} where N is the order and k is an integer value. The elements alternate between a series connection and a parallel connection. The bandpass is determined by specifying cut-off frequencies and can be calculated using Equation 2.13, where Δ is the passband, ω_1 is the first cut-off frequency, ω_2 is the second cut-off frequency and ω_0 is the cut-off frequency.[26]

$$\Delta = \frac{\omega_2 - \omega_1}{\omega_0} \tag{2.13}$$

The elements connected in series are converted into LC circuits and their values are given by Equations 2.14 and 2.15, where L'_k is the inductor value, C'_k is the capacitor value, Δ is the passband, g_k is the prototype element value and ω_0 is the cut-off frequency.[26]

$$L'_k = \frac{\Delta g_k}{\omega_0} \tag{2.14}$$

$$C'_k = \frac{1}{\Delta g_k \, \omega_0} \tag{2.15}$$

The elements connected in parallel are converted to LC series circuits and their element values can be calculated using Equations 2.16 and 2.17. They make use of the same parameters as Equations 2.14 and 2.15 [26].

$$L'_k = \frac{1}{\Delta g_k \, \omega_0} \tag{2.16}$$

$$C'_k = \frac{\Delta g_k}{\omega_0} \tag{2.17}$$

2.6 Rectifiers and Regulators

The output of the system requires a DC voltage to power the trailer lamps. Throughout the system, an AC voltage is used as this is essential for both magnetic induction as well as differentiating the different signals using frequencies. The AC voltage, therefore, is rectified and then filtered. Lastly, the voltage is regulated to protect the lamps. Figure 2.28 below shows the process of converting a sinusoidal voltage into a regulated DC voltage, following the previously mentioned stages.

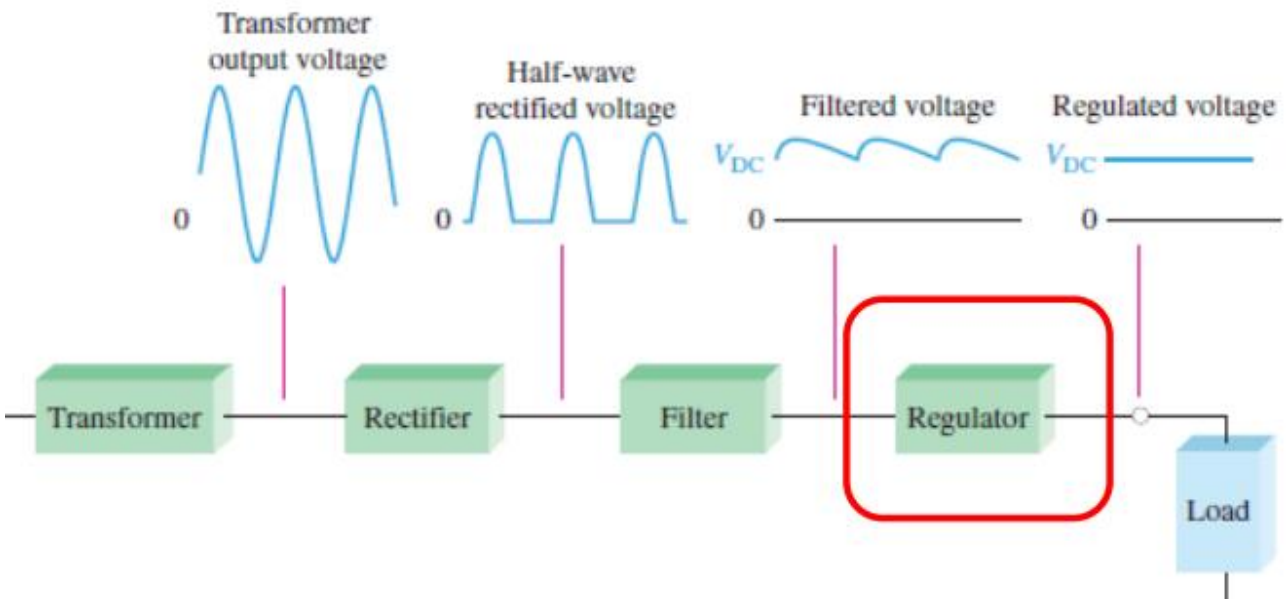

Figure 2.28 Conversion process from AC to DC Voltage [29]

The rectifier converts the AC voltage into a pulsating DC signal. Next, the filter removes any large fluctuations coming from the rectifier. Finally, the regulator ensures that a constant DC voltage is maintained.

A bridge full-wave rectifier is an implementation of four diodes that converts both halves of an AC source to a DC signal. Bridge wave rectifiers allow for smaller transformers to be used at the cost of having more diodes. This cost is welcomed as diodes are cheaper and easier to source as opposed to large transformers. Therefore, they are typically the rectifier of choice. Figure 2.29 is a depiction of a bridge full-wave rectifier. Four diodes are seen which strategically allow signals to pass through.

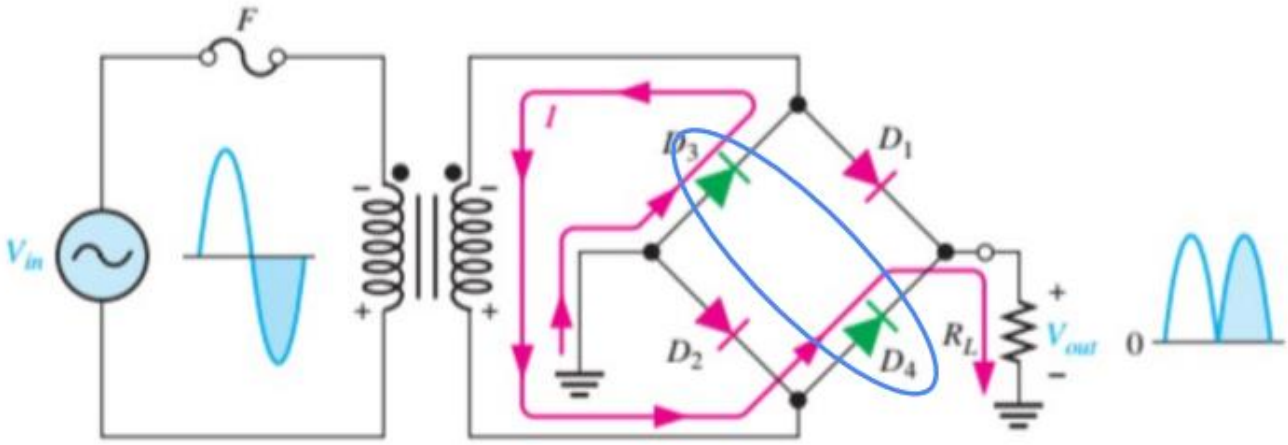

Figure 2.29 Bridge full-wave rectifier [30]

Voltage regulators are complex to design, and the theory related to them are abundant. This is considered beyond the scope of the project. The regulator is therefore sourced based on its performance.
The performance is based on the line regulation and the load regulation. The line regulation is the change in the output voltage when the input voltage changes by a volt. The load regulation, however, is the change in the output voltage from no-load to full-load. Equations 2.18 and 2.19 govern these measures.[30]

$$Line\ Regulation = \frac{\left(\frac{\Delta V_{OUT}}{V_{OUT}}\right)100\%}{\Delta V_{IN}} \tag{2.18}$$

$$Load\ Regulation = \left(\frac{V_{NL} - V_{FL}}{V_{FL}}\right)100\% \tag{2.19}$$

2.7 Conclusion

The literature review covers the five major topics that are essential to system design. Relevant theories are discussed as well as current implementations in the industry. Furthermore, research into the topics is analysed. A major gap in the review is due to the project never being attempted before, therefore all the work has to be done by scratch. This makes combining theories and sections more complex. Finding literature on oscillators and amplifiers was trivial as only the theory is needed. However, with regards to filters, the range and variety prove challenging. This is because it is unclear, the frequency the system will operate at. Microwave filters have less theory than simple low-frequency filters and this lack of information could be troublesome. Lastly, and most importantly, there are many gaps with magnetic induction that needs to be filled. Most of the research online has been done on resonant inductance. This project has more than one signal, making resonant inductance seem unlikely to work. With pure magnetic coupling, although the theory is abundant, its application is not so ample. Therefore, this project will aim to fill in gaps about this theory mainly the frequency it is most effective at, and the geometry (shape) of coils that work best.

3. Methodology

3.1 Overview

The following methodology gives a brief overview of the plan of action of the project. The method involves designing and testing various circuitry and transformers to achieve the ultimate goal. First, the requirements and current implementations (the root of the problem) are investigated. Next, various oscillators are designed with the desired frequencies. Following the oscillator design, the transformer is designed. The filters to acquire the signal are then designed before being rectified. Finally, the designs are tested on software, before being built and tested on hardware.

3.2 Method for Oscillators

The literature review covered two types of oscillators, namely the Colpitts and Hartley oscillators. The Colpitts Oscillator is chosen as it requires one less inductor, where sourcing inductors is more expensive and harder to find as opposed to capacitors. Using the relevant equations, the values of the capacitors, resistors, and inductors are chosen, based on the desired frequencies. The circuit is then built using **LT Spice** and subsequently simulated. After a satisfactory simulation, outputting the desired sinusoidal voltage, the filters are built using physical components. Using an oscilloscope and signal generator, the oscillators are tested in the labs and the graphs are extracted.

3.3 Method for Amplifiers

This method is similar to the above method for Oscillators. Non-inverting op-amp circuits are designed as op-amps have high gains. However, due to the slew rate the frequency of operation may not be ideal and a BJT amplifier is therefore designed as well. These circuits are first designed on LT Spice before being built. Testing of the physical hardware is then tested using oscilloscopes in the lab.

3.4 Method for Magnetic Coupling

The method for designing transformers is an iterative one. Femm and Feko are looked at as possible software choices to design the magnetic couplers. Ultimately, **Ansys Maxwell** is chosen as the final software for design and simulation as the software offers more results and is more intuitive for the project. Various coils are designed with different ratios and different numbers of turns before a final design is chosen. Simultaneously, the results of these simulations are compared with the best design chosen. The results represent the self-inductance, mutual inductance, and magnetic fields of the coils.

Once the chosen design is finalised, the coils are physically built. This is done by hand using the chosen material and super glue. Next, these coils are tested by connecting them to a voltage source and extracting the data from an oscilloscope.

3.5 Method for Filters

The method for designing filters is also an iterative one. The literature review covers active filters, RC passive filters, and LRC microwave filters. All types of filters are designed and simulated on LT Spice, and the parameters and element values are varied until the desired response is found. The final filter circuits are physically built on a breadboard and tested using a signal generator to provide an input, and an oscilloscope to observe the output.

3.6 Method for Rectifiers and regulators

The method for the design of the rectifiers follows the theory from the literature review directly. This too is tested in LT Spice before the physical diodes are sourced and implemented in hardware. The regulators are chosen based on the requirements and the quality factor. The results of this are given both as LT Spice graphs and signals from the oscilloscopes in the lab.

3.7 Testing

The circuits and coupling are all tested individually as described in the various methods above. Once, the individual testing is completed, the entire system will be tested. This will be done in LT spice where the transformer in Ansys Maxwell will be mimicked to complete the system. Based on the results of the tests, changes may be made before hardware implementation. Finally, the hardware is tested. A car battery will be simulated using a voltage source, and the rest of the is connected to this. The result of this is then displayed.

4. Design of the systems

4.1 Background to the design and current implementation

Trailers lights and caravan lights are currently connected to the car's electrical system via means of a cable, with one end that attaches to a socket on the car and the other end attaching to a socket on the trailer. These sockets are shown in Figure 4.1. The goal of this project is to replace those sockets with a magnetic coupler connection. The electrical system of the car has one source, namely a 12V battery. The DC connection the cable provides is sufficient to power the trailer's electrical system. As seen in the figures below, these sockets can easily be corrupted and corroded by environmental elements.

Figure 4.1 Socket on the vehicle-side (on the left) and socket on the trailer (on the right)

Both connectors have 7 pins, differentiating signals, shown in Figure 4.2 below. The signals are for the indicators, brake lights, fog lights, backlights, and the earth terminal. The configuration is shown in Figure 4.2 labelling each pin.

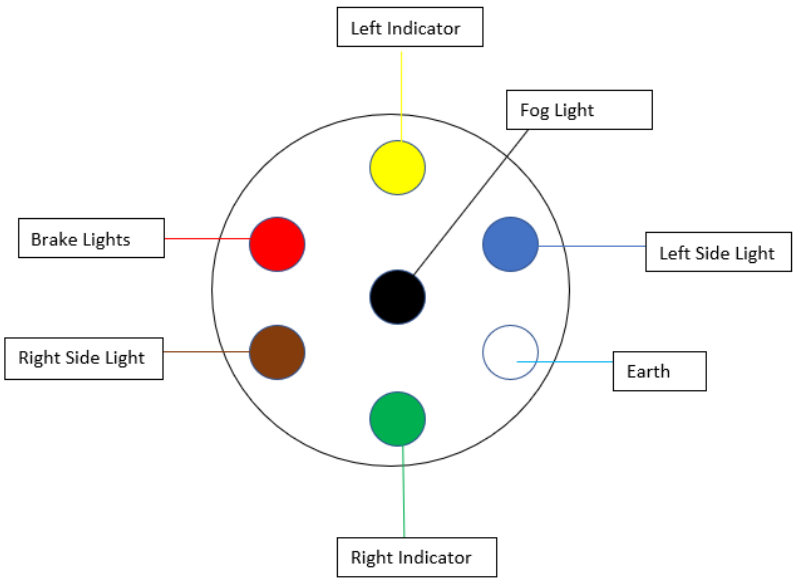

Figure 4.2 7-pin connector layout

It is evident that from the single 12V source, various signals are to be produced. This is achieved by designing and building at least five oscillators. One for the brake lights, two for the respective indicators, one for the backlights, and one for the fog lights. This means five amplifiers, five filters, and five rectifiers need to be designed.

The output of the system should be able to power the incandescent lamps of the trailer. The operating voltage of these lamps is 12V DC, with a power rating of 28W. An example of these lights is shown in Figure 4.3. This product is found from an online shopping website *Takealot.com* (10/26/2021).

Figure 4.3 Trailer lamps from Takealot.com[31]

Basic user requirements and system requirements are shown in Table 4.1. These requirements are general as no specific ones are required at this stage.

Requirement	**Explanation**
Safe	Circuitry needs to be safe and have no adverse effects.
Aesthetically pleasing	As the final build needs to be placed on cars, it should not be too large or unsightly.
Cost-effective	For the device to be worth it, it should not be too much more expensive than current implementations.
Voltage	The lamps are rated st 12V DC
Power	The lamps draw 28W

Table 4.1 User and System Requirements

The V- diagram in Figure 4.4, provides some insight into the design and testing of the project. This is closely followed. Furthermore, an OPM diagram is provided in Figure 4.5 highlighting the interfacing of the system.

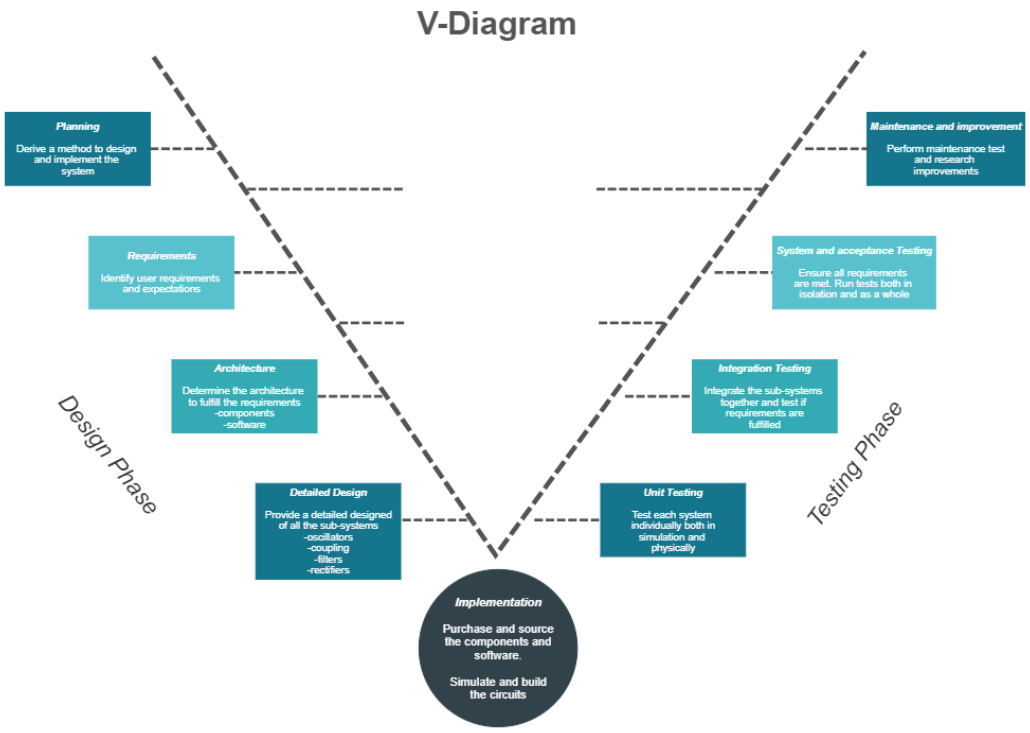

Figure 4.4 V-Diagram

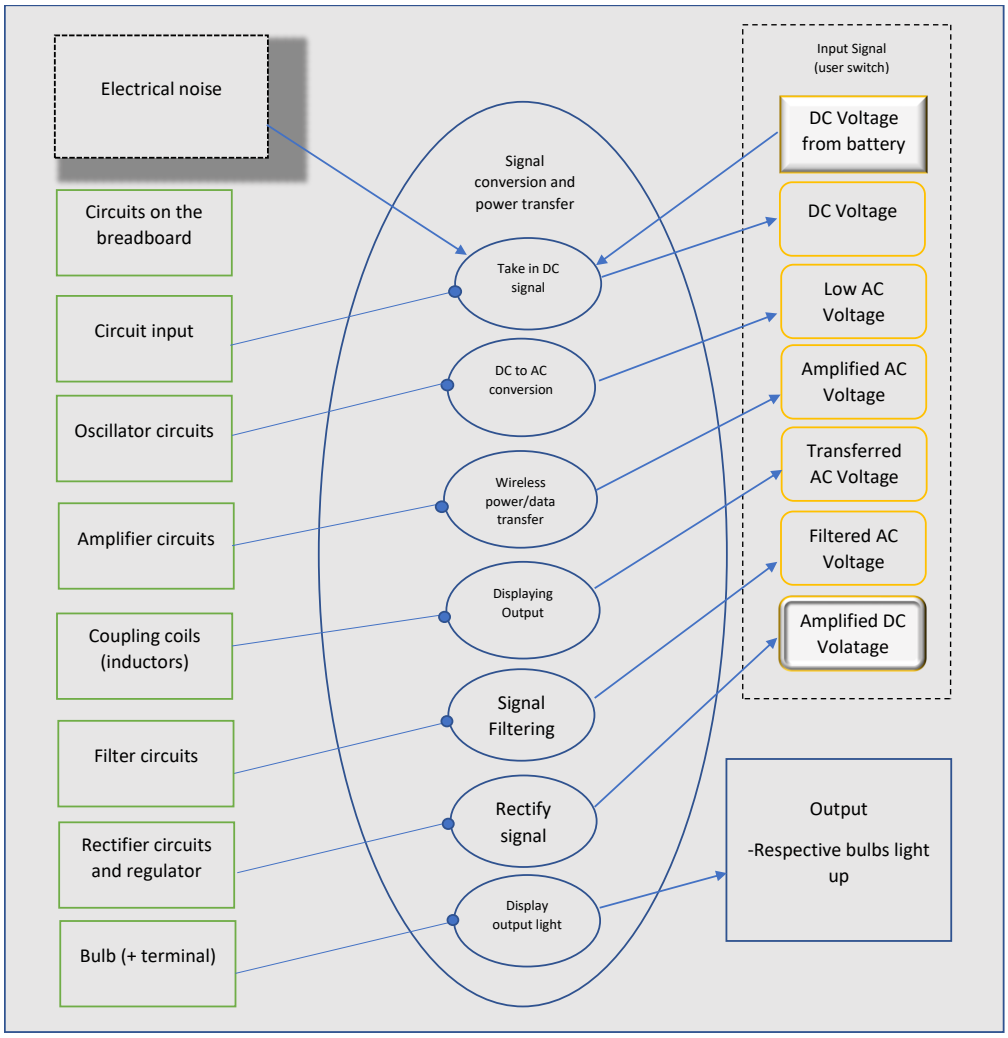

Figure 4.5 OPM

A visual representation of how the system is expected to work is shown in Figure4.6. The signals, controlled by a user switch are first fed through their respective oscillator. The frequency signal and output bulb are chosen arbitrarily as there are no complications with efficient filters. The signal then gets amplified before being transferred across the coils. Next, the signal is filtered and then rectified. Lastly, this output DC voltage is fed into the respective lights. As seen, the 5 different signals are distinct from one another (based on frequency).

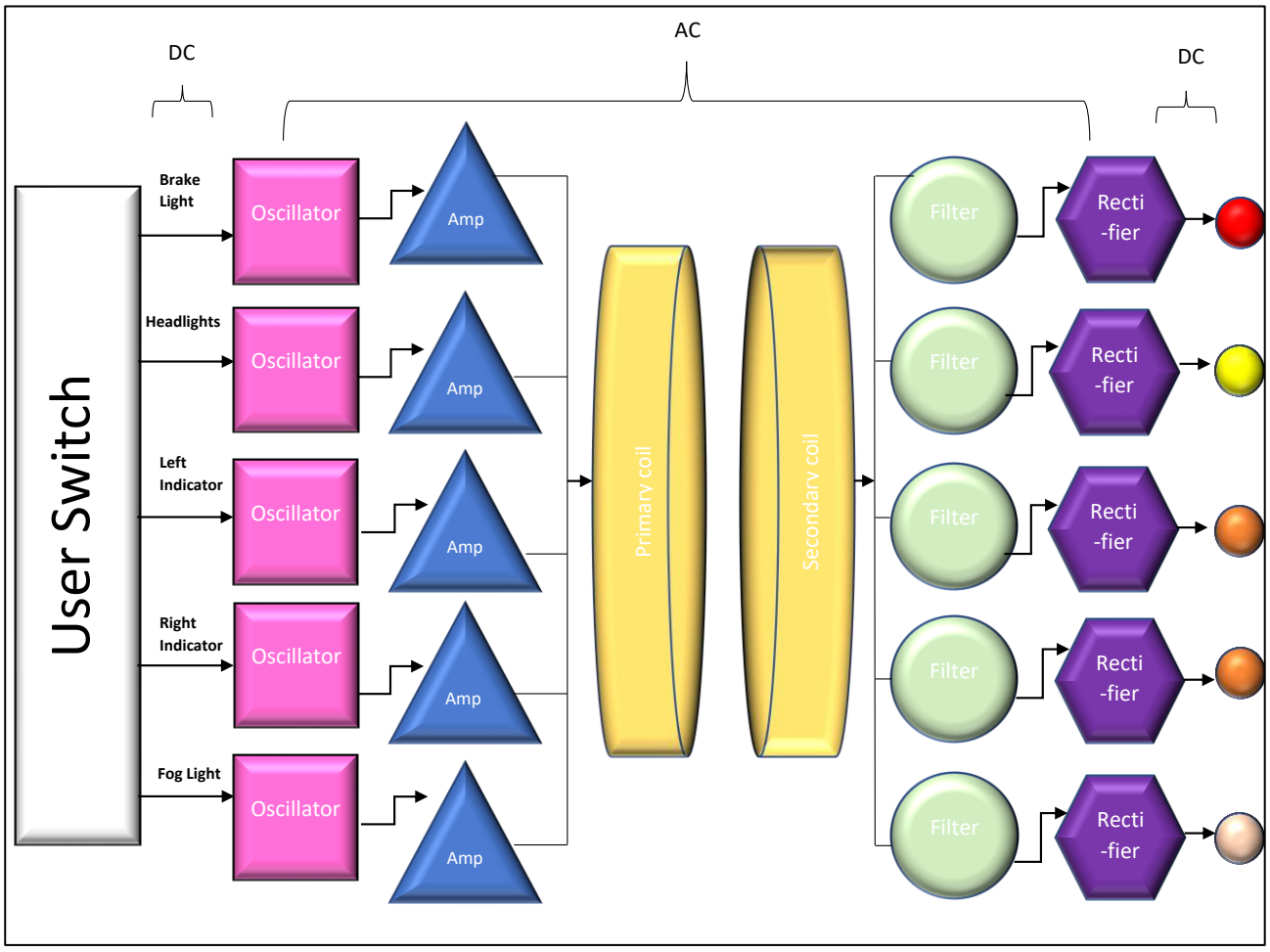

Figure 4.6 System

4.2 Design of the Oscillators

The first circuits that are to be designed are the oscillators. As previously mentioned the system will require 5 signals therefore 5 oscillators are designed. To reinforce the reason for designing oscillators, a quick recap of the theory is given. The car battery supplies a 12V DC voltage. For magnetic induction to take place an AC voltage is required at specific frequencies.

There are many ways to design and build oscillators, using switching circuits and microcontrollers. The Colpitts oscillator is the chosen oscillator as the BJT, resistors, capacitors, and inductors are the least time-consuming to source as well as the most cost-efficient. It does take more time to build and design, however, the trade-off is worth it.

Upon physical testing it was discovered, that the coupling worked best at frequencies between 2MHz and 6MHz. Therefore, the oscillators are designed to meet frequencies between this range. Equation 2.1 is used to achieve the desired frequencies.

$$f_r \cong \frac{1}{2\pi\sqrt{LC_T}} \tag{2.1}$$

4.2.1 Simulation Design

Figure 4.7 shows the circuit of the 2MHz oscillator designed in LT spice. All the Oscillators have the same design apart from the capacitors in the tank circuit, which is changed to suit the required frequency. Figure 4.8 shows the tank circuit in isolation for clarity.

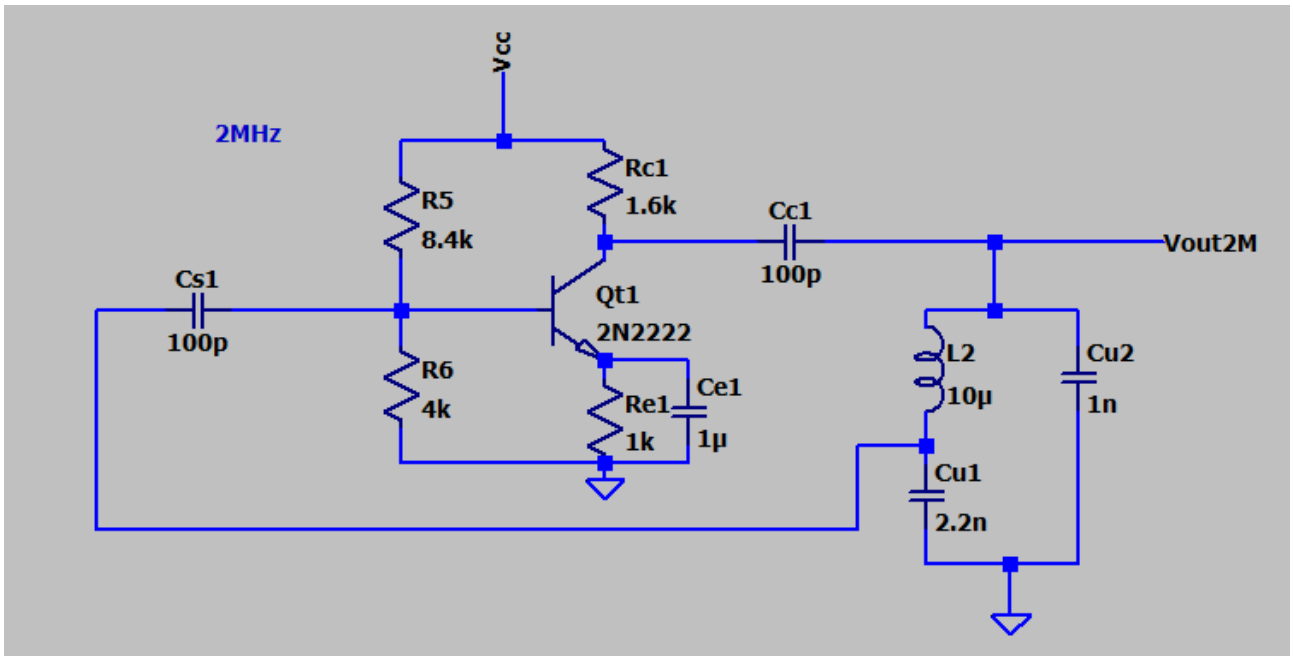

Figure 4.7 Colpitts Oscillator design in LT Spice

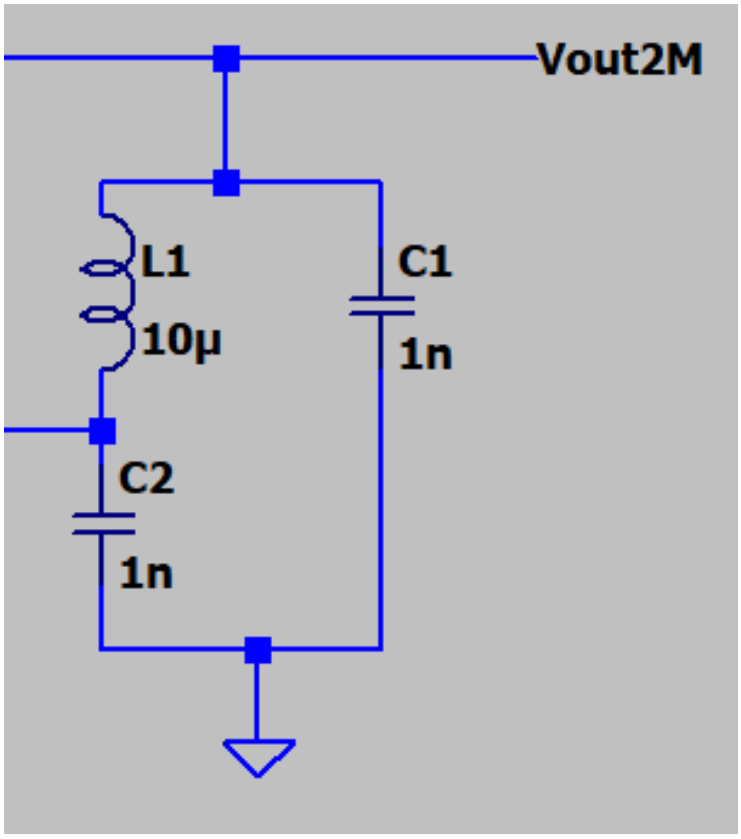

Figure 4.8 Tank Circuit design in LT Spice

The 5 different oscillators are designed to meet various frequencies by setting C1, C2, and L1 in the tank circuit. Table 4.2 shows the values for these components for the required frequencies. These are the only values that affect the frequency of oscillation. It is important to note that the theoretical frequency according to Equation 2.1 and the simulated frequencies is substantially different. This is further discussed in the results. Furthermore, the capacitors used are ones readily available in the University of Cape Town labs and therefore designs are tweaked for this.

Theoretical Frequency(MHz)	Desired Frequency(MHz)	C1 (F)	C2 (F)	C_{total} (F)	L1 (H)
1.92	2	1n	2.2	0.5n	10µ
3.18	3	500p	500p	250p	10µ
4.38	4	330p	220p	165p	10µ
6.06	5	100p	220p	68.75p	10µ
6.98	6	220p	68p	51.94p	10µ

Table 4.2 Capacitor and Inductor values for different frequencies

Calculations of the resistors and coupling capacitors:

First, the values of the resistors to bias the BJT are calculated to be used as an amplifier. Biasing the BJT allows for it to function at the correct operating point for it to output a voltage. Various methods can be used to bias the BJT such as a voltage divider, fixed bias, emitter bias, and self-bias. The first is implemented and is shown in Figure 4.9. The decision is justified as this method allows for good stability, the amplitude is independent of changing β (gain) and resistor value. Furthermore, there is easy control regarding biasing currents. [32]

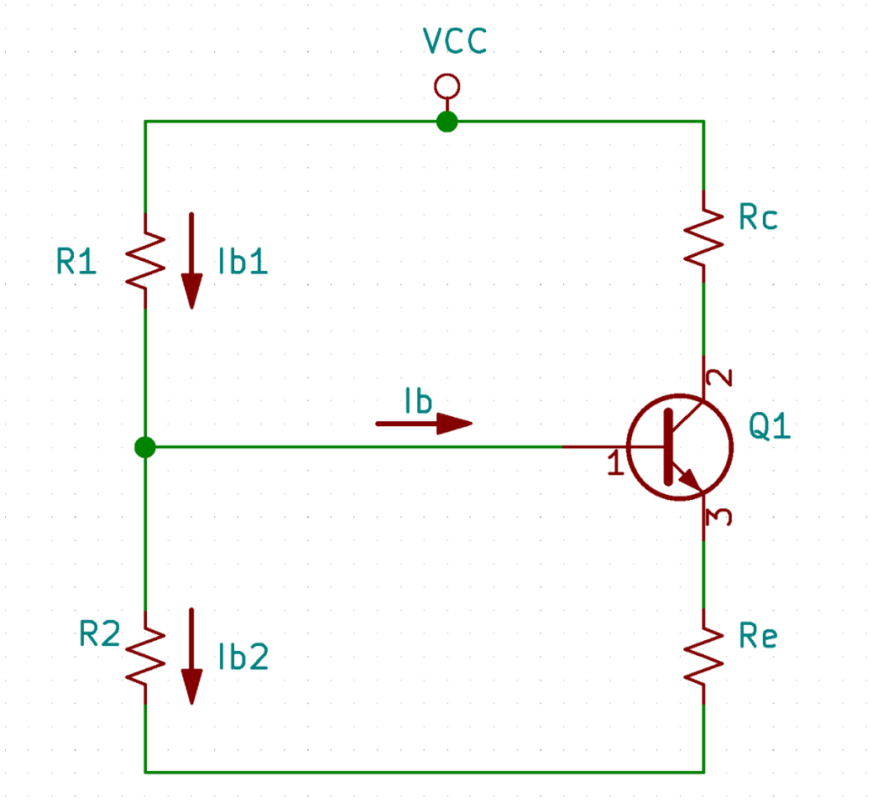

Figure 4.9 Voltage divider biasing of BJT circuit done on KiCad

Figure 4.10 depicts what the optimal operating point (Q) is. It is found in the middle of the active region. The biasing is done to achieve this with the rules implemented. The circuited design uses an NPN BC548A BJT, as this is similar to the literature that was found and reviewed, which produced satisfactory results.

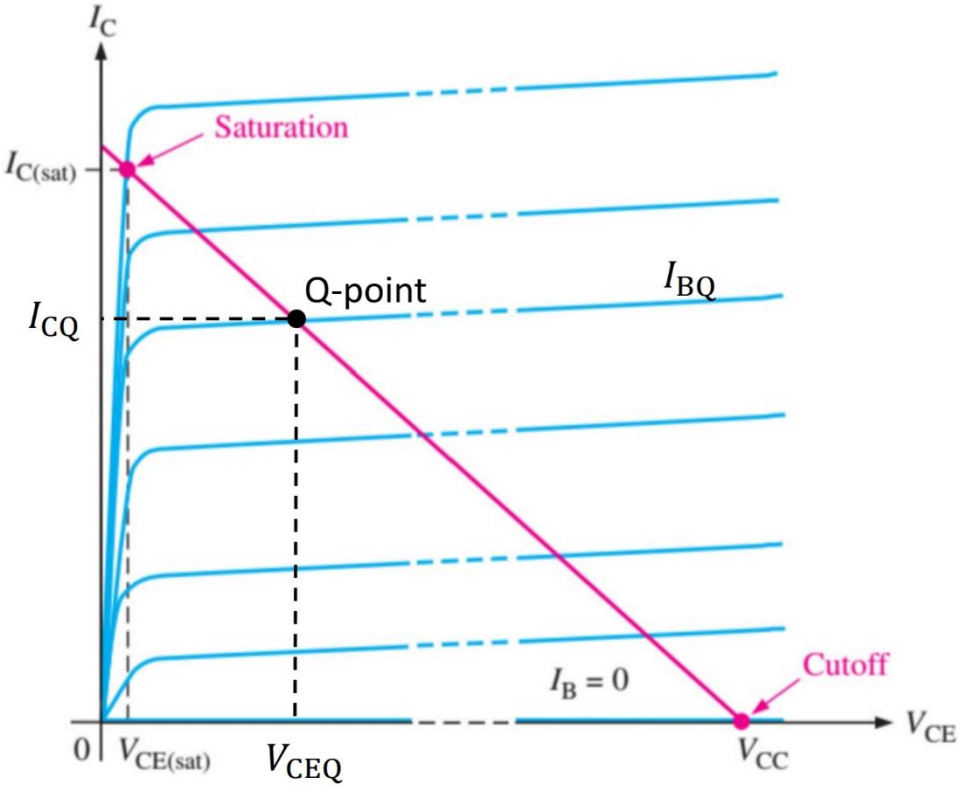

Figure 4.10 DC load-line and Operating point (Q) [33]

Table 4.3 is created using the specifications from the datasheet. This table highlights the various terminal voltages as well as the gain values. The calculations follow the literature from the University of Diyala [32].

Specification	Value
V_{BE}	0.65V
V_{CE}	0.5V
β_{min}	110
β_{max}	220
$V_{CE(sat)}$	0.6
f_T	100Mhz
β_{avg}	156

Table 4.3 Datasheet specifications

An assumption for R_2 is made; a commonly accepted one for circuit design; is shown in Equation 4.1. [32]

$$R_2 \leq \frac{\beta R_e}{10} \tag{4.1}$$

Letting $R_E = 1k\Omega$:

$$R_2 \leq \frac{156 * 1000}{10} \leq 15.6k\Omega$$

R_2 is set to 4kΩ to satisfy this.

From Figure 4.10, Equation 4.2 is derived.

$$I_{b1} - I_{b2} = I_b \tag{4.2}$$

Another accepted assumption is made for the currents I_{b1} and I_b shown in Equation 4.3. [32]

$$I_{b1} > 10I_b \tag{4.3}$$

A known condition for the BC548A is shown in Equation 4.4 once more relating I_{b1} and I_b.

$$I_{b1} = 48I_b \tag{4.4}$$

From Equations 4.3 and 4.4, Equations 4.5 and 4.6 are derived.

$$48I_b - I_{b2} = I_b \tag{4.5}$$

$$I_{b2} = \frac{(V_{BE} + (\beta + 1)\, I_b R_e)}{R_2} \tag{4.6}$$

Using Table 4.3, V_{BE} = 0.65V.

$$\therefore I_{b2} = \frac{(0.65 + (156+1)\, I_b * 1k)}{R_2}$$

By subbing (4.7) into (4.5):

$$I_b = 0.0204mA$$
$$I_{b1} = 48I_b = 0.0979mA$$
$$I_c \approx \beta I_b \approx 3.2mA$$

Using Kirchoff's Voltage Law in Figure 4.7:

$$R_1 = \frac{V_{CC} - V_{BE} - (\beta + 1)\, I_b R_e}{I_{b1}}$$
$$= \frac{8.15}{0.9792mA}$$

$$R_1 = 8.4k\Omega$$

Now, using Kirchoff's Voltage Law in Figure 4.9:

$$V_{CE} = V_{CC} - I_c(R_c + R_e)$$
$$0.5 = 12 - 3.2mA(R_c + 1000)$$
$$R_{c=}1.67\ k\Omega$$

The capacitors $C_c\ and\ C_s$ are used for DC coupling. Changing C_c alters the peak voltage of the signal whereas changing C_s alters the time for oscillations to begin. Setting both of these capacitors to 100pF yields sufficient results. This is determined using many simulations and trials. Further research needs to take place but the results may be accepted at this stage.

The above calculations are designed for a BC458A transistor, however, due to a lack of availability both on LT Spice and physically, it is substituted with the more common NPN 2N2222 BJT. This substitution is valid as the specifications are similar, yielding similar outcomes, as is seen in the results.

4.2.2 Hardware Design

The NPN 2N2222 has 3 pins, namely the emitter, the base, and the collector. This is shown in Figure 4.11. The transistor is fit into the circuit depicted in Figure 4.7, with the pins of the transistor being connected according to the circuit diagram.

PIN	DESCRIPTION
1	emitter
2	base
3	collector, connected to case

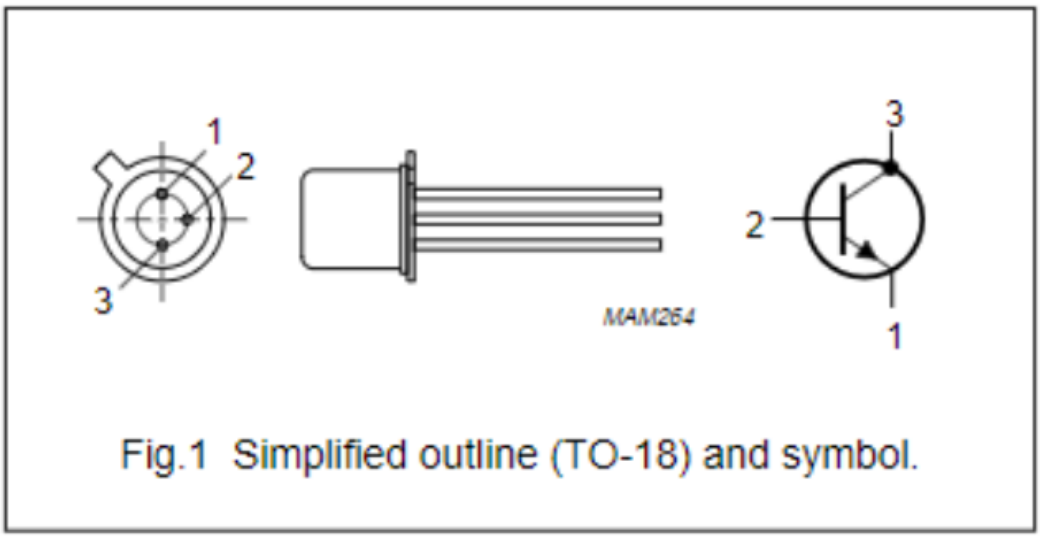

Figure 4.11 Pin Diagram of 2N2222 [34]

The rest of the physical components are connected around the transistor according to Figure 4.7. The final result of the physically built circuit is shown in Figure 4.12. The circuit is implemented on a breadboard with the source coming from a DC voltage power supply. The output for testing is subsequently connected to an oscilloscope. These results are shown later in the report (results section).

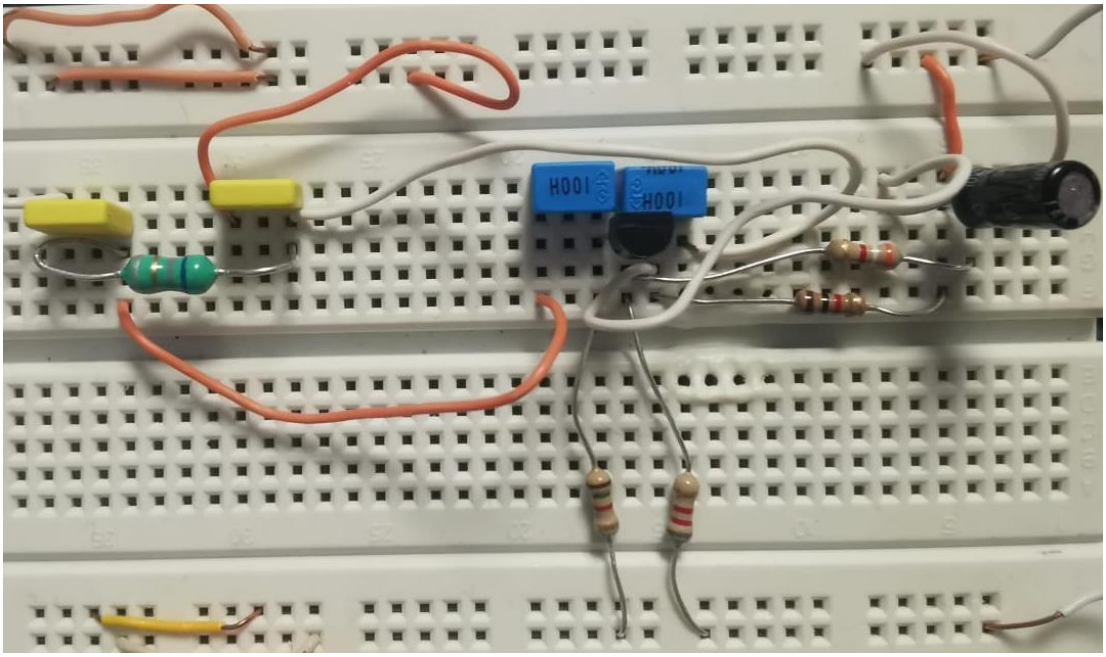

Figure 4.12 Oscillator Circuit on a breadboard

4.3 Design of the Amplifiers

A non-inverting amplifier is required to be designed and constructed for the project. With the Oscillators in Chapter 5 producing signals that have too low a DC voltage, this is necessary. It is important to note that with more research done on the oscillators being done, the amplifiers could be removed. This means that the correct amplification would have to be done in the oscillator stage. The non-inverting amplifier amplifies the low signal from the Oscillator without changing its phase.
The Design of the amplifier takes place by simply calculating the resistor ratio, to satisfy a gain value given by Equation 2.3.

Using Equation 2.3 :

$$A_{(cl)} = 1 + \frac{R_f}{R_i} \tag{2.3}$$

Table 4.4 is created to depict resistor ratios for different gains. The gains needed can only be determined after getting the results of the oscillators. Therefore the output voltage of the respective oscillators is also shown in the table. Furthermore, the actual frequencies from the simulations are shown as well. The output voltages and frequencies are more explicitly shown in the Results of the oscillators. The gain required is calculated by determining the value needed to amplify the voltage back up to approximately 12V. Furthermore, the resistors have standard values which result in an approximation of the required gain. Due to op-amp saturation at the rail voltages (12V) having a gain which higher than required, is not an issue.

Theoretical Oscillator Frequency (MHz)	**Actual Oscillator Frequency (MHz)**	**The output voltage of the Oscillator (V)**	**Gain Required**	$\boldsymbol{R_f}$ **(Ω)**	$\boldsymbol{R_i}$ **(Ω)**
1.92	1.93	4.15	2.9	1k	2k
3.18	3.1	4.5	2.7	1k	1.8k
4.38	4.06	6.14	1.96	1k	1k
6.06	5.17	2.75	4.37	1k	3.6k
6.98	6.1	7.45	1.62	1k	750

Table 4.4 Resistor Values for different Gains

4.3.1 Software Design

The operational amplifier is designed in LT Spice for simulation purposes. Here, the “Universal op-amp” is used (Avol=1Meg GBW=10Meg Slew=100Meg), before looking for available op-amps for the lab. This is suitable for a preliminary design as it commonly translates to “real-world” op-amps. Figure 4.13 depicts how the circuit is constructed in LT Spice. This design represents a non-inverting op-amp with a gain value of 2.

As seen in Figure 4.13 the op-amp is powered by a 12V rail from the battery for Vcc(+) and 0V for Vcc(-). Rf and Ri are the resistors specifying the gain. The input signal comes from the Oscillator. The output of this circuit is fed into the coupling inductor.

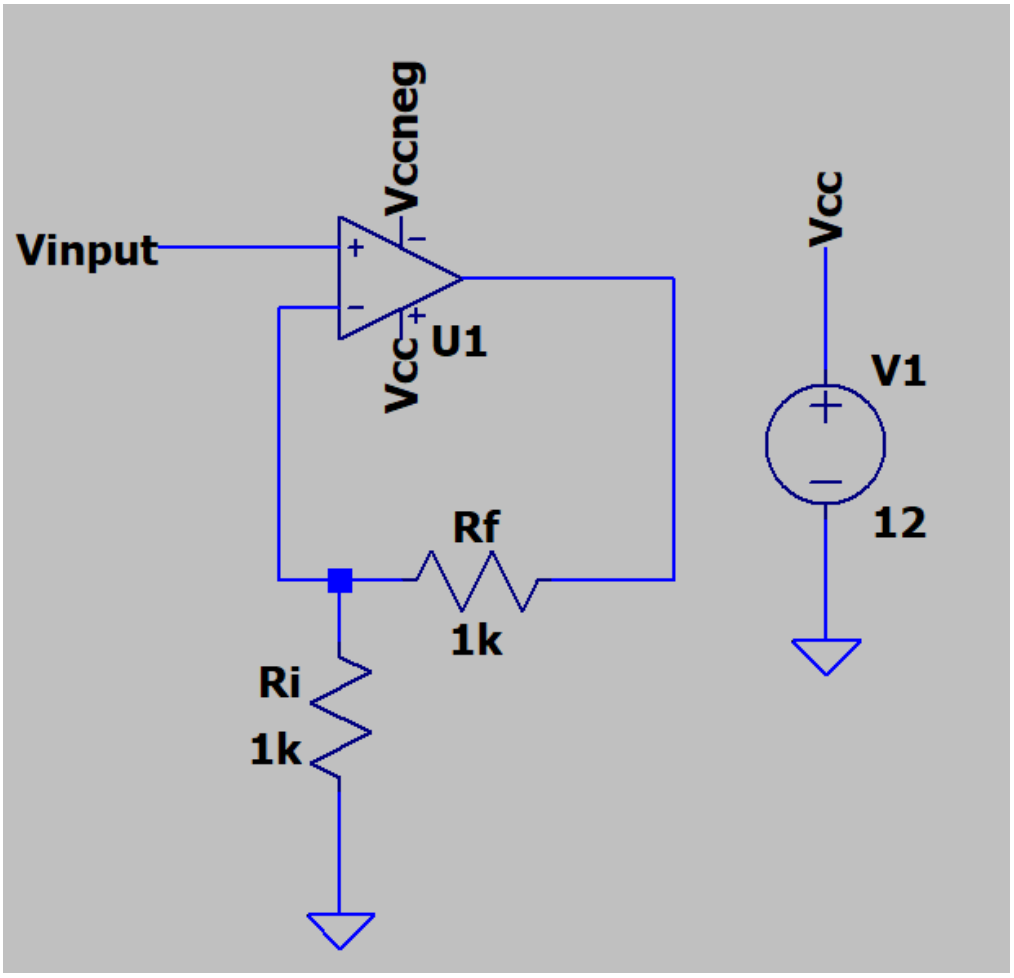

Figure 4.13 Non-inverting amplifier circuit in LT Spice

4.3.2 Hardware Design

The OP07CP the op-amp, an 8-pin Integrated circuit (IC), is used to build the circuit, as the supplier stated it worked for the required frequency range (as per the datasheet). The pin-out diagram from the datasheet is shown in Figure 4.14. [35] The circuit is built by simply following the diagram in Figure 4.13. The op-amp is connected to a DC power supply for power through pins 4 and 7. An AC signal for testing is fed into the non-inverting input, pin 3, with the output pin 1 being connected to R_f. The inverting input pin 2 is connected to R_i which is subsequently connected to R_f and then grounded.

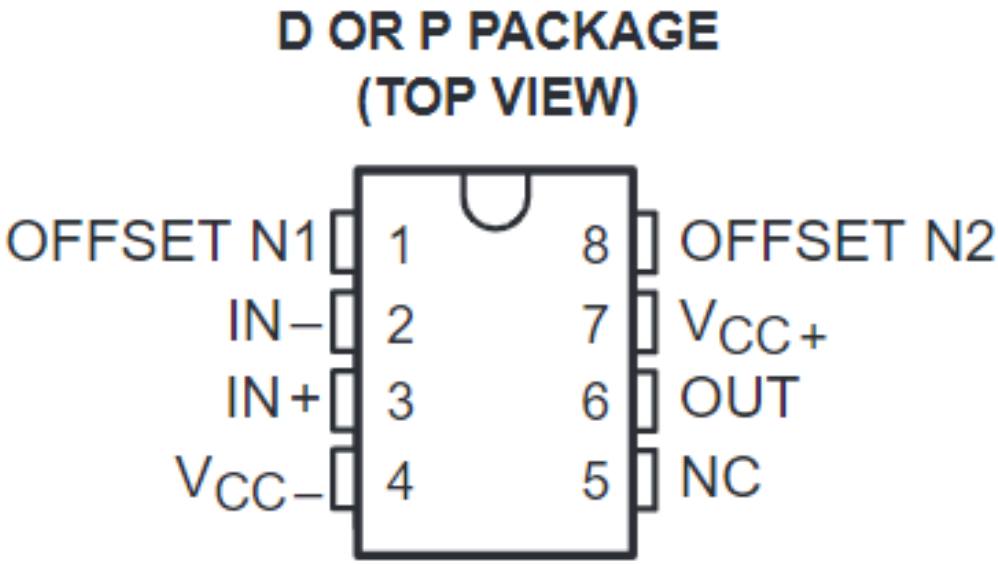

Figure 4.14 Pin-Out diagram of the LM358P [35]

Figure 4.15 is a visual representation of the circuit described, built on a breadboard using physical components. The results of this circuit are displayed later on in the report. The green/white wires are connected to the rails (Vcc), with the red wire connected to the input and the yellow being grounded. The results of this circuit are displayed later on in the report.

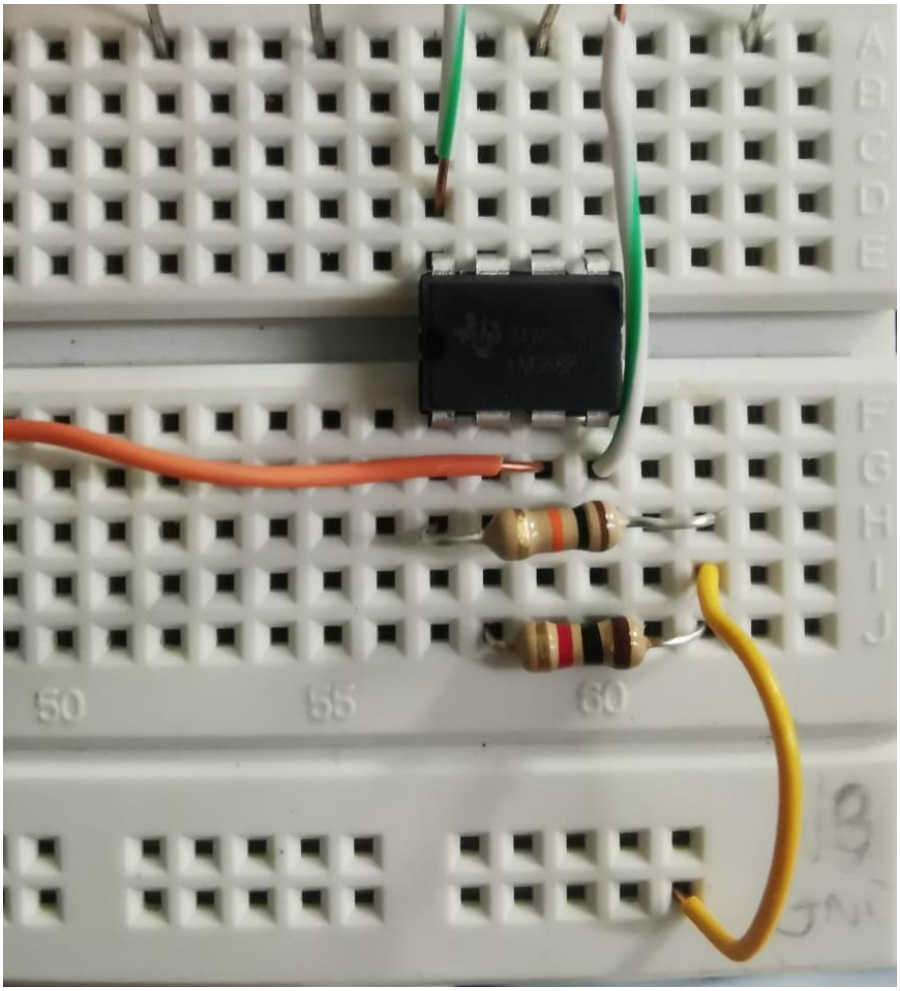

Figure 4.15 Physical Implementation of the Amplifier

4.4 Design of the Magnetic Coupling Coils

The design of the coils for the coupling is an iterative process. The dimensions, geometry, and the number of coils need to be set to maximise efficiency. Therefore many simulations are done to find the most efficient design.

Dimensions of the coils

The size of each coil is important it is the biggest part of the system, and the one that is the most difficult to reduce in size. Currently, the sockets found have a dimension of 135mm x 50m x 150 mm as seen on one such socket from takealot.com.[36] These are similar to the ones seen in Figure 4.1 earlier in the chapter. Therefore, coils similar to this size will work best and be accepted.

The geometry of the coils

Next, the type of coil is to be chosen. Most of the literature review revolves around spiral planar coils as it is well suited to this project. The reasons will be reiterated and emphasised more. Firstly, flat planar coils are less space-consuming than coils with 3 significant dimensions. With, planar coils, 1 plane (usually x-y) dominates the dimensions with the second and third being solely dependant on the thickness of the wire. This is different from helical structures which usually have relatively large dimensions in 3 planes (x-y, x-z, y-z). Moreover, as previously mentioned, the mutual inductance coefficient is much better when the turns of the coil are concentrated along the radius of the coil rather than being distributed at the outer circumference.[9]
A further justification for using a spiral planar coil is derived from a paper by Wuhan University. The authors have simulated and compared the results of three different coils. These coils are namely a helix coil, planar spiral coil, and a square helix coil. A visual representation is shown in Figure 416. Although it is concluded that helical coils offer the highest efficiency, it is still very similar to that of the spiral coil. The efficiencies are 84.65%, 78.7%, and 83% for the helix, spiral, and square coils respectively,[37]
Furthermore, the efficiency decrease verse distance was much steeper with the helix coil as opposed to the spiral coil. This is seen in Figure 4.17, which depicts the efficiency versus distance.

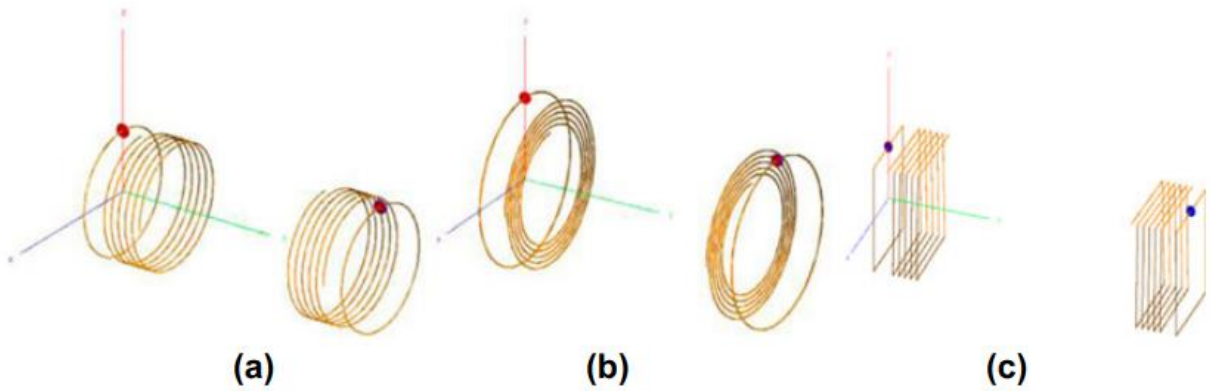

Figure 4.16 Schematics of the coils, (a) helix coil, (b) spiral coil, (c) square helix coil [37]

Specifically, the efficiencies of the WPT systems with helix coils, planar spiral coils, and square helix coils are, respectively, 84.65, 78.67, and 82.99% at the resonant frequency.
Also, reiterating the results of Figure 2.16 in Chapter 2, the coils must be aligned coaxially, as far as possible, to achieve maximum power transfer. This is seen in the final design.

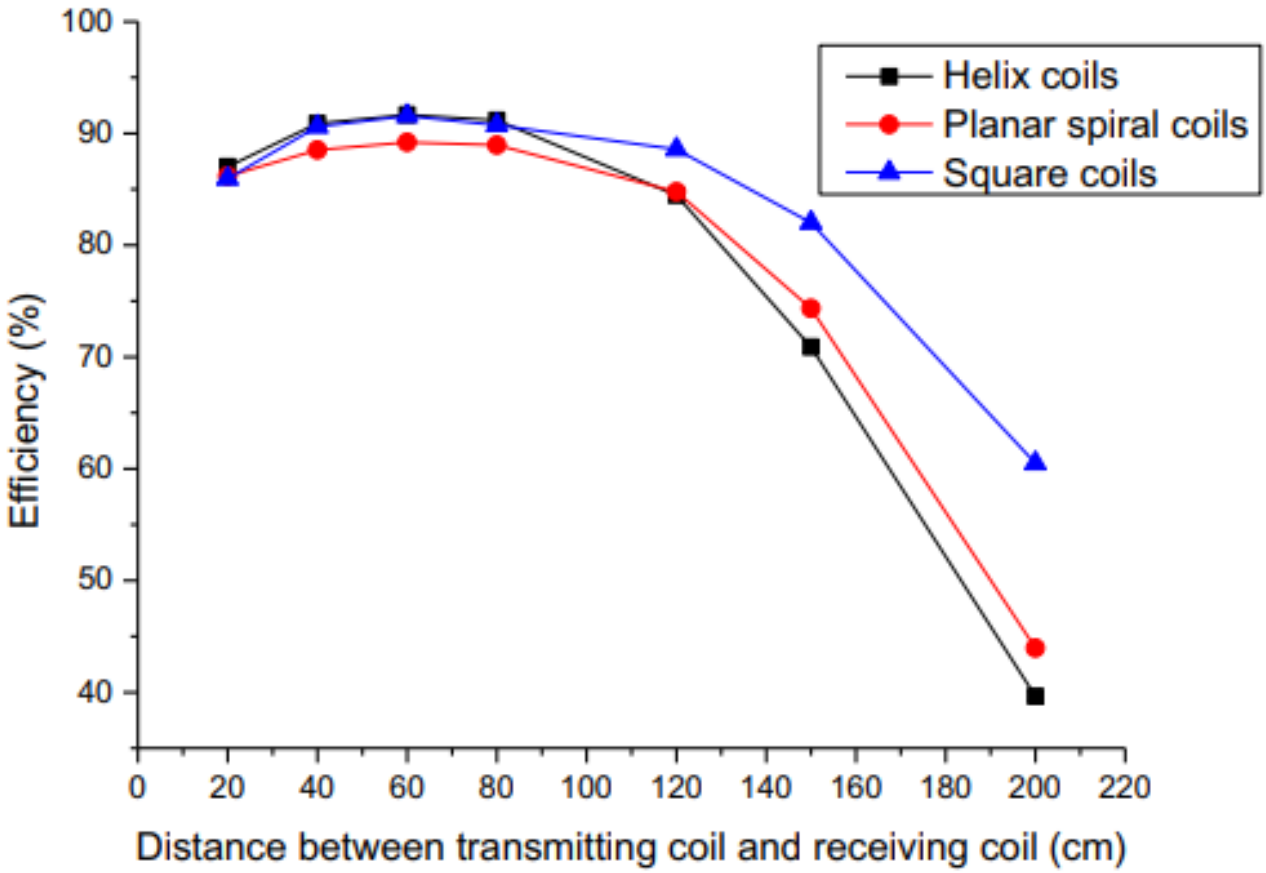

Figure 4.17 Efficiency vs distance between transmitter and receiver coils of the different structures [37]

4.4.1 Software set-up and Design

All the software designs are done in Ansys Maxwell. Ansys Maxwell is an Electromagnetic field solver that is used to simulate transformers, magnets, wireless charging coils, and more. The coils are designed using a user-defined segmented helix.

The user-defined parameters are seen in Figure 4.18. The polygon segments are set to 4 indicating a rectangular wire is used. This is done as it reduces the simulation time and computational expenses. Furthermore, this can be justified, as using a round wire with a specific diameter, has a similar enough outcome as using a rectangular wire with dimensions mimicking the former diameter. [38].

Moreover, the inner diameter of the coil is set by changing the "start helix radius". For the simulations done this set to 10mm. Next, the "RadiusChange is set to 2.05mm" indicating the space between turns. This value was chosen as it is approximately two times the diameter of the wire. The diameter of the wire is set to 1mm by changing "polygon radius". At first 0.6mm wire was used. However, due to the thicker wire being less resistant, and offering greater currents to pass through, 1mm wire is chosen. Furthermore, the cost to make this change is insignificant.

Lastly, the turns are set, according to the simulation requirements. These properties are shown in Figure 4.18, where a 20 turn coil simulation is done.

With the properties set, the changes are applied and the coil is produced by the software. This is depicted in Figure 4.19, where two coils are developed using the beforementioned properties. The second coil appears as a result of duplicating the first, using a copying tool.

Name	Value	Unit	Evaluated Value	Description
Location	syslib			
Version	1.0			
PolygonSegme...	4		4	Number of cross-sectio...
PolygonRadius	1	mm	1mm	Outer radius of cross-se..
StartHelixRadius	10	mm	10mm	Start radius from polygo..
RadiusChange	2.05	mm	2.05mm	Radius change per turn
Pitch	0	mm	0mm	Helix pitch
Turns	20		20	Number of turns
SegmentsPerT...	36		36	Number of segments p...
RightHanded	1		1	Helix direction, non-zer...

Figure 4.18 Properties menu in Ansys Maxwell

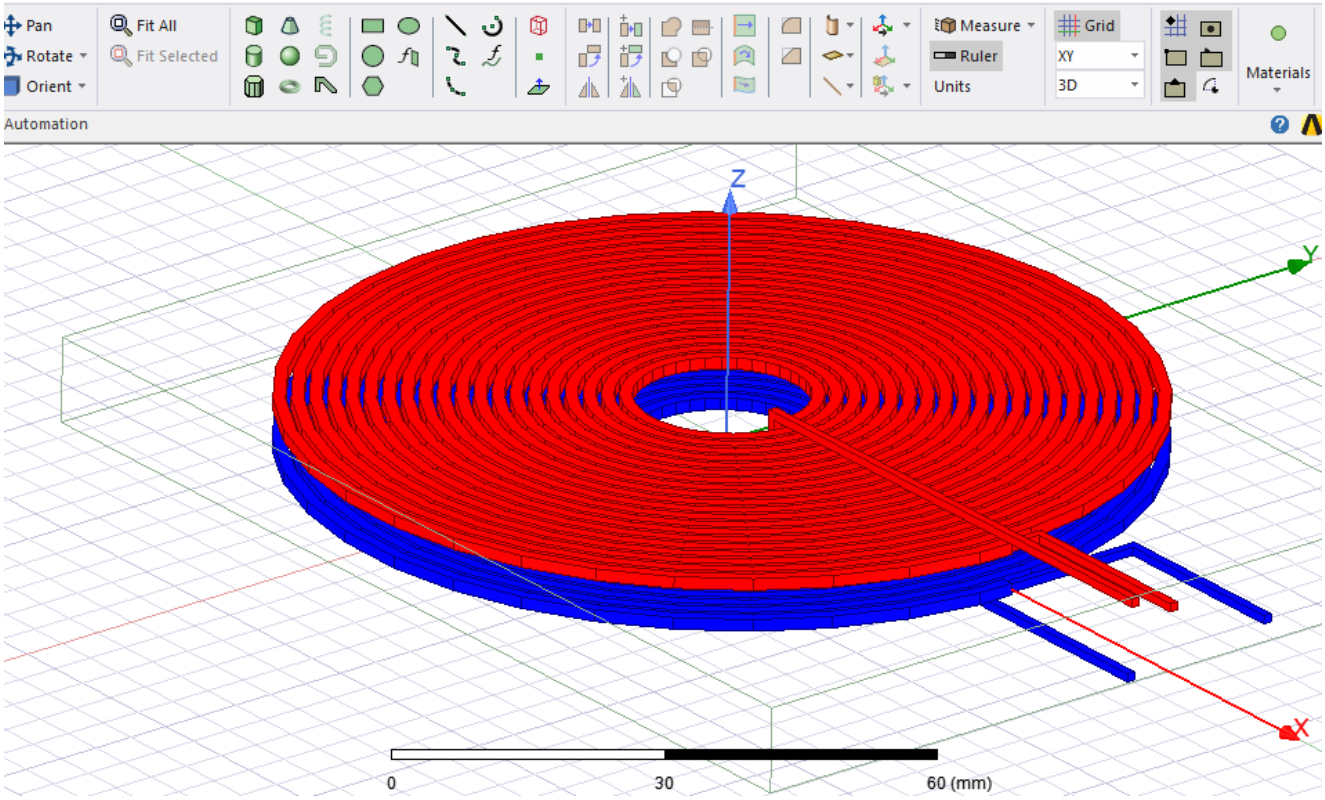

Figure 4.19 Spiral transmitter and receiver coils developed in Ansys Maxwell

The material for the coil is set to copper (relative permeability 0.999) as it is both a cheap and efficient conductor as in Figure 4.20. This justification is shown previously in Chapter 2. Furthermore, the outer boundaries are set by creating a box with a 10% padding distance away from the edge of the coils and with the coil terminal touching it on one end. This box/vacuum is set to air (relative permeability of 1).

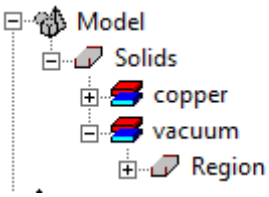

Figure 4.20 Materials of the coil and box

Each terminal is excited with 5A of current (solid) with the directions pointing either into or out of the terminal. In future iterations, 2.3A should be used to match up with the current drawn by the trailer

incandescent bulbs (power consumption of 28W). Each coil has one pair of these currents with alternate directions. This step is necessary to analyse the model. The excitations are shown in Figure 4.21.

Design List: 0_47 - Maxwell3DDesign1

Model | Boundaries | Excitations | Parameters | Mesh Operations | Analysis Setup

Name	Type	Description
Current1	Current	Type = Current, Current = 5A, IsSolid = Solid, Direction = Point into terminal
Current2	Current	Type = Current, Current = 5A, IsSolid = Solid, Direction = Point out of terminal
Current3	Current	Type = Current, Current = 5A, IsSolid = Solid, Direction = Point into terminal
Current4	Current	Type = Current, Current = 5A, IsSolid = Solid, Direction = Point out of terminal

Figure 4.21 Current excitations of the coils in Ansys Maxwell

Lastly, the mesh and convergences are set up. Depicted in Figure 4.22, it is shown that the maximum element length is set to 1mm and the maximum number of additional elements is set to 1000. Moreover, regarding the set-up, a maximum number of 10 passes are initialised with a refinement per pass of 30%. This is clear from Figure 4.23. Furthermore, the simulation is set to stop upon convergence.

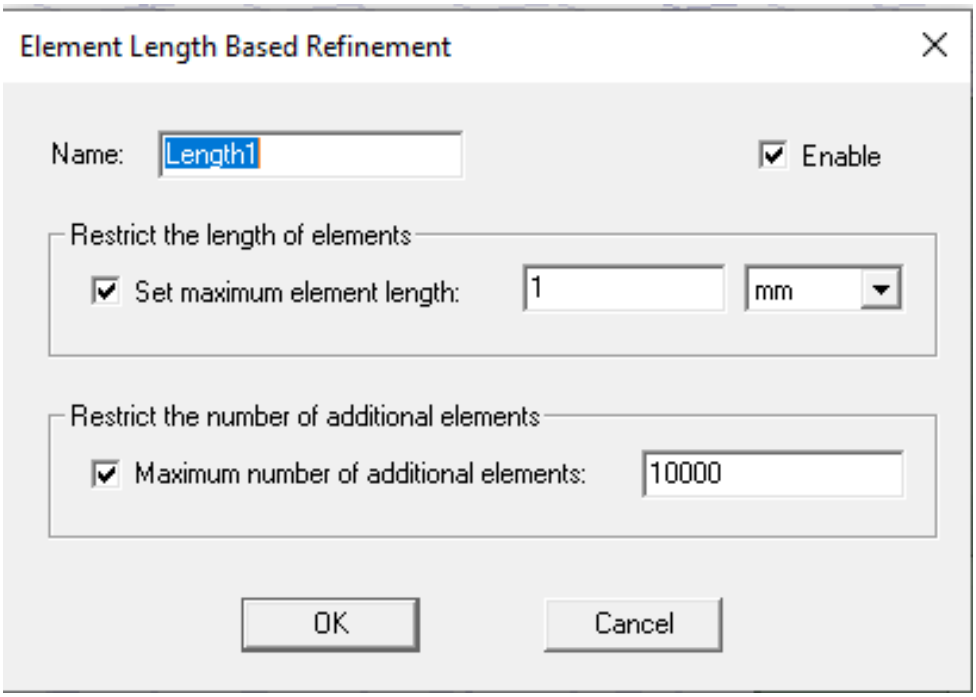

Figure 4.22 Mesh definition in Ansys Maxwell

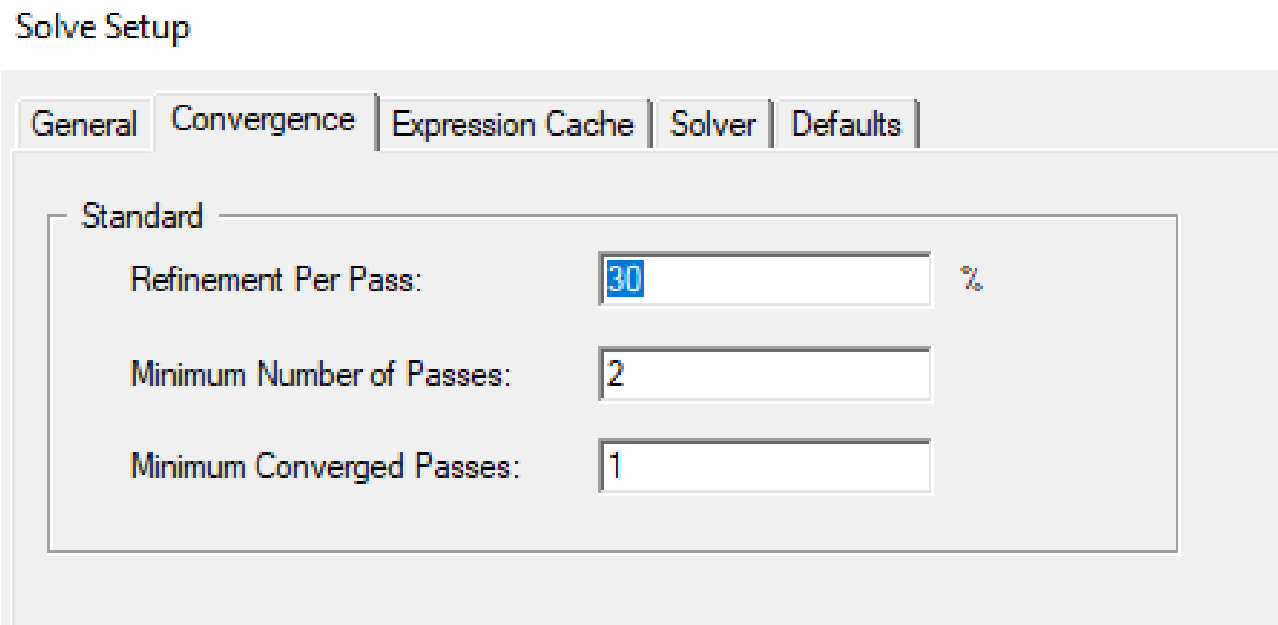

Figure 4.23 Refinement of passes in Ansys Maxwell

Three pairs of coils (transmitter and receiver) are simulated according to these conditions. Table 4.5 provides a detailed look into this. The outer diameter is calculated using a program created in Matlab. The highlighted row is chosen for the final design with reasons discussed later.

Simulation	Transmitter Turns	Receiver Turns	Inner diameter (mm)	Outer diameter (mm)
1	10	10	10	71
2	20	20	10	132
3	40	40	10	254

Table 4.5 Different coils simulated

With the designs completed and simulated in Ansys Maxwell, the coils are transferred to LT Spice with the simulated parameters. A simulation of one such example is shown in Figure 4.24. Here, the Primary inductor on the left is connected to a 12V Sinusoidal voltage as this is what is expected from the previous stage of the system, the amplifier. For the example below the frequency is set to 1KHz which is changed according to results achieved from the physical implementation. As seen, the mutual inductance coupling factor (K) is set in LT Spice. Lastly, the secondary coil is connected to the load to imitate a lamp. This load can be changed to more accurately test the incandescent bulb (Power consumption=28W).

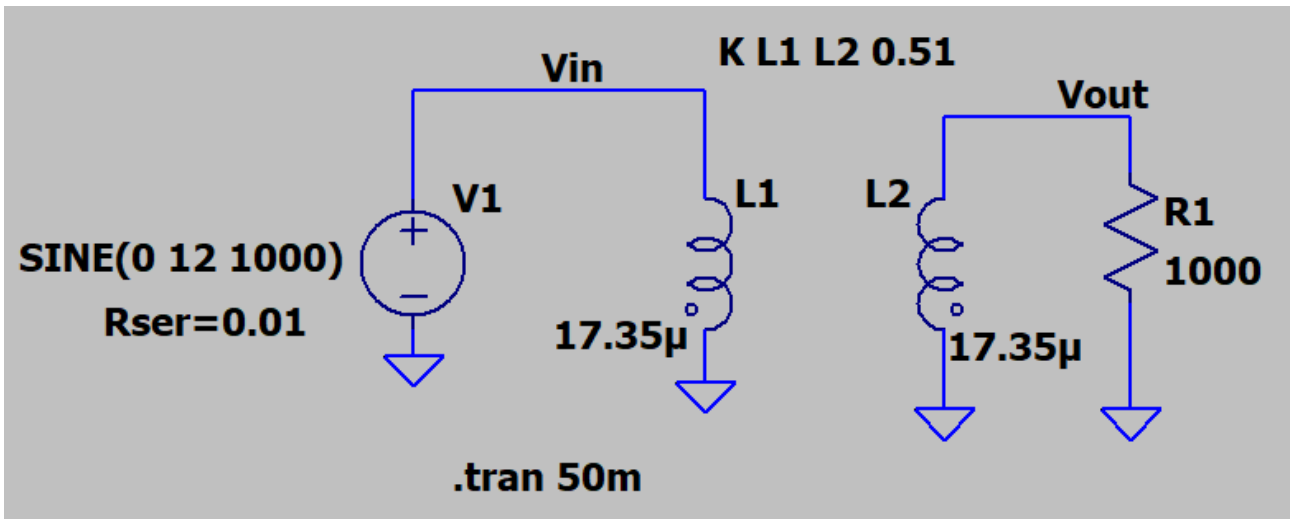

Figure 4.24 LT spice Simulation of the coils

4.4.2 Hardware Design

The physical loops take many iterations to build. Figure 4.25 shows some of the earlier unsuccessful builds. As is shown, both 0.6mm diameter wire and 1mm are tested. These loops are built by hand. A big problem is that coils tend to spiral outwards and upwards, deviating a lot from the simulated coils. The type of wire that is used is a pliable,single-core, copper wire. The copper wire has thin insulation which is scraped off with a knife. This was provided by the University of Cape town without any cost. The wire is priced at R117 per 11m at RS Components (as of 11/1/2021).[39]

Figure 4.25 Early iteration of the physical coil

By the third iteration, the coils are accurate and similar enough to the simulated coils. Q-Bond and clear glue is used to ensure that the loops are kept in place and do not spiral unacceptably. The first desired radius is achieved by using 3 washers which are attached. This forms a wheel that allows the first loop to be created. The subsequent turns were manually created which requires a lot of time and strength. Although Q-Bond is a quick-setting adhesive, a different clear adhesive is used in conjunction with this. The clear adhesive sets overnight. The final built coil, along with the materials used are displayed in Figure 4.26. The coils built each contained 20 turns. As will be shown, in the results these coils provide satisfactory results in simulation, therefore their construction is justified. Also, they are less space-consuming than the 40 turn coils.

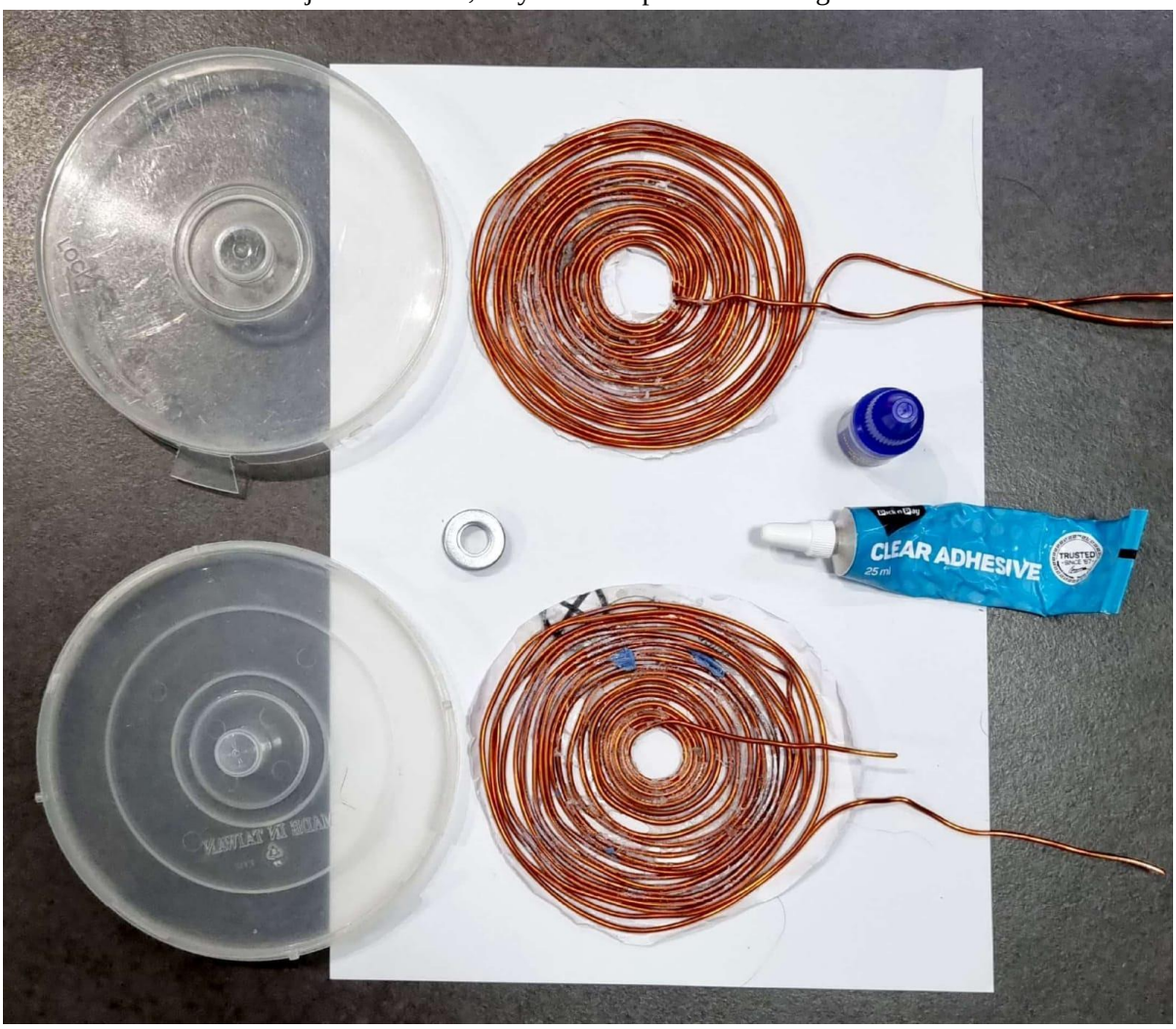

Figure 4.26 Final coils (20 turns) built with the materials used

The dimensions of the coil are as follows. It has an inner radius of 10mm and an outer radius of 110mm. This is similar to the theoretical dimensions. More importantly, it is similar to the currently implemented sockets which were discussed earlier. The outer radius is calculated before building the coils using a Matlab program created. However, having a coil already built, the dimensions are simply measured. The amount of material (copper wire) used is also calculated using a Matlab program. A code snippet is shown in Figure 4.27.

Editor - C:\Users\aekha\OneDrive\Documents\MATLAB\Untitled3.m

Untitled3.m

```
sum=0;
turns=20;
inner_R=10;
wire_thickness=1.025;

for v = 0:turns
    length = 2*pi*(10+wire_thickness*v);
   disp(length)
   sum=sum+length;
end
```

Figure 4.27 Matlab function to determine the length of the wire

3D Printing

A 3-printed housing is designed for the coils as seen in Figure 4.28. The design is done in Tinkercad and with the dimensions indicated by the figure. The housing consists of two disk-like structures that fit into each other. Moreover, the housing has holes on the edges for the terminals to be fed through. The final printed design is shown in Figure 4.29.

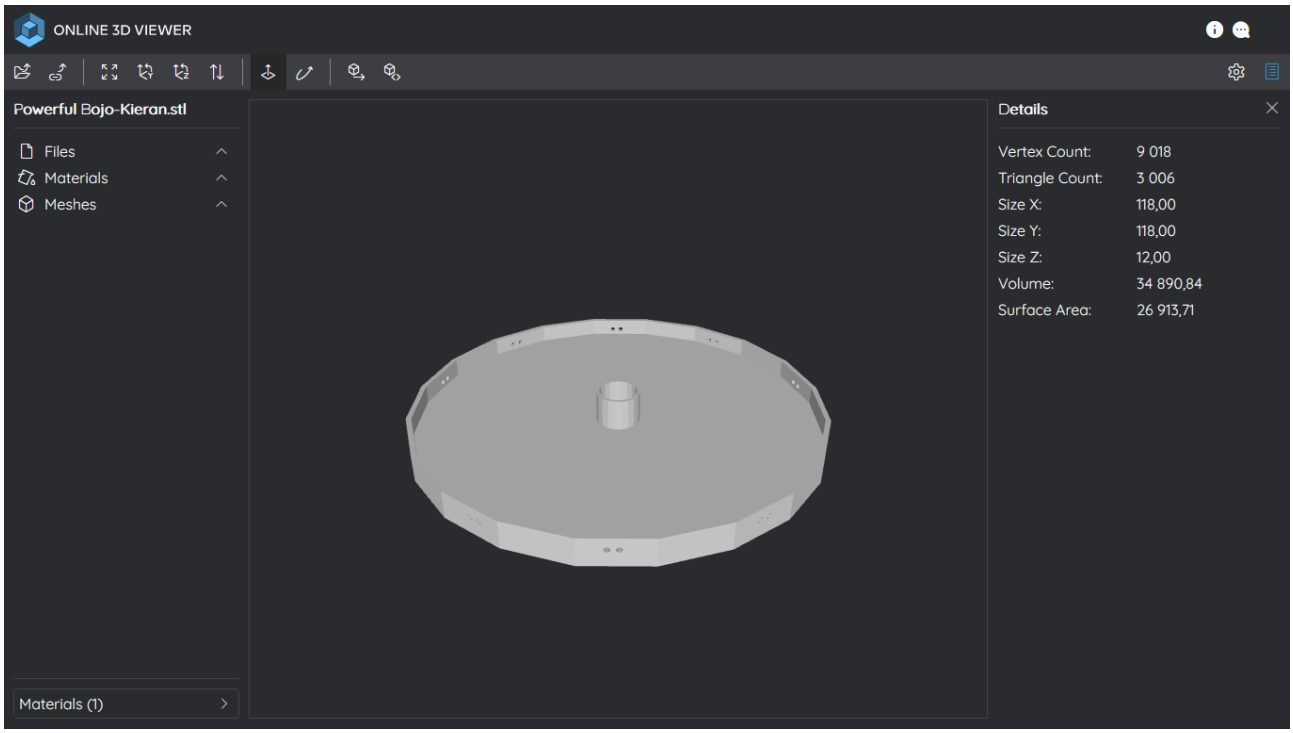

Figure 4.28 Design

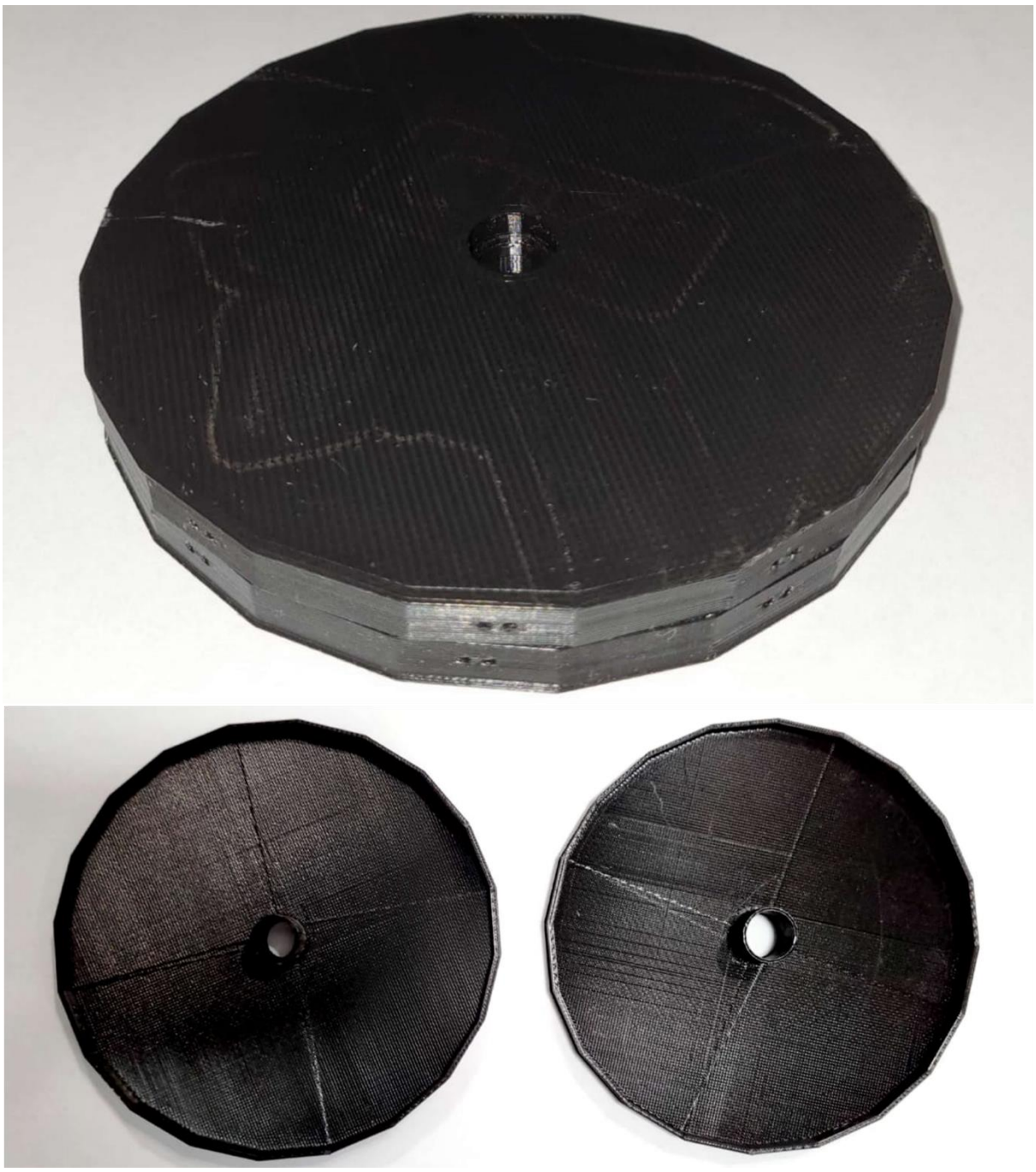

Figure 4.29 3-D printed housing

4.5 Design of the Filters

Five bandpass filters are designed, and each is required to isolate the frequency of oscillation for each of the five oscillators. To fulfill its purpose, the filter needs to have a short bandwidth that isolates the oscillation frequency assigned to it, as well as a roll-off that is steep enough to attenuate the other oscillation frequencies. At the same time, the filter output needs to remain stable. As previously mentioned, filters can be sub-categorized according to whether they are active or passive, high pass or low pass, their response type, or their order. Before the final design is created, multiple types of filter designs are simulated on LT Spice, and their characteristics are altered until the most optimized output is obtained. The final filter designs that are chosen for this project are third-order bandpass microwave LRC filters, as they effectively isolate their respective oscillation frequencies, provide stable outputs, and are also cost-efficient due to the simplicity of passive components. Note that the theoretical oscillation frequencies, which can be seen in Table 4.2 from the oscillator design section, are used as the peak frequencies.

4.5.1 Simulation Design

The first iteration is of an active third-order Butterworth bandpass filter shown in Figure 4.30. This filter was simulated to obtain a steep roll-off and to avoid the loading effect problem associated with passive filters. However, active components such as operational amplifiers are costly and active filters are not suitable for high-frequency applications because they amplify noise and they are also bandwidth limited.

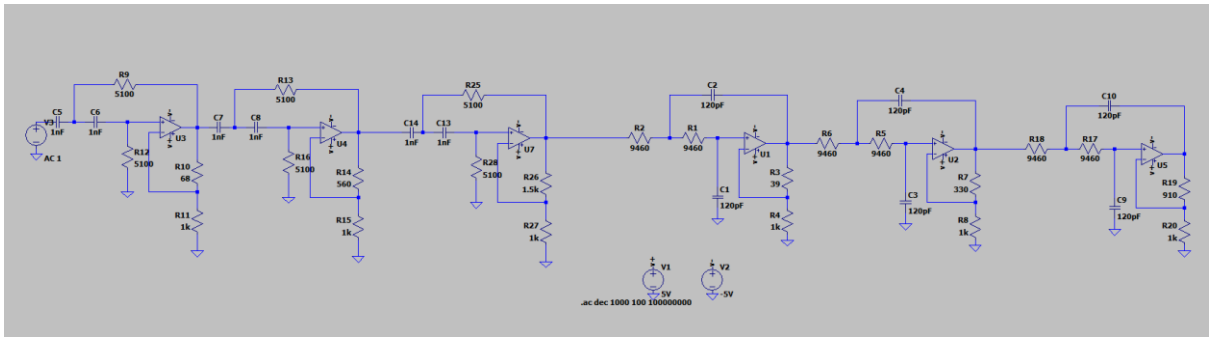

Figure 4.30 Active third-order Butterworth bandpass filter simulated on LT Spice

The next few iterations are of passive RC bandpass filters with increasing orders to increase the steepness of the roll-off. RC passive filters are cost-effective, practical and the outputs are stable as long as the order is not too high. To reduce the effects of loading, the impedance of each successive stage is designed to be ten times greater than the previous. The component values are calculated using a Python program shown in Figure 4.31 to avoid tedious hand-written calculations for each iteration. Figures 4.32, 4.33, and 4.34 show second, third, and fourth-order passive RC bandpass filters, respectively. The second-order filter has a very gentle roll-off rate and would not be able to effectively attenuate undesirable frequencies. Although the fourth-order filter would attenuate frequencies around the oscillation frequencies at a faster rate, too many components are required to build it making it cost-ineffective. The frequency responses of these filters are shown later and analysed further in the results section.

```python
import math
#third order passive filter
#calculate the corner frequency using the cut-off frequency
n = 3
f_cutoff = 1*(10**3)
f_corner = f_cutoff/(math.sqrt((2**(1/n))-1))
print ("Corner Frequency: ",f_corner)

#resistor values
r1 = 100
r2 = 10*r1
r3 = 100*r1

#capacitor values
c1 =  1/((4*((math.pi)**2)*(f_corner**2)*r1*r2*r3*(1/1000))**(1/3))
c2 = c1*0.1
c3 = c1*0.01

print("c1: ", c1)
print("c2: ", c2)
print("c3: ", c3)
```

```
Corner Frequency:  1961.4591767006195
c1:  1.8742487877548346e-05
c2:  1.8742487877548347e-06
c3:  1.8742487877548347e-07
```

Figure 4.31 Python program used to calculate the component values for passive RC filters

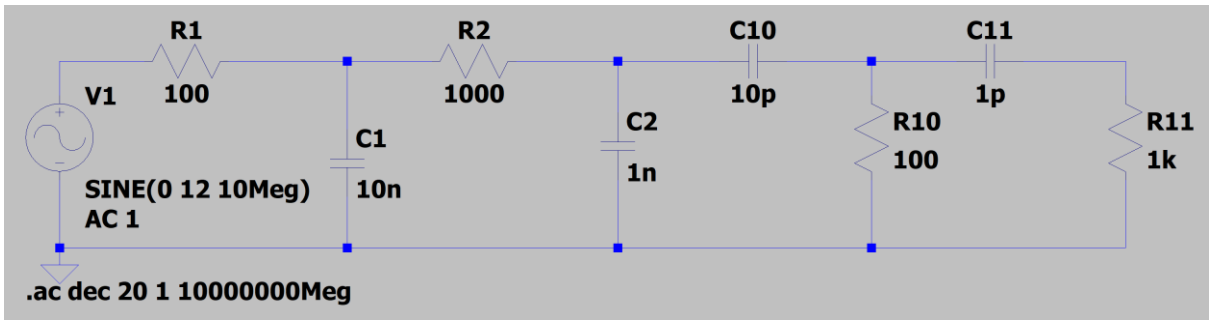

Figure 4.32 Second-order passive bandpass filter simulated on LT Spice

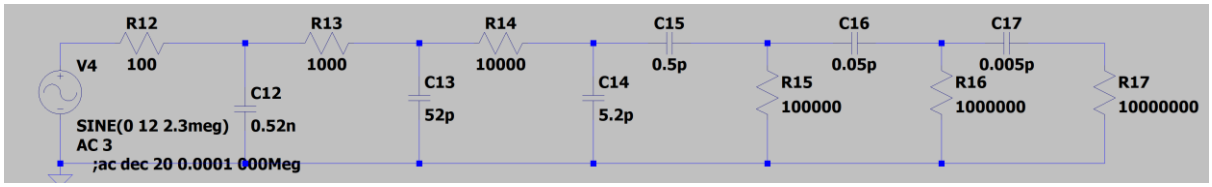

Figure 4.33 Third-order passive RC bandpass filter simulated on LT Spice

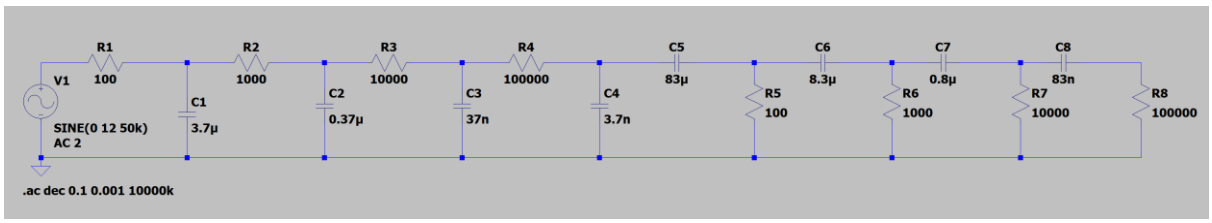

Figure 4.34 Fourth-order passive bandpass filter simulated on LT Spice

As previously mentioned, second-order filters do not attenuate undesirable frequencies at a fast enough rate and fourth-order filters require too many components to build, and thus, a third-order filter was decided upon. RC filters are not suitable for high-frequency applications and therefore microwave LRC filters are considered. The first iteration of a microwave filter is of a Chebyshev with a 0.5dB ripple. Although a ripple in the passband is not exactly a positive characteristic, a Chebyshev filter was considered due to its desirable high roll-off rate. Figure 4.35 shows a 0.5dB rippled Chebyshev microwave filter circuit designed to have a peak frequency of 1.92MHz, which is the oscillation frequency for the first oscillator. Although this filter has a fast roll-off, the output is attenuated by a very high factor, and therefore a Butterworth filter is decided upon for the final design of the filters for this project.

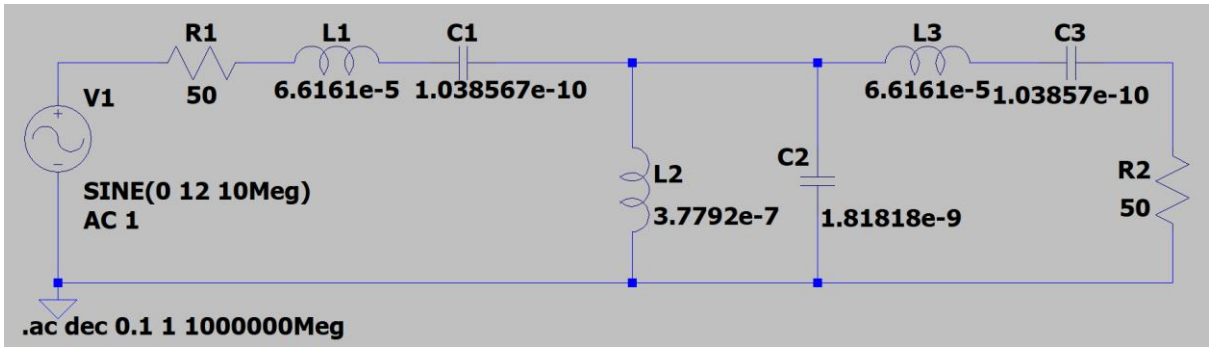

Figure 4.35 Chebyshev microwave filter simulated on LT Spice

The Butterworth microwave filter is used to isolate the frequencies of oscillation for each of the five oscillators. The insertion loss method was used as described in the literature review. The component values were calculated using a Python program shown in Figure 4.36, which makes use of Equations 2.14, 2.15 2.16, and 2.17. The bandwidth value for each filter is varied until the most optimized output is generated. This meant that undesirable frequencies must be attenuated, and the peak frequency must not be attenuated by a large factor. A fixed resistor of 50Ω is chosen for the input and load resistance, as it is a standard value commonly used in microwave filter designs. The peak frequencies are chosen according to the theoretical frequencies of oscillation and their values are shown in Table 4.6. Figure 4.38 shows the microwave filter designed for the 1.92MHz peak frequency. All filters have the same design but with varied element values to obtain the desired peak frequencies and these values can be seen in Table 4.7.

```python
import math
f0 = 1.92*(10**6)
w0 = 2*math.pi*f0
g1 = 1
g2 = 2
g3 = 1
bandwidth = 0.1
R0 = 50
L1 = (g1*R0)/(w0*bandwidth)
C1 = (bandwidth)/(g1*R0*w0)
L2 = (R0*bandwidth)/(g2*w0)
C2 = (g2)/(R0*w0*bandwidth)
L3 = (g3*R0)/(w0*bandwidth)
C3 = (bandwidth)/(g3*R0*w0)
```

Figure 4.36 Python program used to calculate component values for microwave filters

Frequency of Oscillation (MHz)
1.92
3.18
4.38
6.06
6.98

Table 4.6 Theoretical frequencies of Oscillation

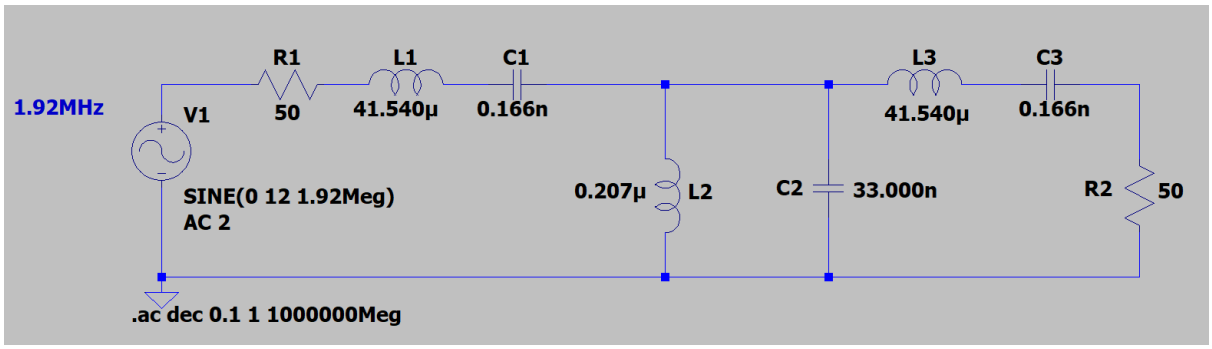

Figure 4.37 Microwave filter design in LT Spice with a 1.92MHz peak frequency

Peak Frequency (MHz)	Bandwidth Δ (%)	R1 & R2 (Ω)	C1(F)	C2(F)	C3(F)	L1(H)	L2(H)	L3(H)
1.92	10	50	0.166n	33.000n	0.166n	41.540µ	0.207µ	41.540µ
3.18	10	50	0.100n	20.019n	0.100n	25.024µ	0.125µ	25.024µ
4.38	20	50	0.182n	5.814n	0.182n	7.267µ	0.227µ	7.267µ
6.06	10	50	52.526p	10.505n	52.526p	13.130µ	65.658n	13.130µ
6.98	25	50	0.137n	3.040n	0.137n	3.800µ	0.170µ	3.800µ

Table 4.7 Element values and parameters for different peak frequencies

4.5.2 Hardware Design

Figure 4.38 shows the first microwave filter that is built and tested on a breadboard. A signal from the signal generator is inputted and the output is observed on the oscilloscope. Due to there being a limited supply of components, the exact values of inductors are not able to be sourced. Inductors with values that are as close to the simulated values as possible are used instead. This, however, causes the peak frequency, which is intended to be 1.92MHz, to change to 2MHz and is attenuated more than anticipated. The inductor values are altered in the LT Spice according to the hardware values and the circuit was simulated again. The process was repeated for the other four filters and the results were similar.

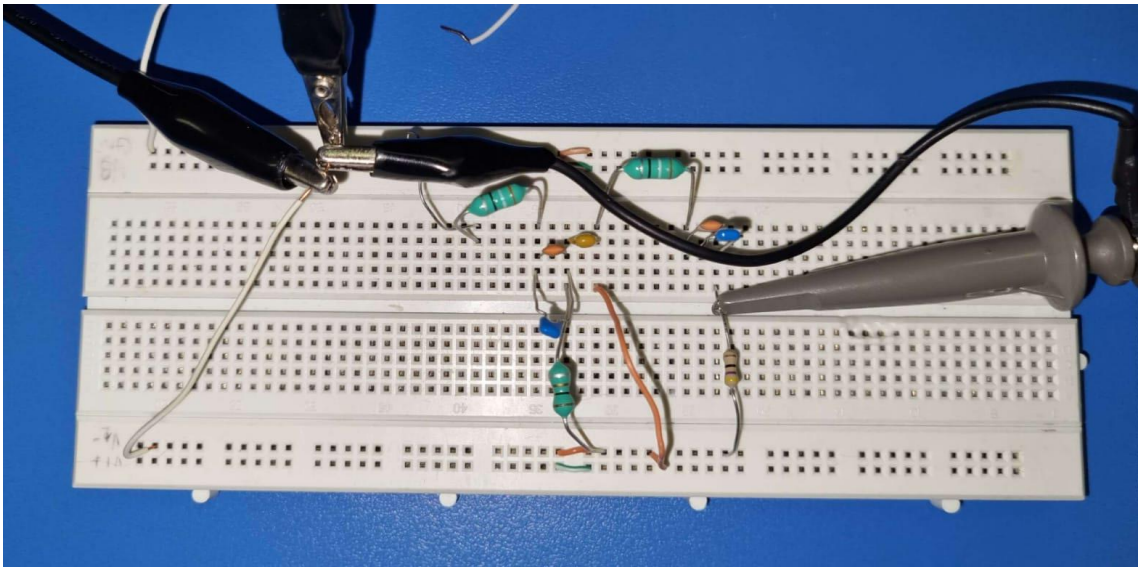

Figure 4.38 Hardware circuit setup of the first microwave filter

4.6 Design of the Rectifiers and Regulators

The final part of designing the project involves converting the AC voltage that was used to achieve magnetic induction, back into its original DC voltage. Many lamps and bulbs do operate with an AC voltage, however, the trailer lights are explicitly stated to use DC voltage. Therefore, simple rectification circuits are designed to achieve this. More precisely, five identical ones. Furthermore, for the protection of the lamps, regulators are implemented. In this project, this may not be too important as there is no expectation for the output to have a voltage greater than 12V. Therefore, regulators are sourced rather than built from scratch. Furthermore, this addition will help with future iterations.

The IN5404 diodes are chosen as they have a maximum average forward current of 3 A, as seen in the datasheet.[40] This is sustainable for the circuits and bulbs used in the project. Four of these are required in a diamond configuration, which was discussed in the literature review. Furthermore, a smoothing capacitor is used in parallel with the load. This converts the full-wave rectified signal into a more linear one, similar to a DC voltage. The calculation of the capacitor value follows Equation 4.7, where I is current, f the frequency of oscillation, c the capacitance and $V_{(ripple)}$ the voltage ripple. [29] A 1000µF capacitor is concluded upon.

$$V_{(ripple)} = \frac{I}{f * c} \tag{4.7}$$

A regulator is used to make the output voltage constant. The 7812CT regulators are used as they have an output voltage of 12.5V, close enough to the desired 12V. Furthermore, they have a load regulation of 100mv and a line regulation of 60mv. These values may be confirmed in the datasheet. [41]

4.6.1 Simulation Design

The circuit shown in Figure 4.39 below is the general structure of the ones to be simulated in Lt spice. The 5.14Ω resistor imitates the load (lamps with a power consumption of 28W). Diodes(1N194) with similar specifications to the IN5404 are used. The 1N194 has a forward voltage drop of 1V as opposed to the IN5404's drop of 1.2V. Furthermore, an input AC voltage source of 12V is seen as this is expected from the previous circuitry. A transient analysis to 10ms is chosen for the set-up.

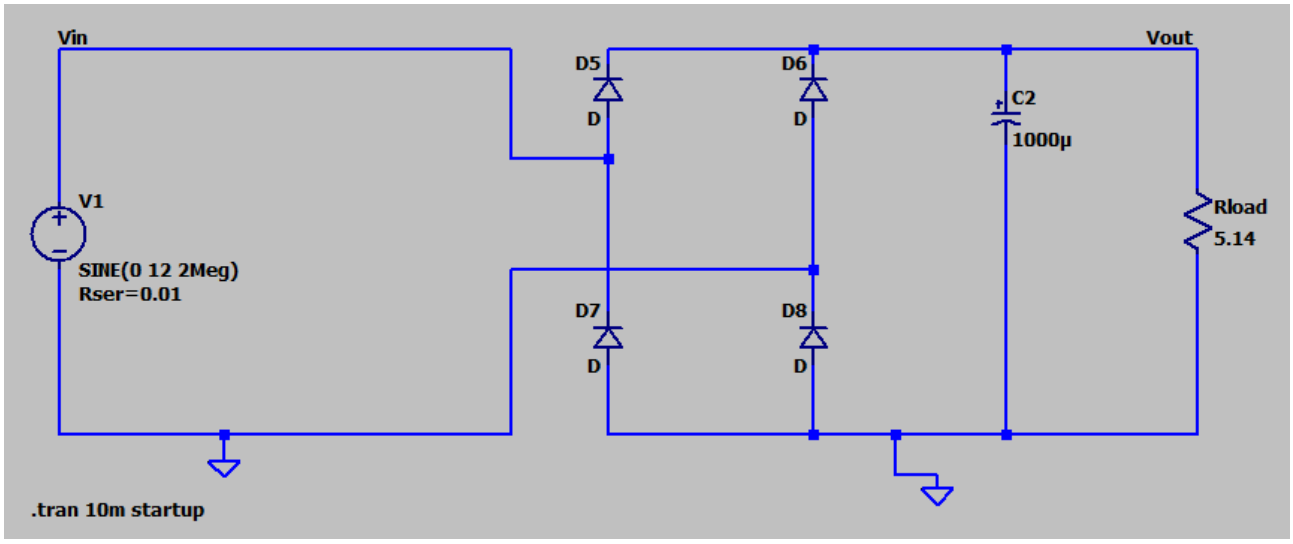

Figure 4.39 Rectifier circuit in LT Spice

The regulator is not added in as the result of this is trivial. Especially considering that based on the previous outcomes of the report the regulator's effect will not be seen. As a note, the regulator simply would fit in after the smoothing capacitor.

4.6.2 *Hardware Design*

The physical designs and pinout of the regulator(7812CT) and diodes(IN5404) are shown in Figure 4.40 and Figure 4.41 respectively. In Figure 4.40 it is apparent that the regulator has 3 terminals. Contrary, in Figure 4.41 we see the diode has only two terminals, namely the cathode(black band) and the anode.

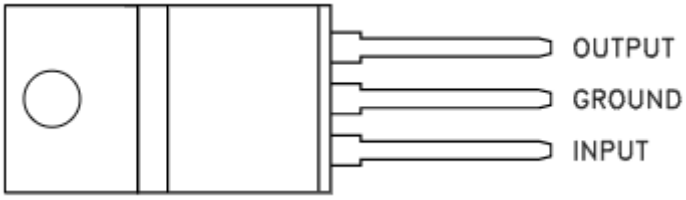

Figure 4.40 Layout of the regulator[41]

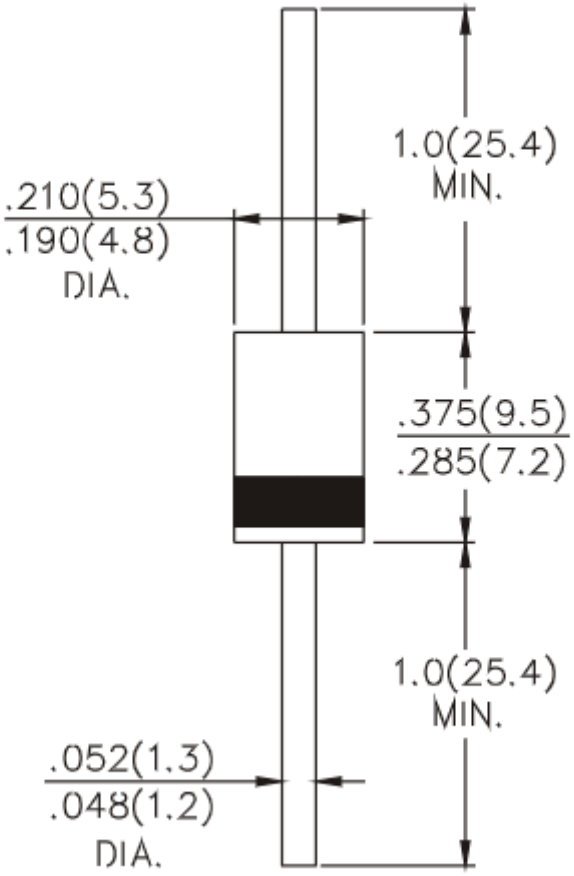

Figure 4.41 Layout of the diode [40]

The diodes are physically soldered together as seen in Figure 4.42. This follows the design of the simulated LT Spice circuit. Moreover, the capacitor is connected in parallel to the output as is expected. Lastly, Figure 4.43 is a depiction of the physical regulator. It is seen with a casing and heat sink for thermal protection. This is shown not connected.

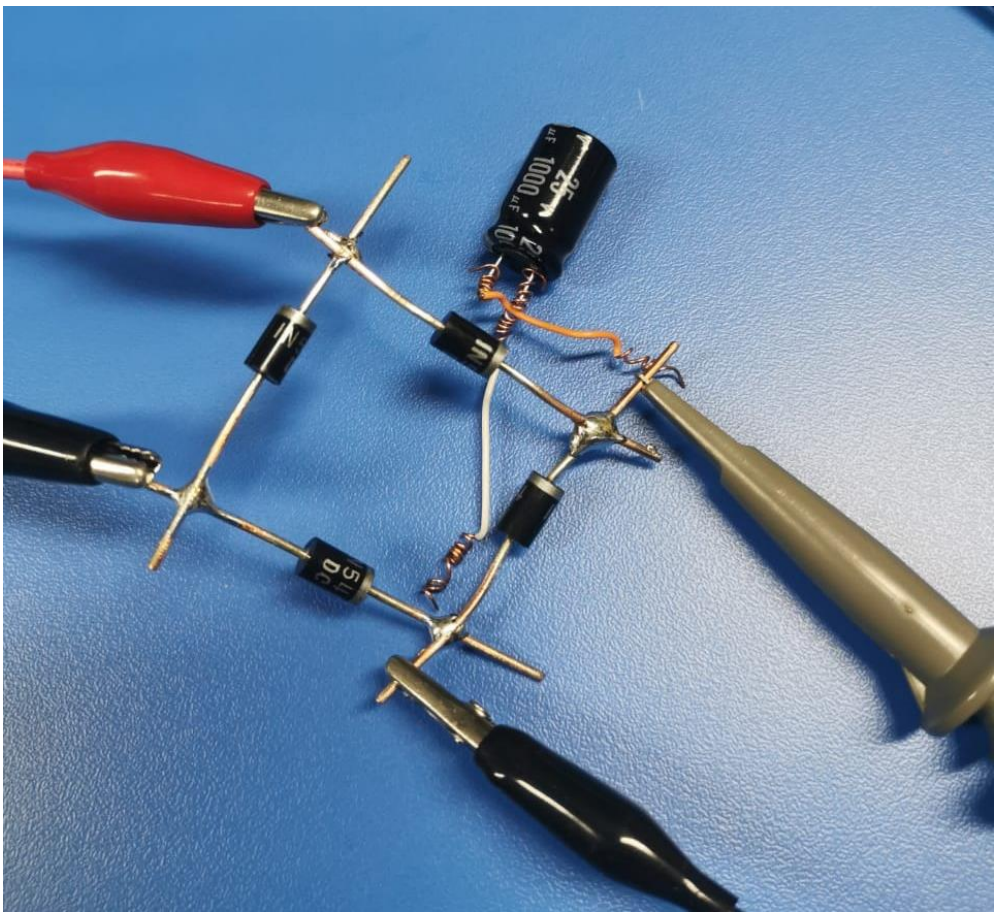

Figure 4.42 Diodes(IN5404) soldered together with the capacitor on the output

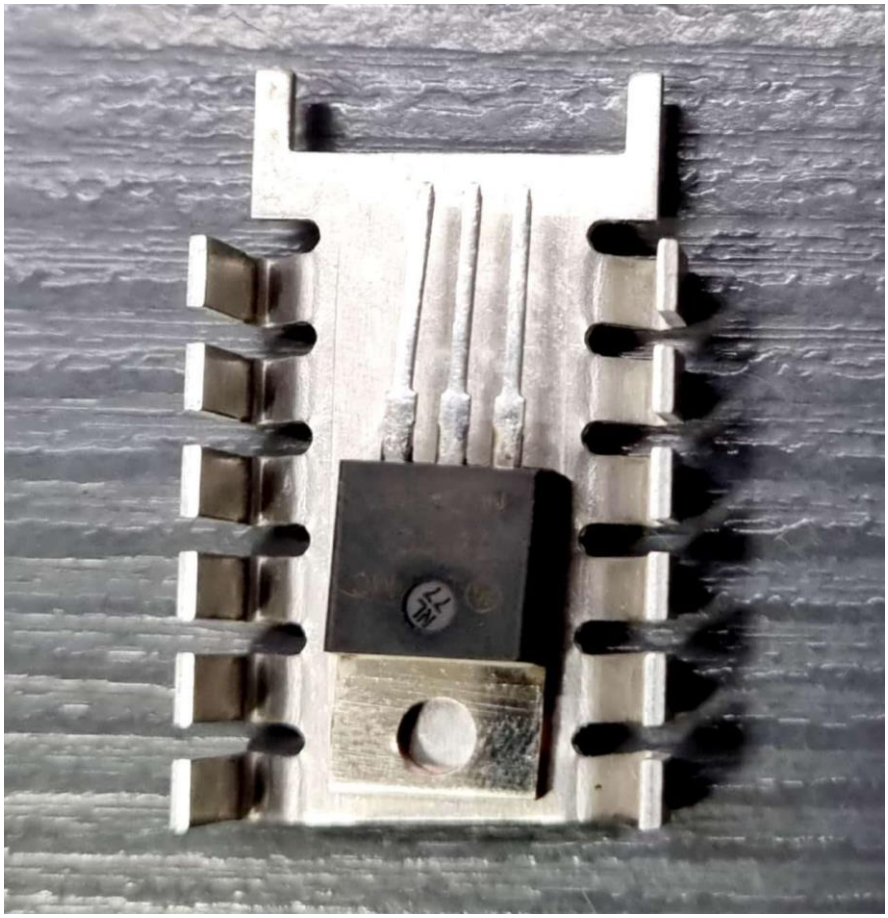

Figure 4.43 The physical regulator(7812CT) in its casing

4.7 Complete Design and Integration into the Test Rig

With all the circuits designed they are combined. Firstly, to replicate users changing signals, switches are implemented as inputs. Next, with the prototype, the five oscillator circuits, and five amplifiers, which are to be connected on the vehicle side, are left on the breadboards. In the future, this circuitry may be made smaller using PCB boards as well as boxing them.

The housing of the inductor coils is a cylinder which was discussed earlier. This can be attached to many parts of the vehicle. Figure 4.44 shows an example of where the housing may be placed. This is fixed with nuts and bolts. Next, there is a cable running from the housing to the vehicle and another from the housing to the trailer. These cables connect to their respective “boxes” of circuitry. The input to the “box” of the vehicle is a 12V line from the battery. The output of the trailer “box” is fed into the lights.

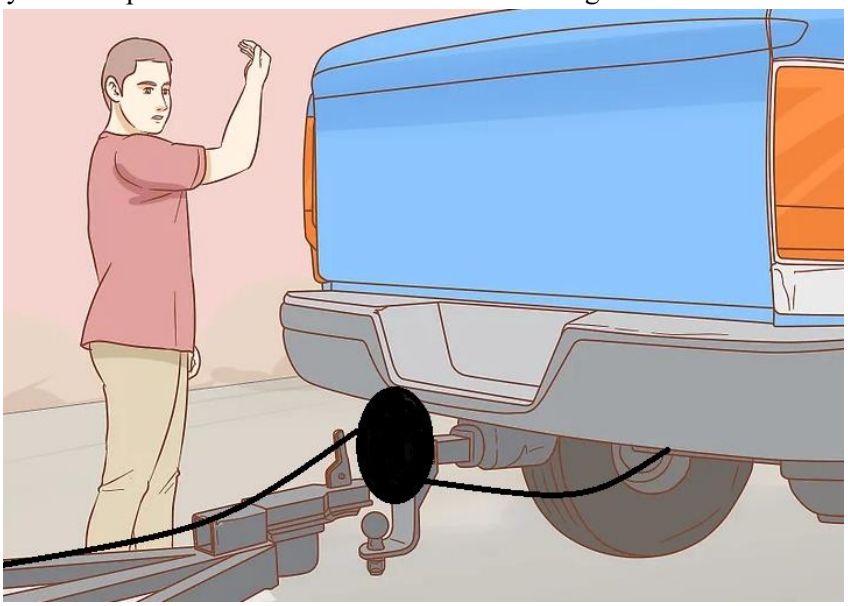

Figure 4.44 Physically attaching the system [42]

Similar to the oscillators and amplifiers, the five filters and five rectifier circuits are left on the breadboards. They too can be made smaller in later prototypes and closed off to public view. They make up the “box” of circuitry on the trailer's side.

The battery is mimicked using a voltage source set to 12V. The output of the prototype is LEDs. This is due to a lack of trailer light bulbs. However, these LEDs do provide for sufficient testing of the system. Furthermore, the output is connected to an oscilloscope to ensure more accurate voltages and currents are achieved. A complete depiction of the prototype is shown in Figure 4.45. The separate circuits are not connected at this stage, and only one line signal is shown due to a lack of physical space. The full schematic from LT spice is depicted in Figure 4.46.

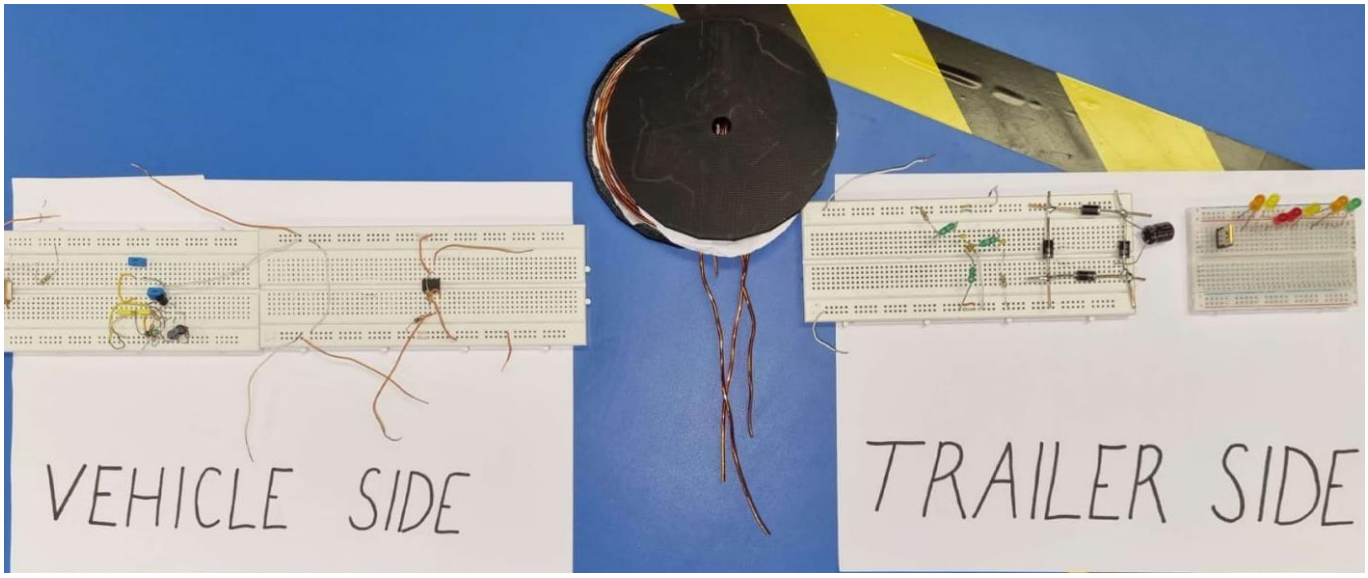

Figure 4.45 Prototype of the system for one signal line

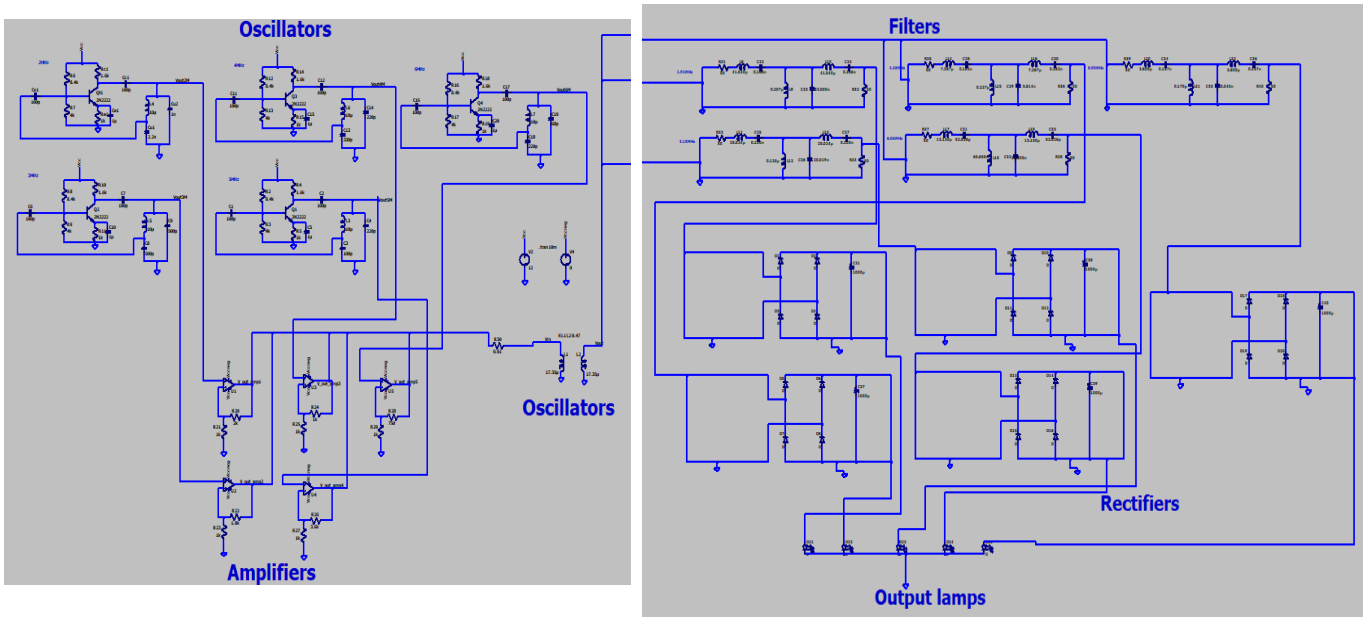

Figure 4.46 Schematic on LT spice

5. Results

5.1 Results of the Oscillator designs

Software Results

All the software results for the oscillators are achieved in LT Spice. Figure 5.1 depicts the five oscillators that are simulated ranging from 2MHz to 6MHz. A transient analysis to 100ms is done to see the results. The output to be shown is when the probes are placed on the respective Vout(frequencies).

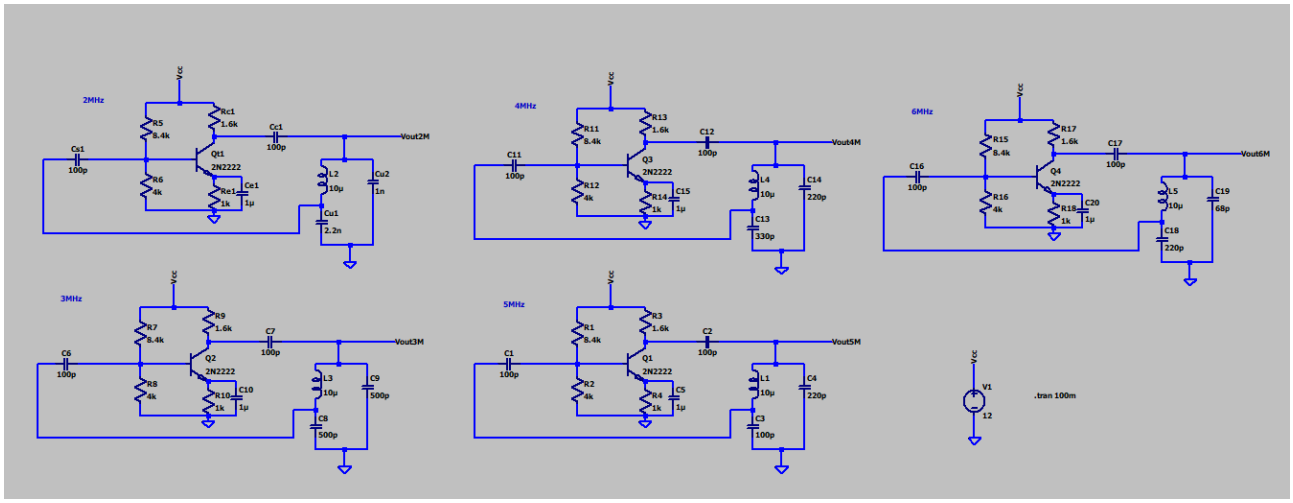

Figure 5.1 Oscillator Circuits which are simulated on LT Spice

The output of the theoretical 2MHz oscillator is shown in Figure 5.2. As is seen oscillations begin rapidly due to the high capacitor value (100pF) at the base. Moreover, Vcc is seen as a 12V DC voltage. A more detailed and zoomed-in output is shown in Figure 5.3. At roughly 56µs the oscillator reaches its peak voltage of about 4.15V. This is clear from Figure 5.4.

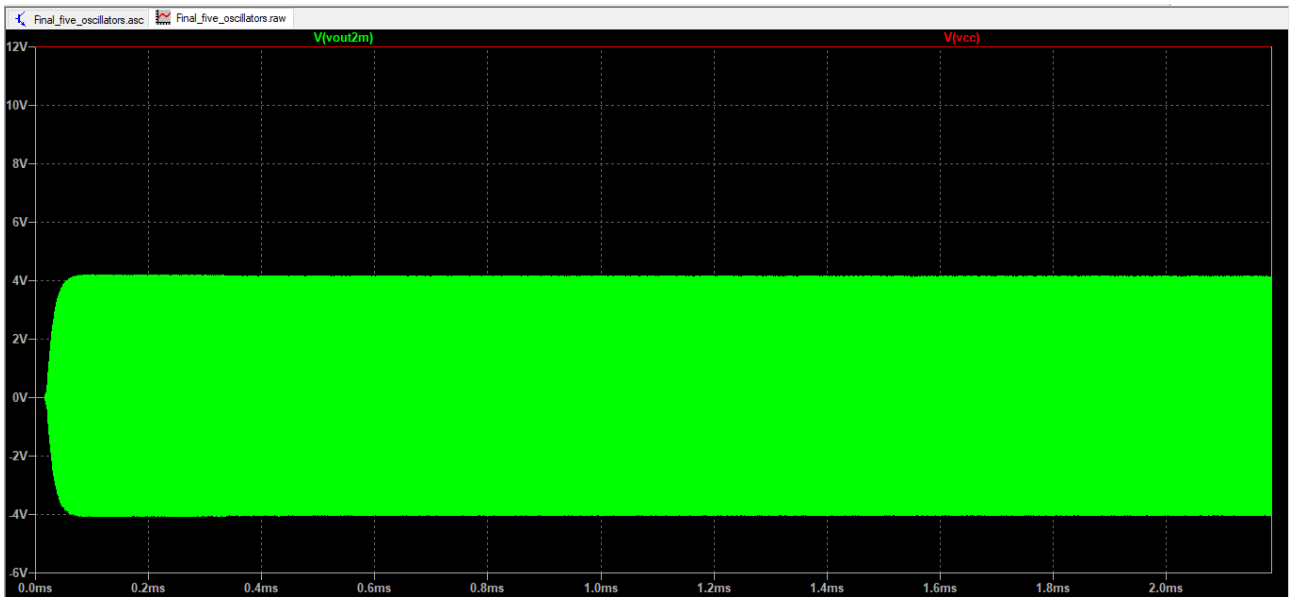

Figure 5.2 Output of the 2MHz Oscillator

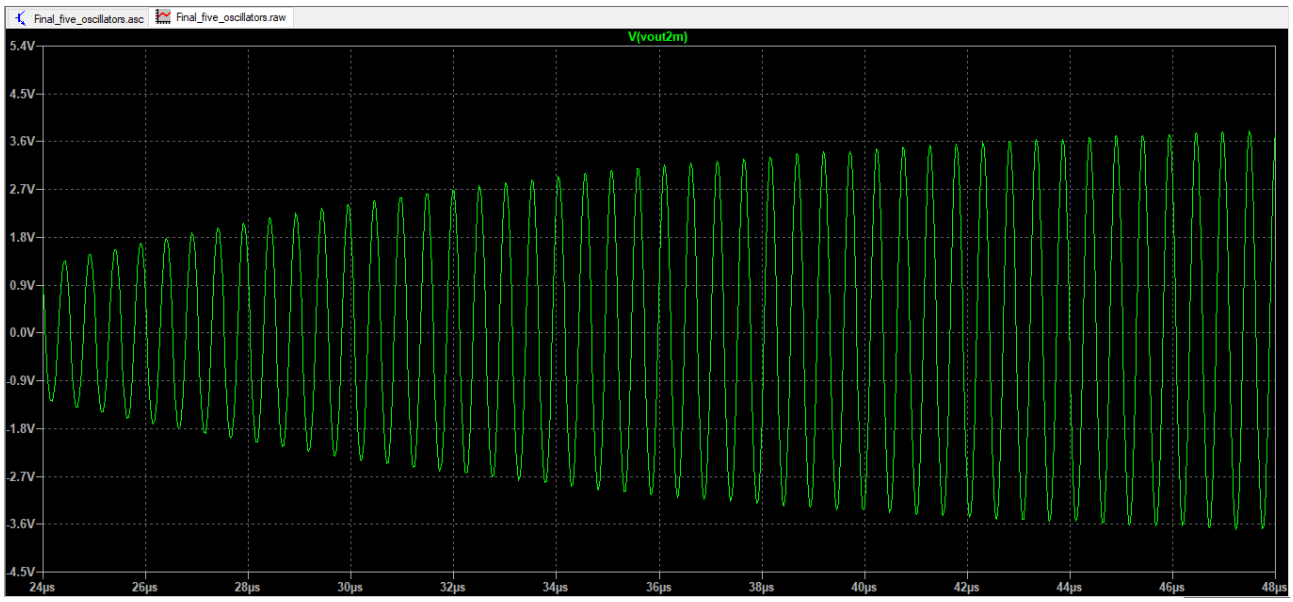

Figure 5.3 Zoomed-in output of the 2MHZ Oscillator to see the start of oscillations

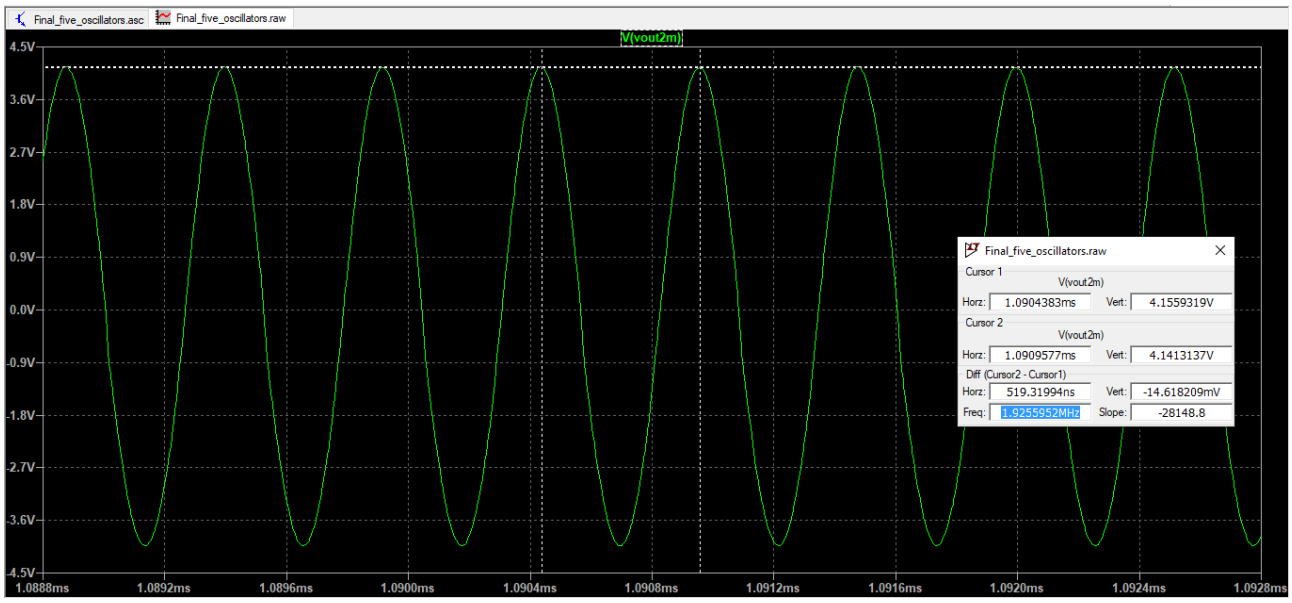

Figure 5.4 Further zoomed-in output of the 2MHz Oscillator

For completeness, the rest of the Oscillator outputs are shown in Figure 5.5. It is clear to see that each oscillator has its own frequency (as per the labels) and that all the oscillators have a different peak voltage. Due to the peak voltages being less than 12V the amplifiers are introduced in the next section. It is important to note that setting the correct resistor values in the oscillator circuit could make the use of the amplifiers redundant. However, due to time constraints, this is unachievable.

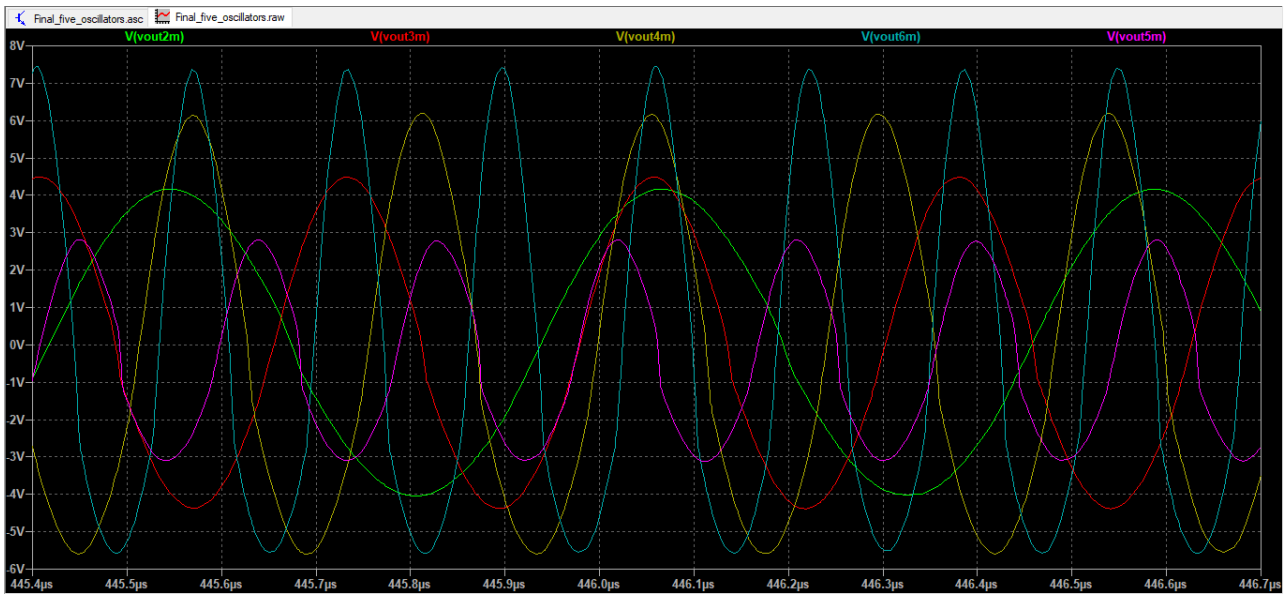

Figure 5.5 The outputs of the different oscillator circuits

Lastly, Table 5.1 gives the values of the frequency of oscillation and the different peak voltages achieved by the oscillator circuits. These results are used in the next section to determine the gains required of the op-amps.

Theoretical Oscillator Frequency (MHz)	**Achieved Oscillator Frequency (MHz)**	**The output voltage of the Oscillator (V)**
1.92	1.93	4.15
3.18	3.1	4.5
4.38	4.06	6.14
6.06	5.17	2.75
6.98	6.1	7.45

Table 5.1 Output frequencies and voltages in LT spice

Hardware Results

The simulations are then transferred to physical hardware as discussed in Chapter 4.1. With the input voltage set to 12V DC, the output of the 2MHz oscillator, on the oscilloscope is shown in Figure 5.6. Here a major flaw is seen. The frequency of oscillation is at 50Hz which is completely off from the simulated result. This error is seen in all the other oscillator circuits. This points to incorrect usage of physical components which cannot be fixed due to the time constraint.

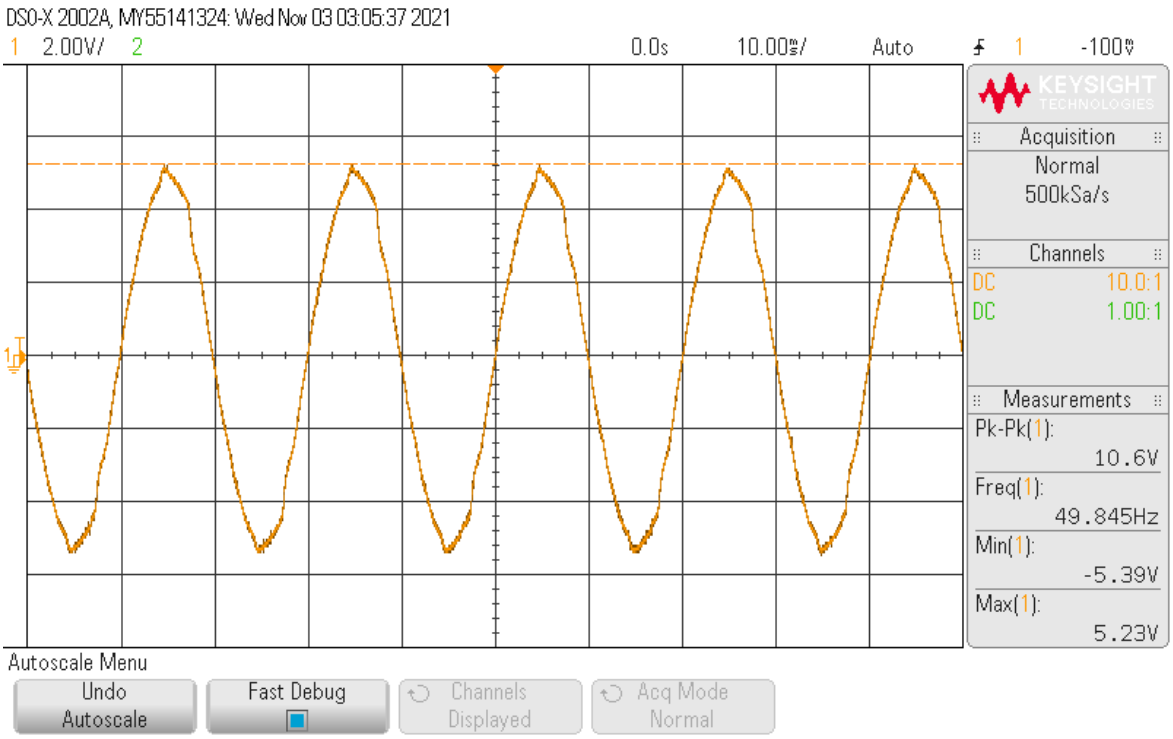

Figure 5.6 Output of the physical oscillator on the oscilloscope

In an attempt to get the desired oscillations, a different approach is used. This involves using a crystal as shown in Figure 5.7. However, the results are similar to the previous ones as can be seen in Figure 5.8. More research into this topic needs to be done, regarding physical component usage.

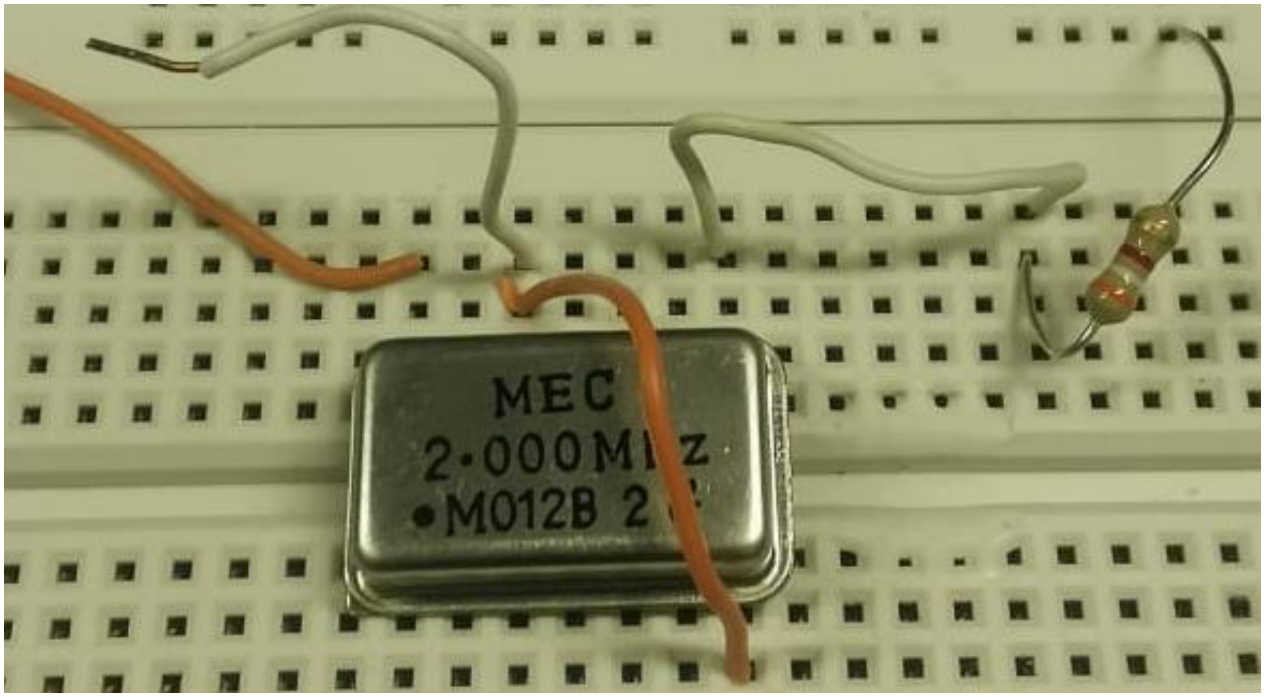

Figure 5.7 Crystal Oscillator circuit

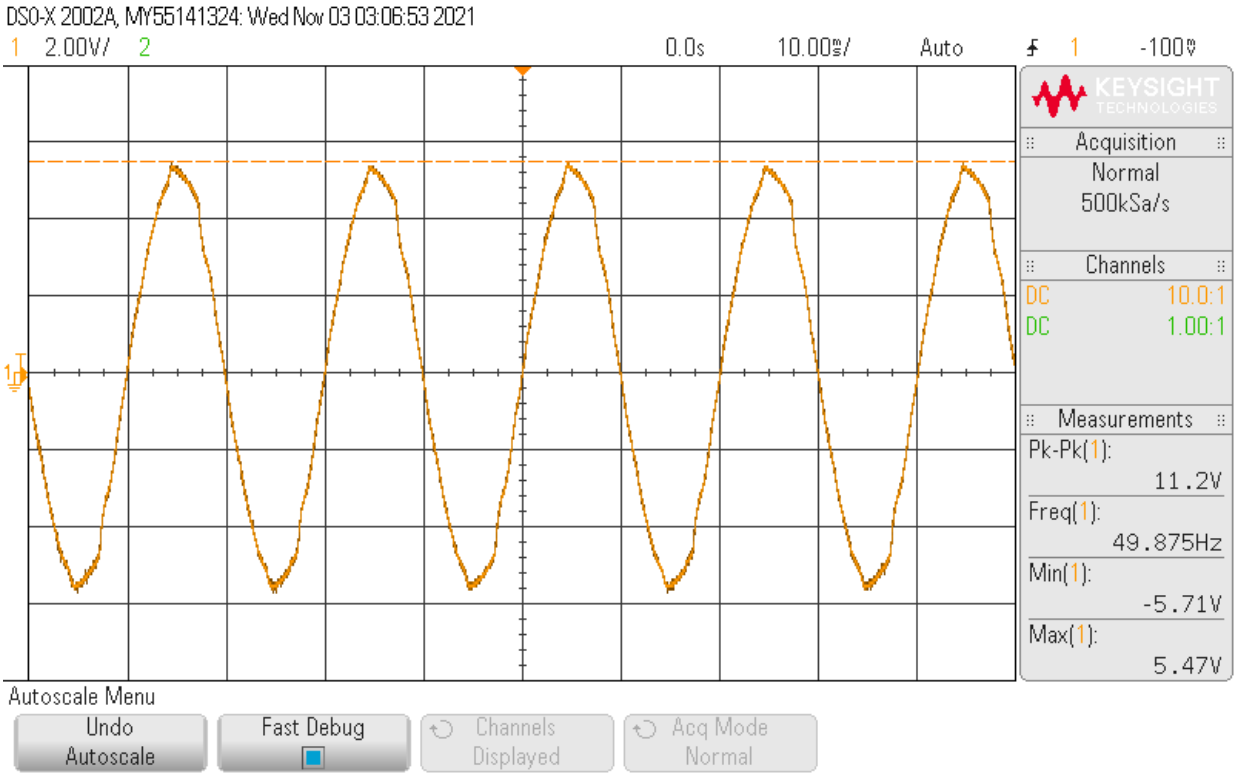

Figure 5.8 Output of the Crystal Oscillator

5.2 Results of the Amplifier designs

Software Results

All the software results for the amplifiers are gathered in LT Spice. Figure 5.9 depicts the five amplifiers that are simulated for the different signals. A transient analysis to 2ms is done to see the results. The output to be shown is when the probes are placed on the respective Vout(amp number).

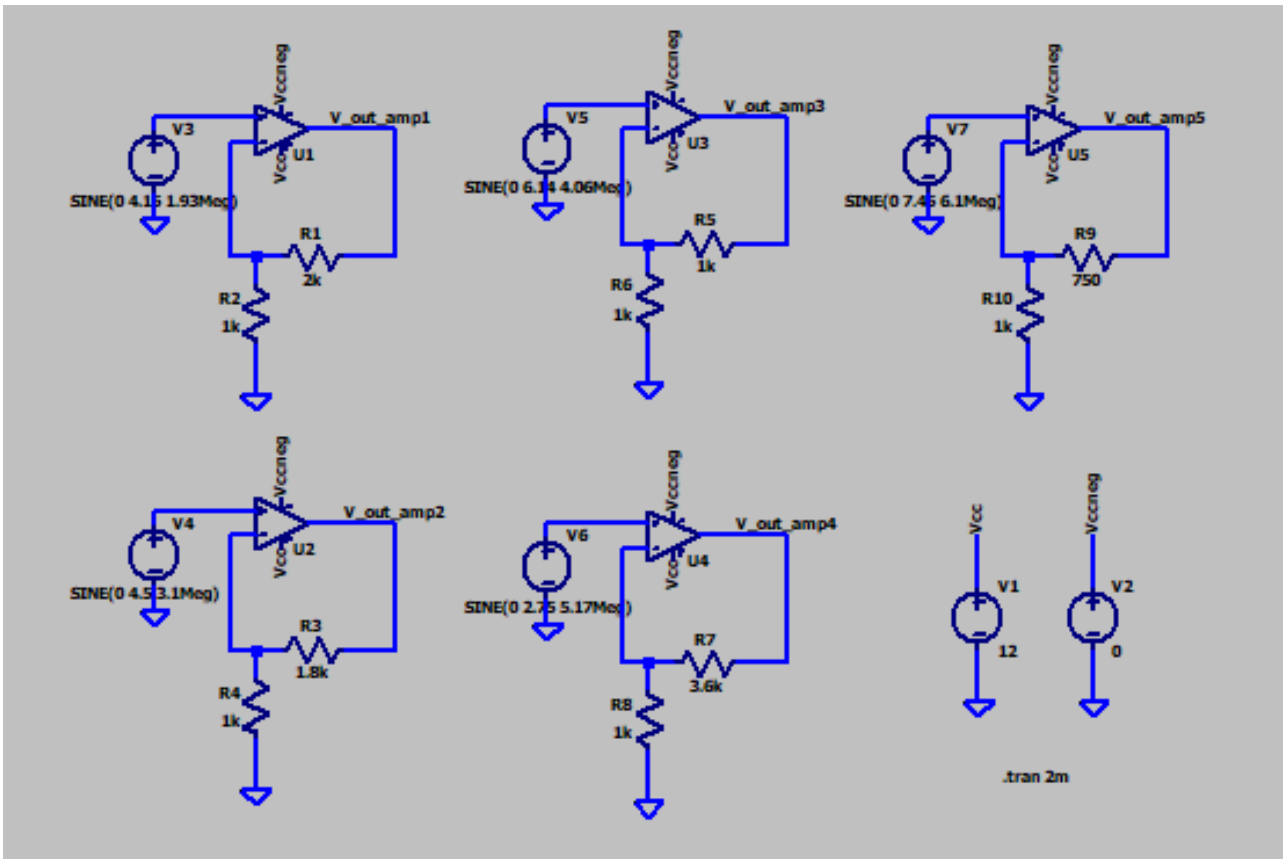

Figure 5.9 Non-Inverting amplifier circuits which are simulated

The output of the theoretical amplifier at 2MHz is shown in Figure 5.10. The output is at the same frequency as the input which is promising. Furthermore, it is clear that the voltage has been amplified which was desired. However, for the peak voltage criteria, a problem is encountered. The output is improved by increasing the slew rate (slew=1000Meg) as seen in Figure 5.11. This is still concerning as this part may be difficult to source. Moreover, the signal only shows the positive cycle. This is due to the negative rail voltage being grounded. Due to the frequency being high, this may not be problematic.

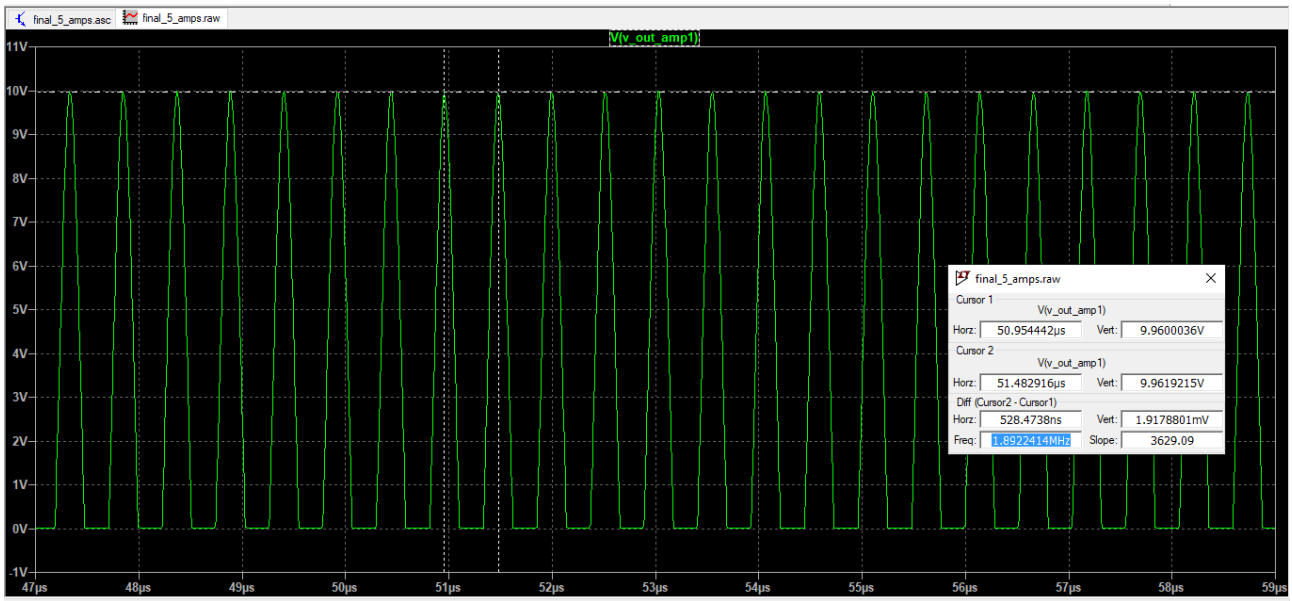

Figure 5.10 Output of the amplifier with the op-amp set to (Slew=100Meg)

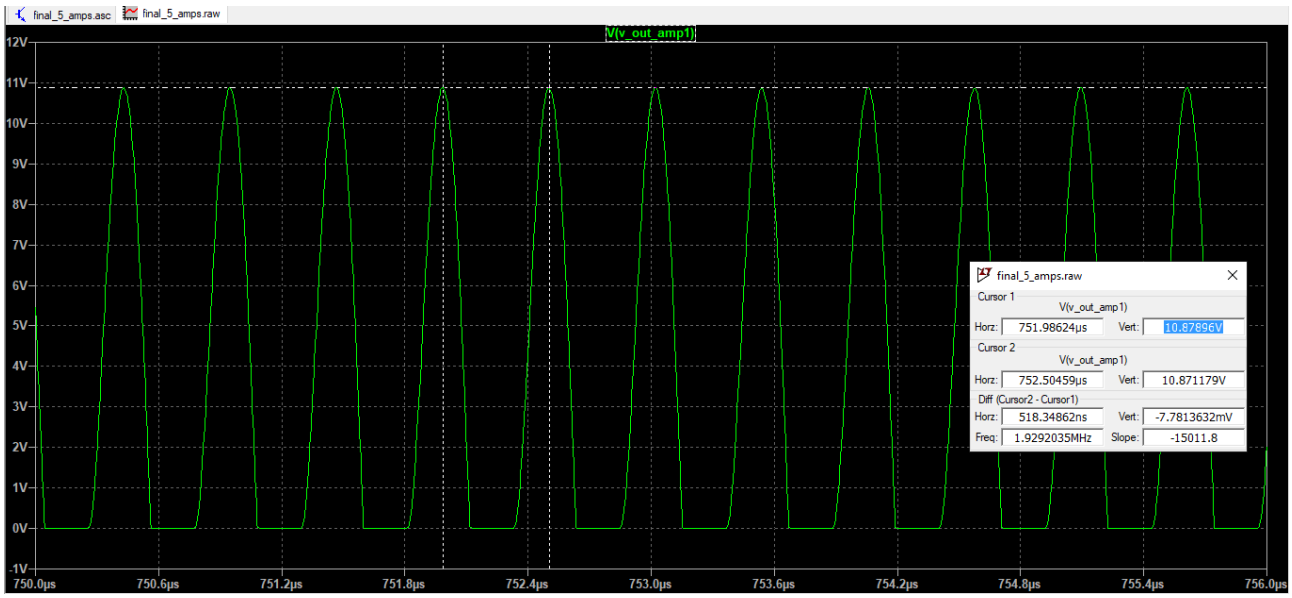

Figure 5.11 Output of the amplifier with the op-amp set to (Slew=1000Meg)

The results of the remaining amplifiers are shown in Figure 5.12. Their peaks are slightly too low. More research into the gain-bandwidth product and slew rate need to be done to improve this. The problem is extremely bad for the signal at 4MHz. As mentioned earlier, it would be ideal to improve the oscillators, to remove the amplifiers from the system. This is due to the unstable nature of op-amps at high frequencies.

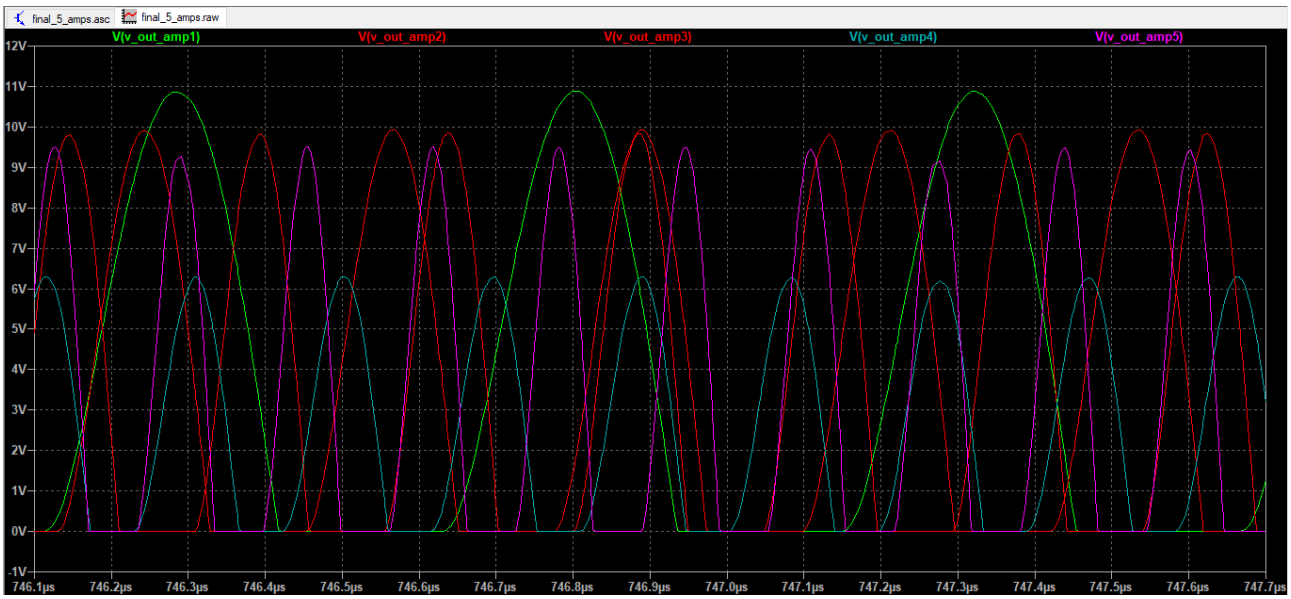

Figure 5.12 Outputs of the amplified signals on LT Spice

Hardware Results

The hardware implementation is done using the OP07CP op-amp. First, the op-amp is powered by a Vcc(+) of 12V and a Vcc(-) of -12V, with a 4.15 AC voltage @2MHz input to mimic the 2MHz signal that resulted from the oscillators. The output of the implemented non-inverting amplifier configuration is shown in Figure 5.13. An identical approach is done to all the other signals. From Figure 5.13 two pairs of graphs are displayed. The green is the input signal and the orange is the output signal. The top plot indicates testing done at 2MHz. It is discovered here, that the component (OP07CP), although believed to have an operating frequency in the Megahertz range, is unsuitable. Furthermore, the slew rate is too low therefore a pure sinusoidal output is not achieved. Therefore, the bottom plot shows a result where the frequency is set to 100KHz and the correct output is displayed, to justify the theory.

Figure 5.14 has the exact implementation as Figure 5.13 bar one detail. The Vcc(-) is set at 0V which is more realistic and what the simulations are based on. Therefore, only the positive half cycle has a non-zero voltage. It is important to note that in both figures the voltage is saturated by the rails.

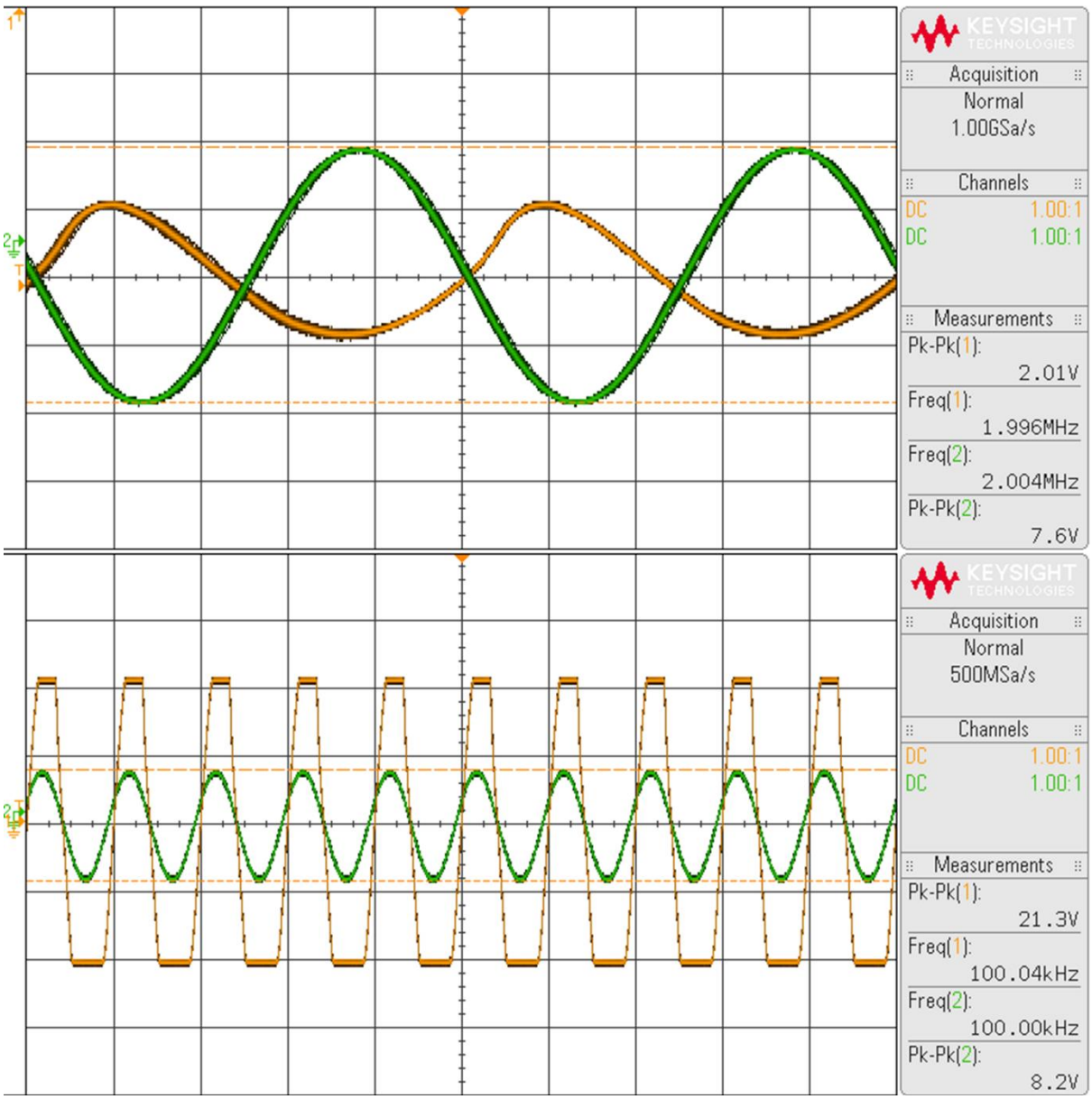

Figure 5.13 Output of the physical amplifier at 2MHz (full wave)

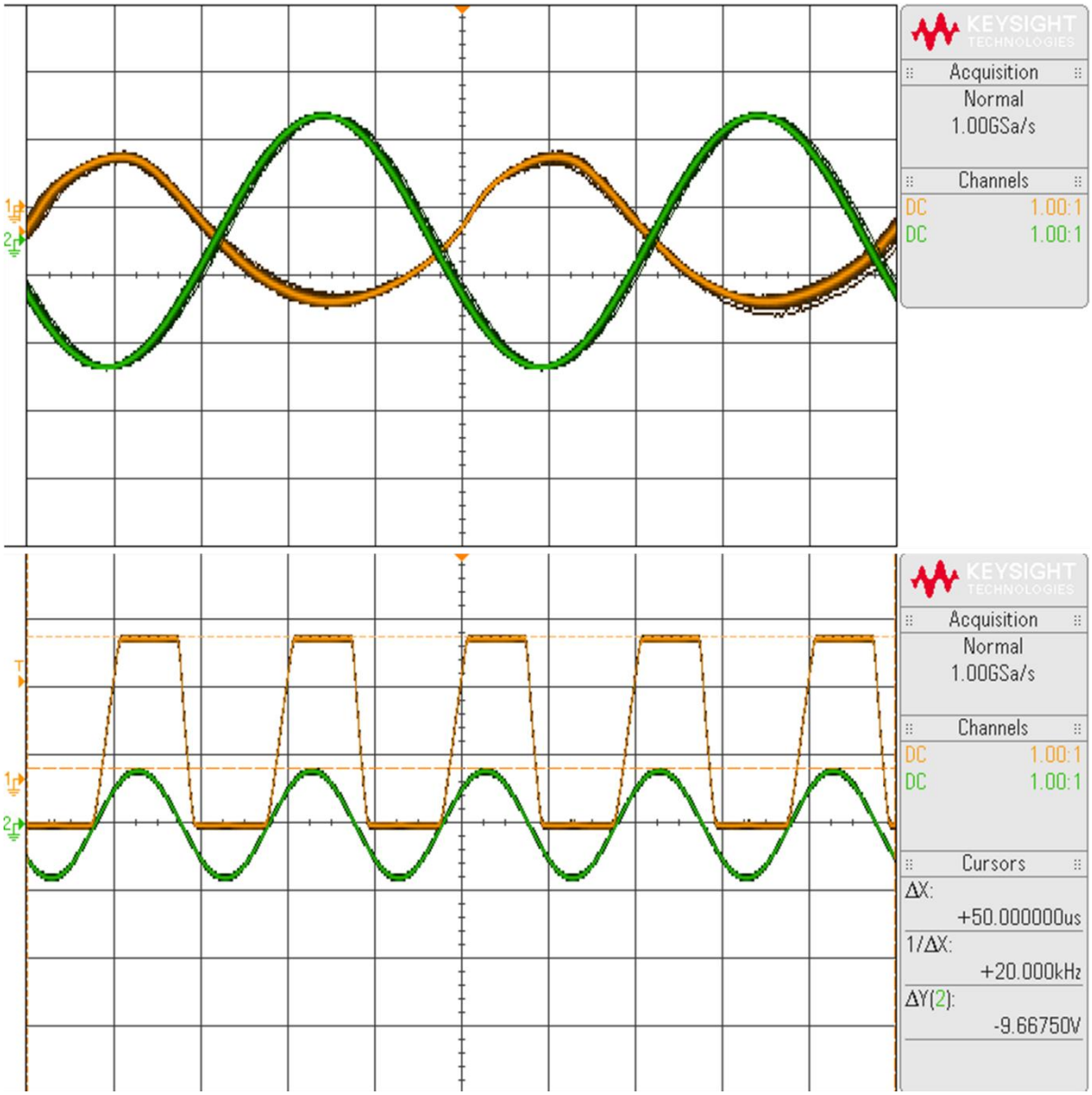

Figure 5.14 Output of the physical amplifier at 2MHz (half-wave)

5.3 Results of the Magnetic Coupling Coil designs

Software Results

As mentioned earlier, the coils were simulated in Ansys Maxwell. The image shown in Figure 5.15 serves as a refresher of this where the transmitter coil is shown in red and the receiver coil is shown in yellow. The set-up of the software and simulation conditions is found more detailed in the design chapter.

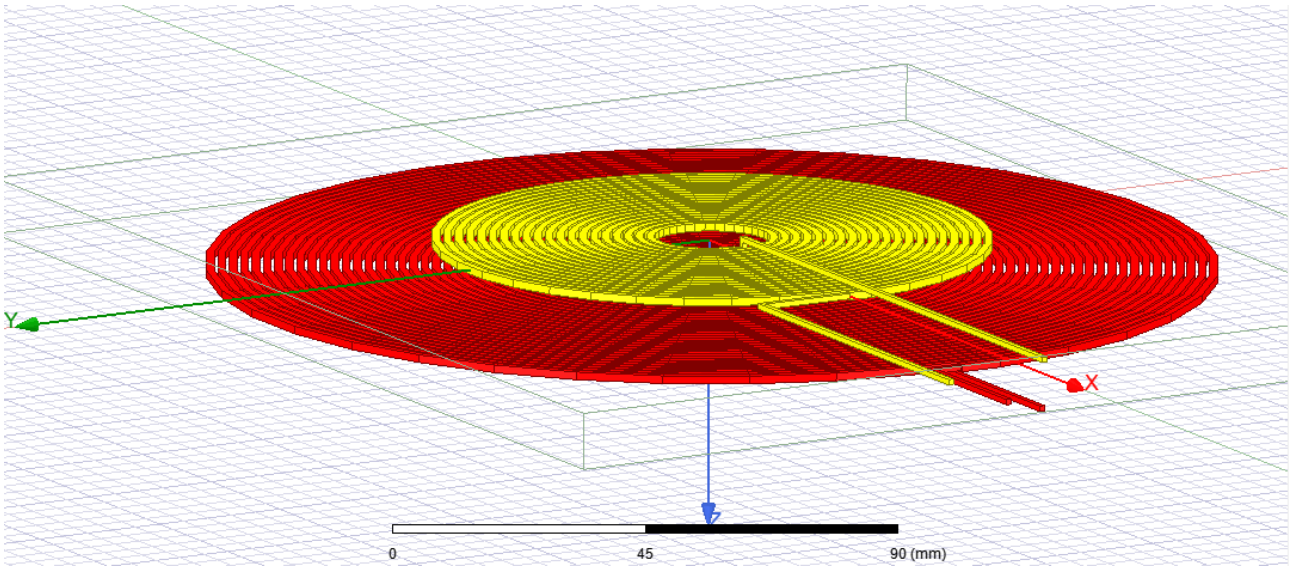

Figure 5.15 Visual representation of an arbitrary simulation set-up in Ansys Maxwell

The results of three different coils with different turns ratios are discussed as follows. Figure 5.16 is the results of a 40:20 coil simulation indicating the transmitter coil has 10 turns and the receiver coil has 10 turns. Figure 5.17 has a ratio of 20:20 and Figure 5.18 has a ratio of 40:40.

The tables shown are directly extracted from Ansys Maxwell. Current(1,1) is the excitation of the transmitter with Current(3,3), the excitation of the receiver. Current(1,3 & 3,1) represents the mutual excitation. With this, the self inductances, mutual inductances, and coupling coefficients are shown.

	$distance [mm]	Matrix1.CplCoef(Current3,Current1) Setup1 : LastAdaptive	Matrix1.L(Current1,Current1) [uH] Setup1 : LastAdaptive	Matrix1.L(Current3,Current1) [uH] Setup1 : LastAdaptive	Matrix1.L(Current3,Current3) [uH] Setup1 : LastAdaptive
1	5.000000	0.216297	13.617704	1.594228	3.989285

Figure 5.16 Simulation with coil ratio of 40:20

	$distance [mm]	Matrix1.CplCoef(Current3,Current1) Setup1 : LastAdaptive	Matrix1.L(Current1,Current1) [uH] Setup1 : LastAdaptive	Matrix1.L(Current3,Current1) [uH] Setup1 : LastAdaptive	Matrix1.L(Current3,Current3) [uH] Setup1 : LastAdaptive
1	4.000000	0.462468	4.723206	1.994638	3.938481
2	9.000000	0.158357	1.532142	0.402675	4.220212
3	14.000000	0.101683	1.771614	0.291286	4.632054
4	19.000000	0.071493	1.990926	0.223402	4.904415
5	20.000000	0.067040	2.032531	0.212650	4.950295

Figure 5.17 Simulation with coil ratio of 20:20 (Chosen design)

	$dist [mm]	Matrix1.CplCoef(Current3,Current1) Setup1 : LastAdaptive	Matrix1.L(Current1,Current1) [uH] Setup1 : LastAdaptive	Matrix1.L(Current3,Current3) [uH] Setup1 : LastAdaptive
1	4.000000	0.514082	17.353934	17.358404
2	10.047546	0.173333	5.532841	19.491249
3	15.000000	0.122275	6.351953	21.546770

Figure 5.18 Simulation with coil ratio of 40:40

From the figures above it is evident that having a turns ratio of 1:1 is the most efficient for the current design. This is seen as the 0.216 coupling factor in Figure 5.16 is the lowest of the three simulations. Another observation is that increasing the distance of separation between the transmitter and receiver, depicted in

Figures 5.17 and 5.18, decreases the coupling factor as expected. Lastly, the coupling factor is the greatest when turns are the highest. However, due to physical constraints, the coils with a 20:20 turns ratio are chosen as the final design. The coupling factor is only 0.46, but this is fair. In the future, a transformer will be implemented to step up the battery voltage, to account for the losses.

Next, an Electromagnetic analysis is done on the chosen design. Figure 5.19 shows the magnitude of the Magnetic Flux Density (B) with Figures 5.20 and 5.21 showing the flux density vectors. The maximum flux density reaches a value around 0.0036T concentrated in the centre of the coil. Furthermore, from Figure 5.20 it is seen that the field lines point in the z-direction as the field moves toward the centre of the coil. Figure 5.22 simply depicts a cross-section of the other figures.

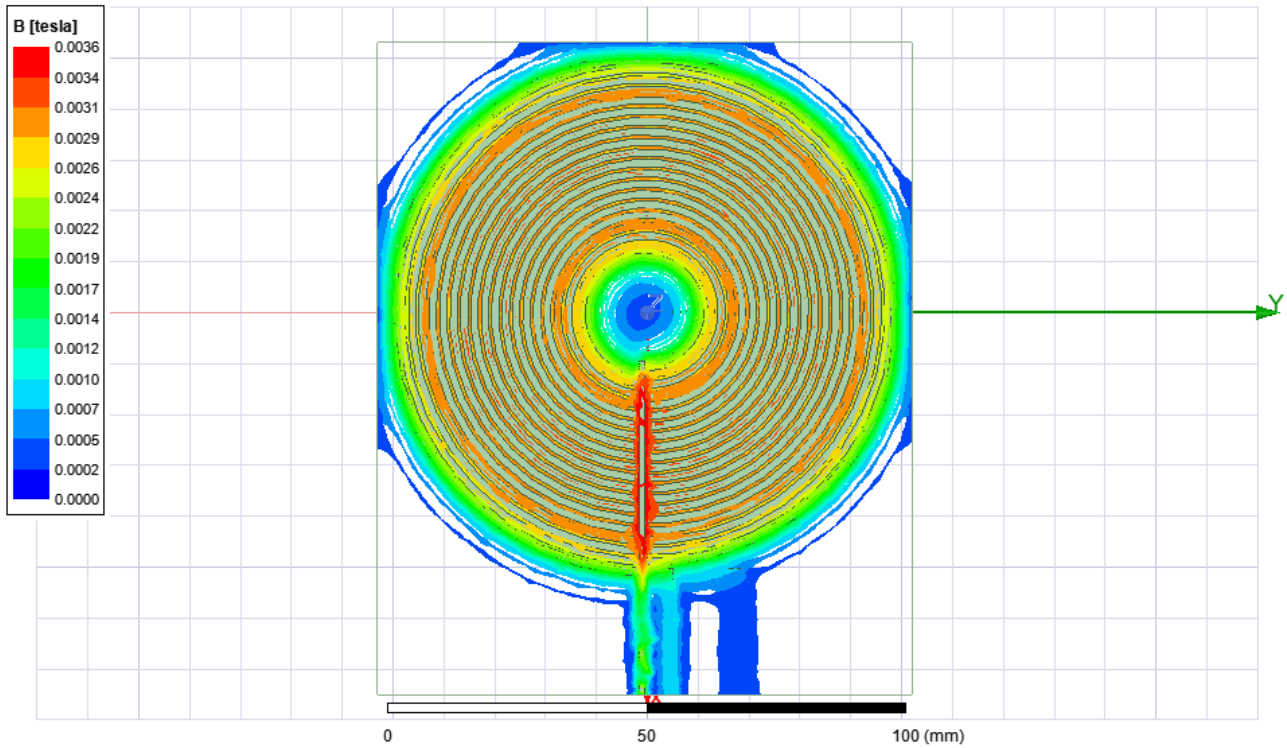

Figure 5.19 Top view of the Magnetic Flux Density magnitude plot

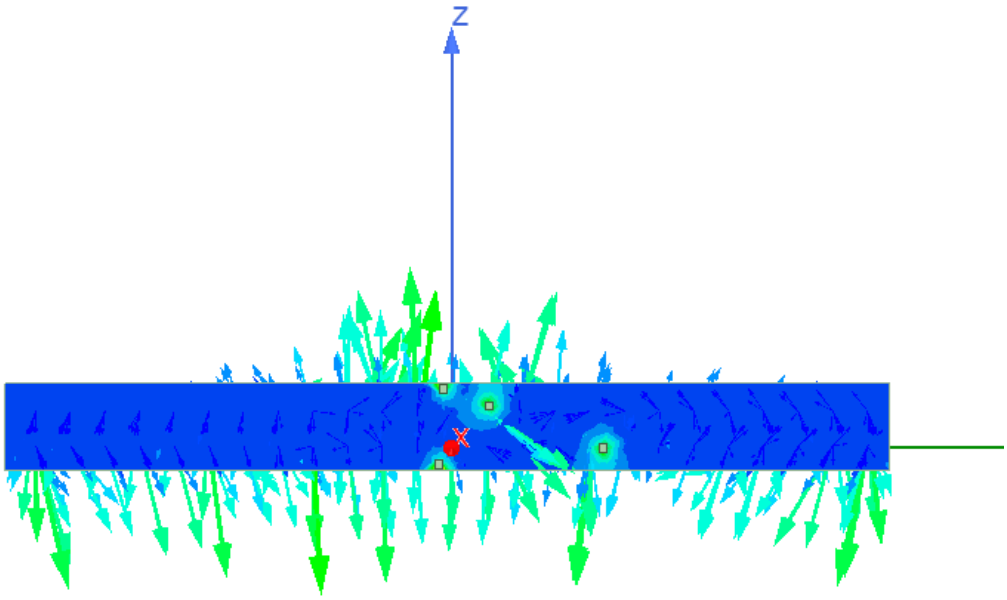

Figure 5.20 Side view of the Magnetic Flux Density vector plot

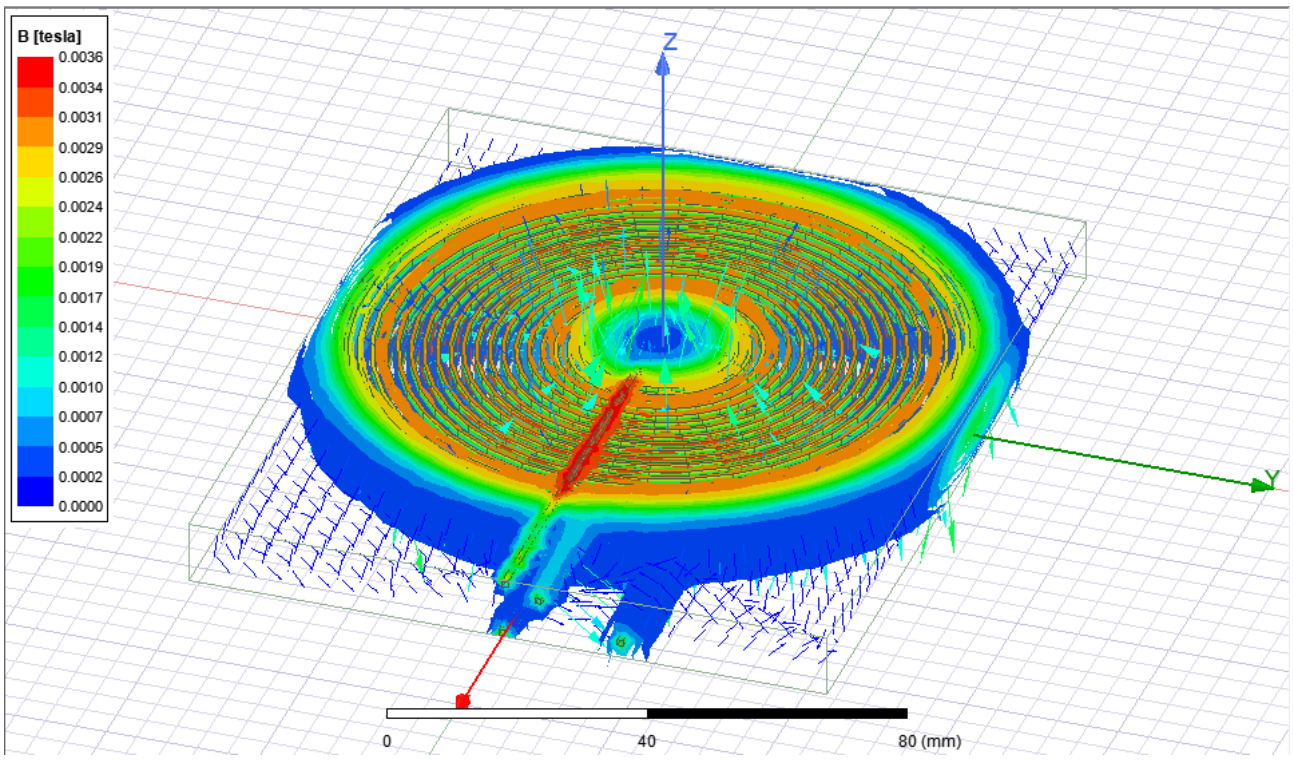

Figure 5.21 Angled view of the Magnetic Flux Density vector plot

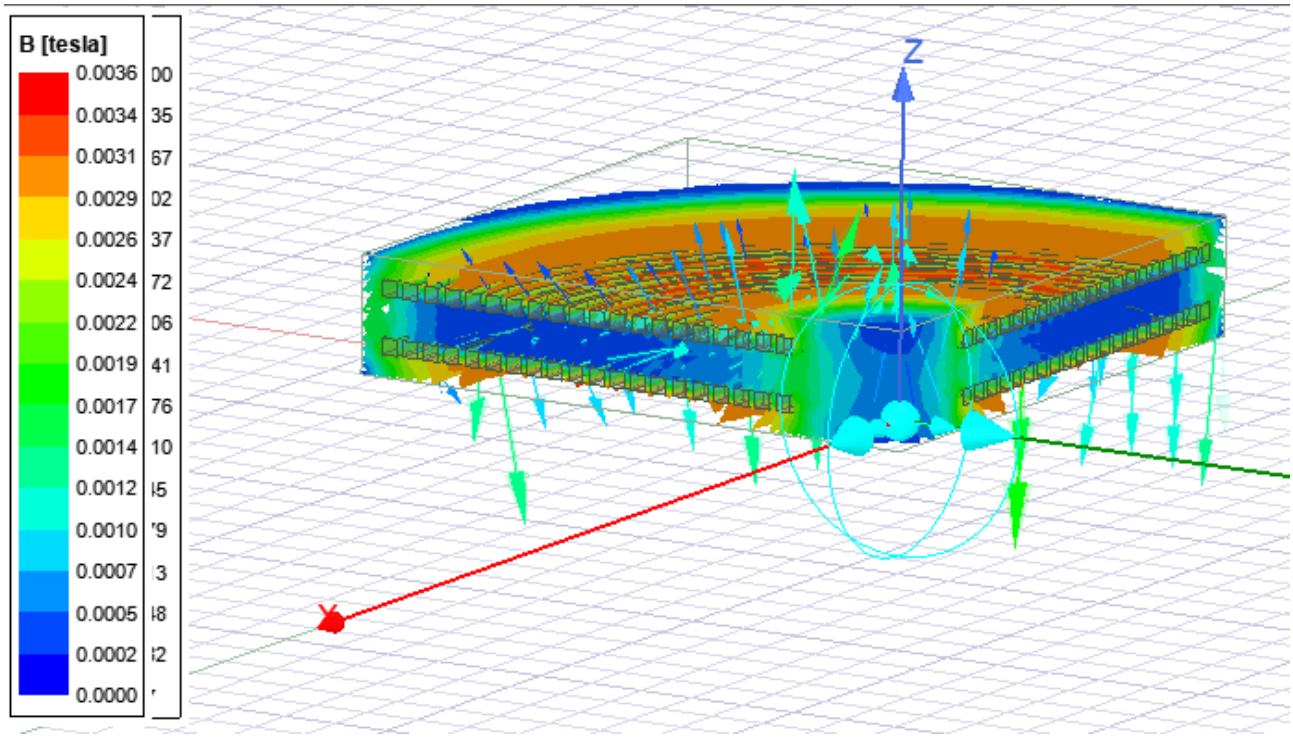

Figure 5.22 Cross-sectional view of the Magnetic Flux Density vector and magnitude plot

Figure 5.23 shows the magnitude of the Magnetic Field Intensity (H) with Figure 5.24 showing the field intensity vectors (field lines). The maximum field intensity is around 2800 A/m concentrated in the centre of the coil. From Figure 5.24 it is evident that the field lines tend to point more in the z-direction at the centre of the coil. As for the B field, Figure 5.25 shows a cross-section of the other Figures.

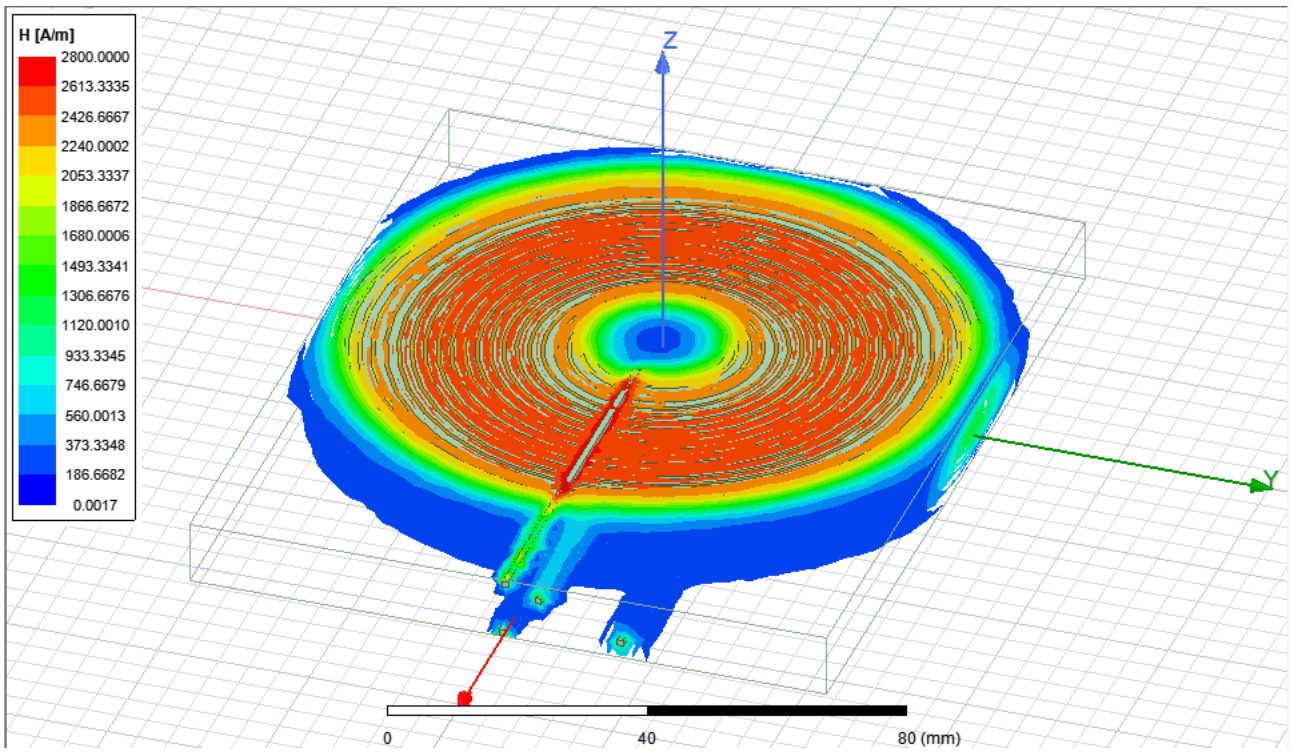

Figure 5.23 Angled view of the Magnetic Field Intensity magnitude plot

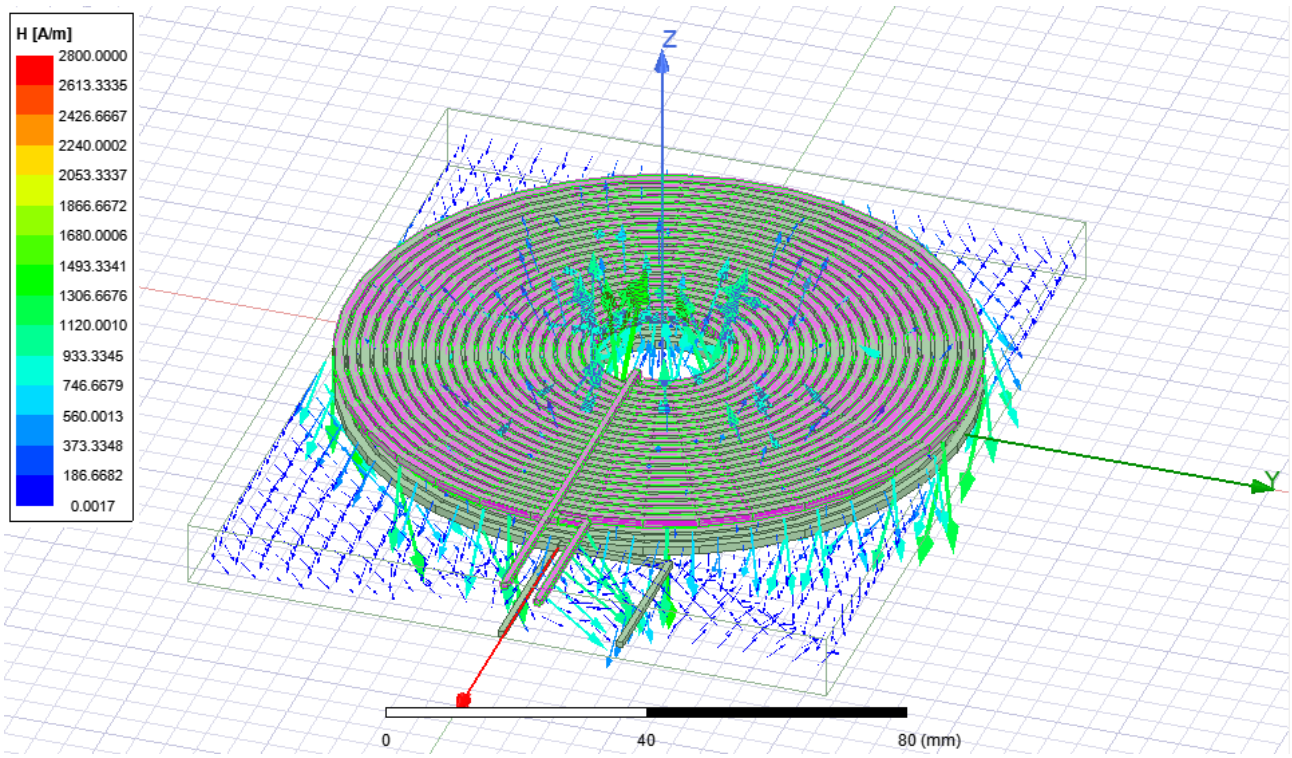

Figure 5.24 Angled view of the Magnetic Field Intensity vector plot

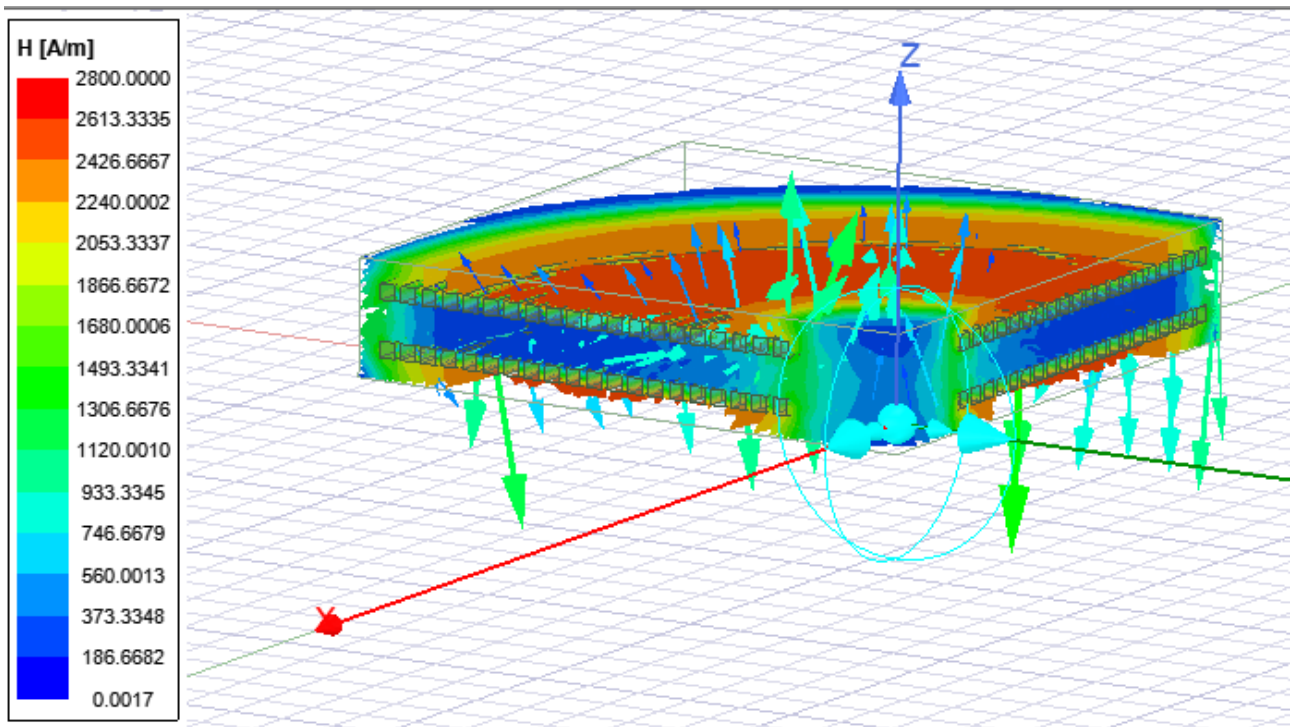

Figure 5.25 Cross-sectional view of the Magnetic Field Intensity vector and magnitude plot

With the analysis in Ansys Maxwell completed, the coils(inductors) with their respective inductances and coupling factor are transferred to LT Spice. The circuit using them is shown in Figure 5.26. This circuit, with an input of 12V AC (expected output from the amplifier in the previous section), is simulated. The 12V is the amplitude, meaning the negative amplitude is -12V. This does not follow from the amplifiers section due to the negative rail being grounded, but this does not affect the testing. The frequency of the input is varied from 2MHz to 6MHz. In Figure 5.27 the input and output signal of the 2MHz signal is shown. The results are consistent for the other signals as well.

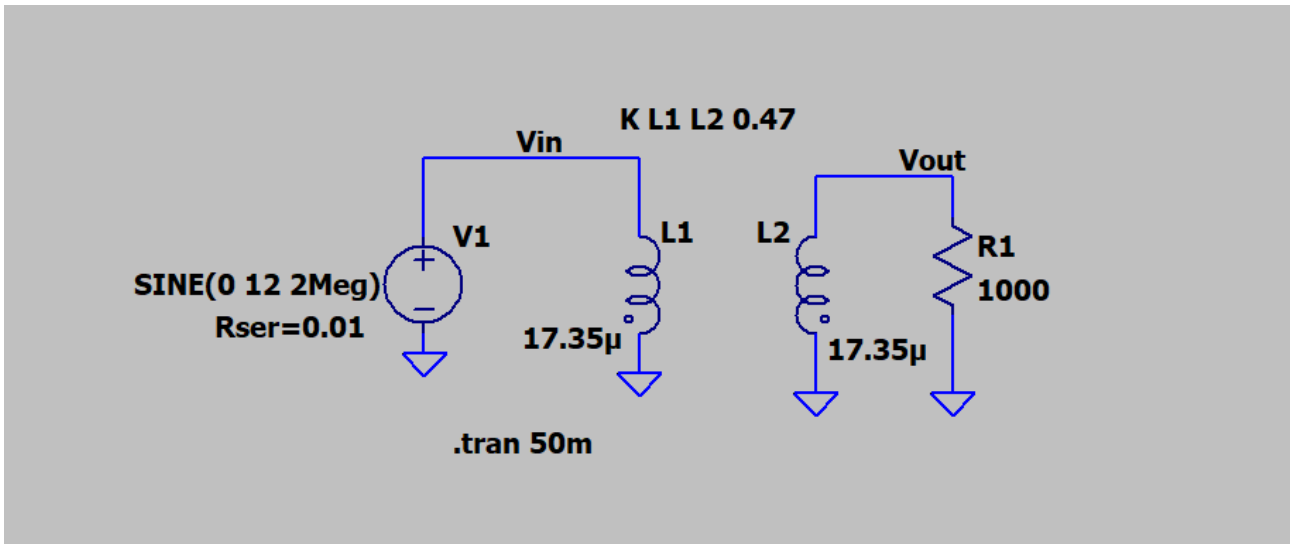

Figure 5.26 Coupling circuit simulated in LT Spice

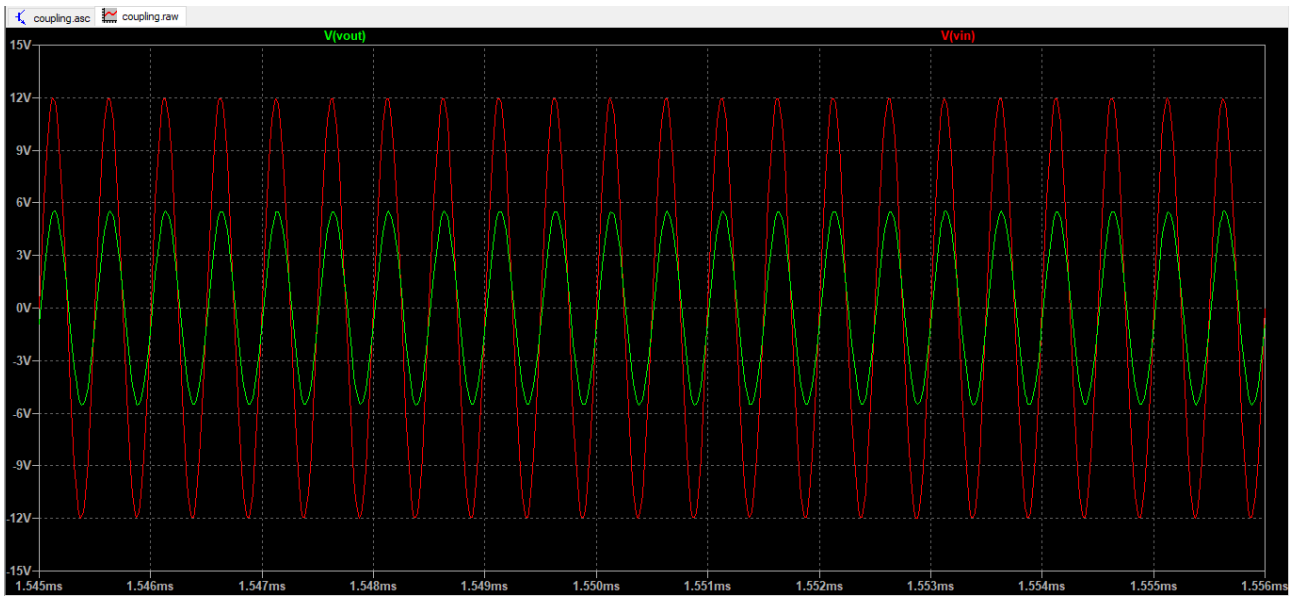

Figure 5.27 Input and output signal of the coupling circuit

Hardware Results

The hardware set-up of the circuit is shown in Figure 5.28. The input comes from a voltage source with the output being connected to an oscilloscope. These tests were done without the coil housing, however, this is not a problem as the material of the housing should not affect the results.

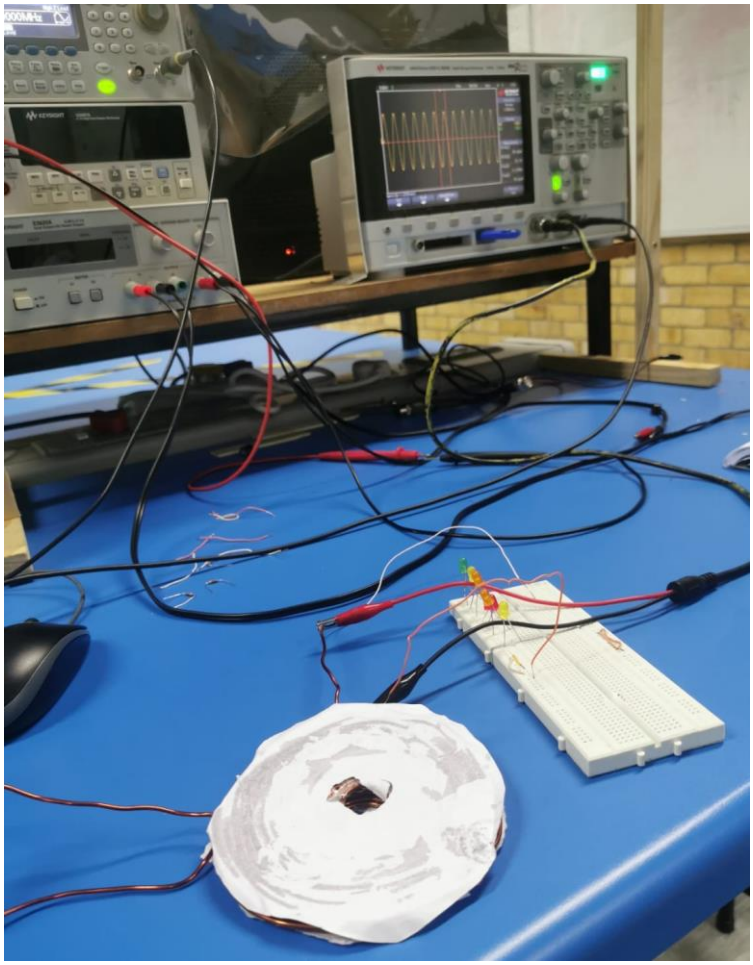
Figure 5.28 Physical set-up of the coupling circuit

Due to the upper limit of the signal generators being 15V peak-to-peak AC, the coupling is tested at this voltage, which is the closest to the required value. It is here, where it is discovered that the magnetic coupling

works best between 2MHz and 6MHz. More research needs to take place to identify the reason for this. Lower frequency signals make the efficiency nearly 0%. The input voltage source is fed into the terminals of the transmitter coil and the output is tested at the terminal of the receiver coil.

Figure 5.29 shows the input voltage at 2MHz on the oscilloscope, with Figure 5.30 showing the corresponding output voltage. As is seen the frequencies are the same with the coupling factor at 0.87 (12.3/14.1). This is much higher than the 0.47 from the simulation. An appropriate explanation for this is due to the mismatch between the simulated and physical devices built. This is due to it being very difficult to manually wind the coil to its exact specification.

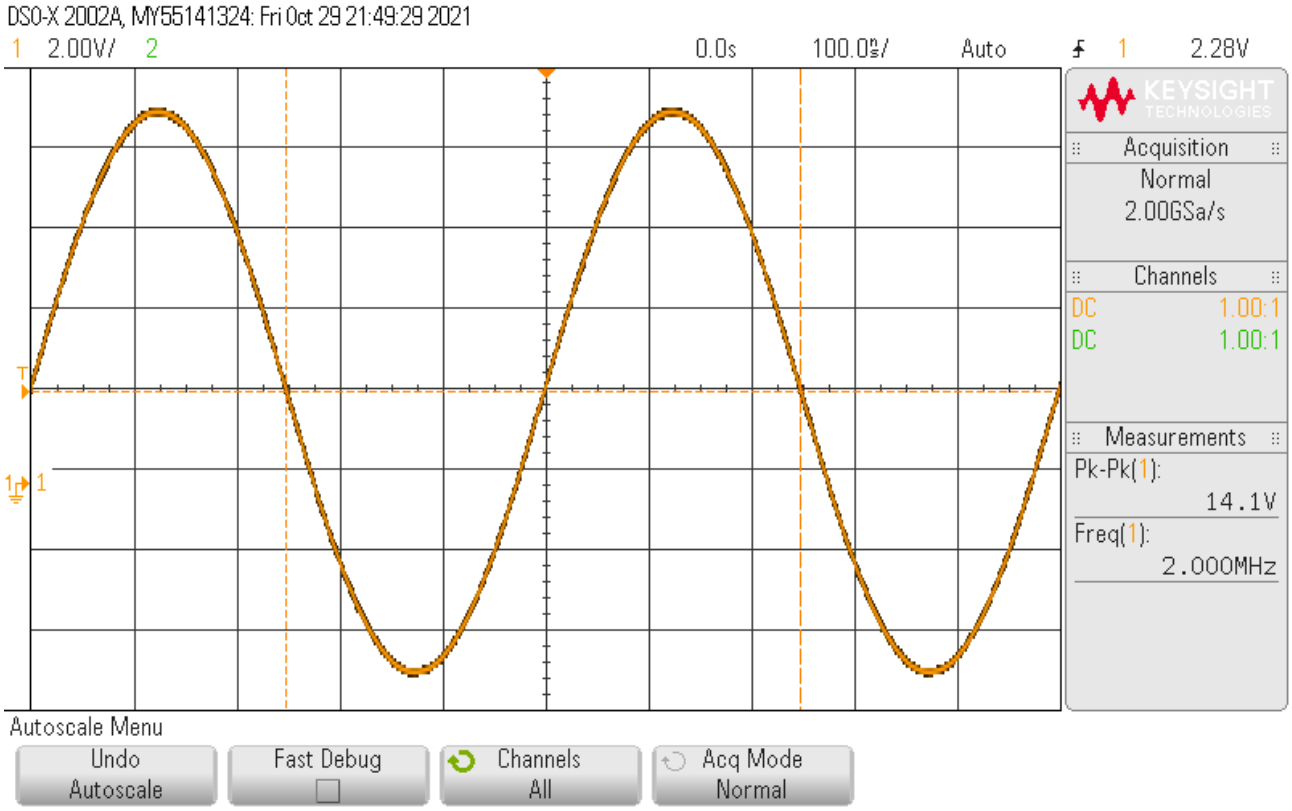

*Figure 5.29 Voltage source signal at **2MHz** on an oscilloscope*

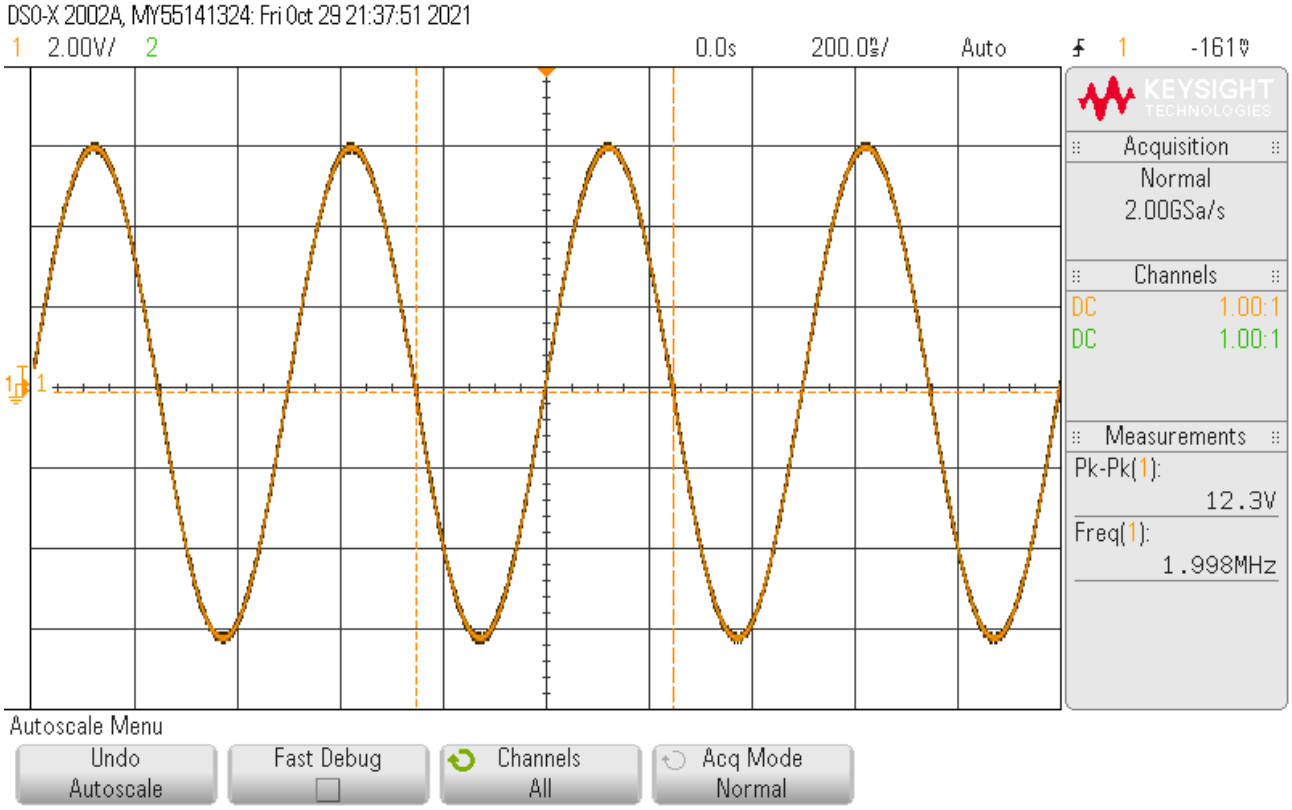

*Figure 5.30 Voltage output signal at **2MHz** on an oscilloscope*

Next, the 6MHz results are shown. Figure 5.31 shows the input voltage at 6MHz on the oscilloscope, with Figure 5.32 showing the corresponding output voltage. Again the frequencies are the same but the coupling factor is now 0.41 (6.2/15.1). This is lower than the 0.47 from the simulation. The reason for this was previously discussed. As the signals are traversed (2MHz-6MHz signals), the coupling factors are reduced. These results are not shown, but an important piece of information comes from these tests. These tests are the sole justification for designing the signals to be between 2MHz and 6MHz.

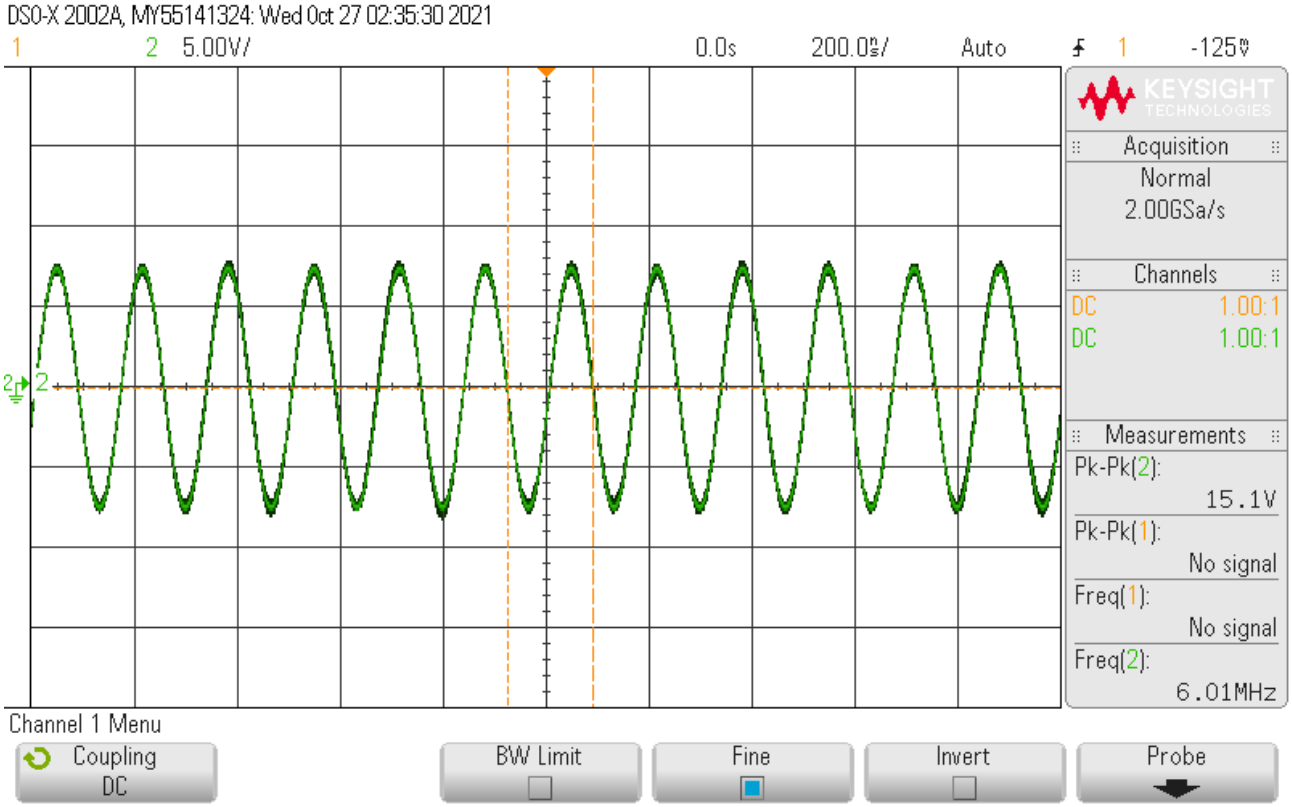

*Figure 5.31 Voltage source at **6MHz** signal on an oscilloscope*

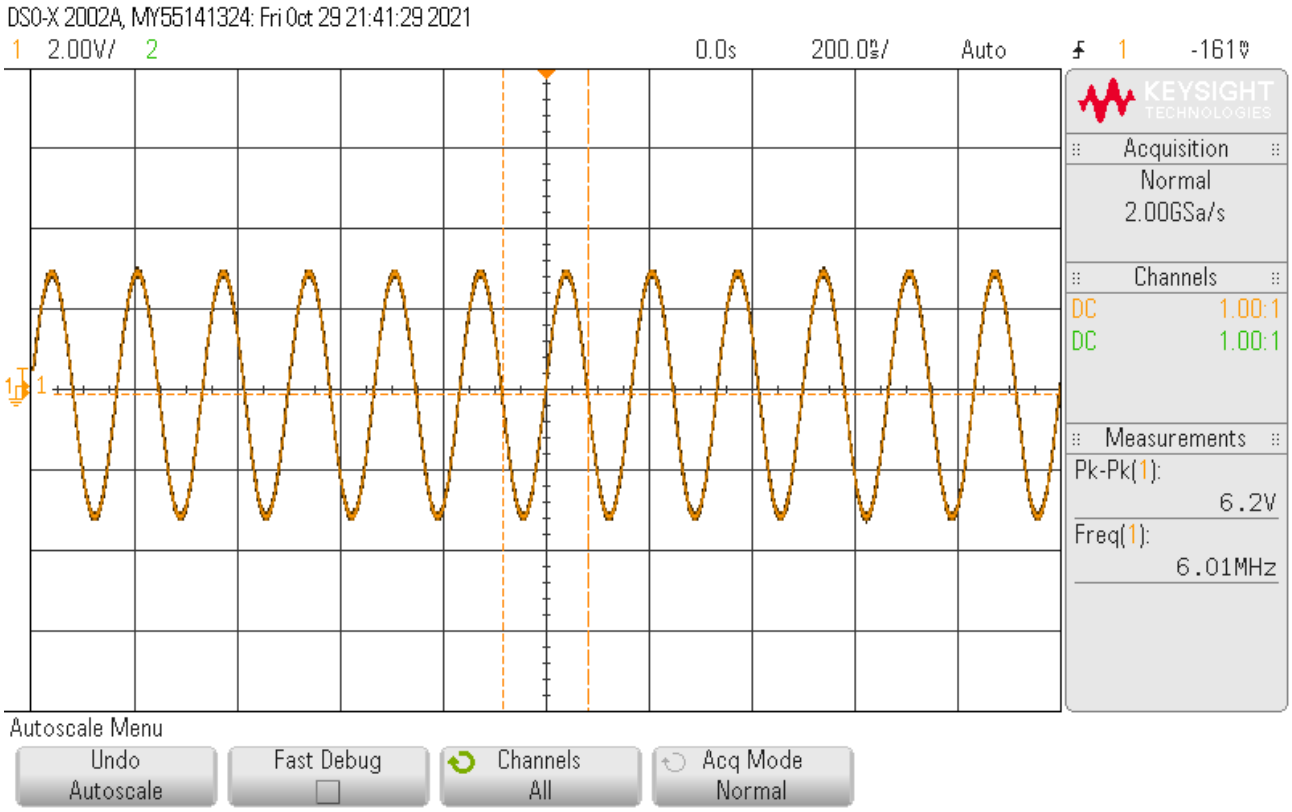

*Figure 5.32 Voltage output at **6Mhz** signal on an oscilloscope*

Lastly, the same test is done using a 12V at 6MHz input signal. However, this time the coils are kept as close together as physically possible. This is done by manually “squashing” the two coils together. The result in

Figure 5.33 shows that in doing this, the coupling factor is greatly increased based on the high output voltage. This is as expected.

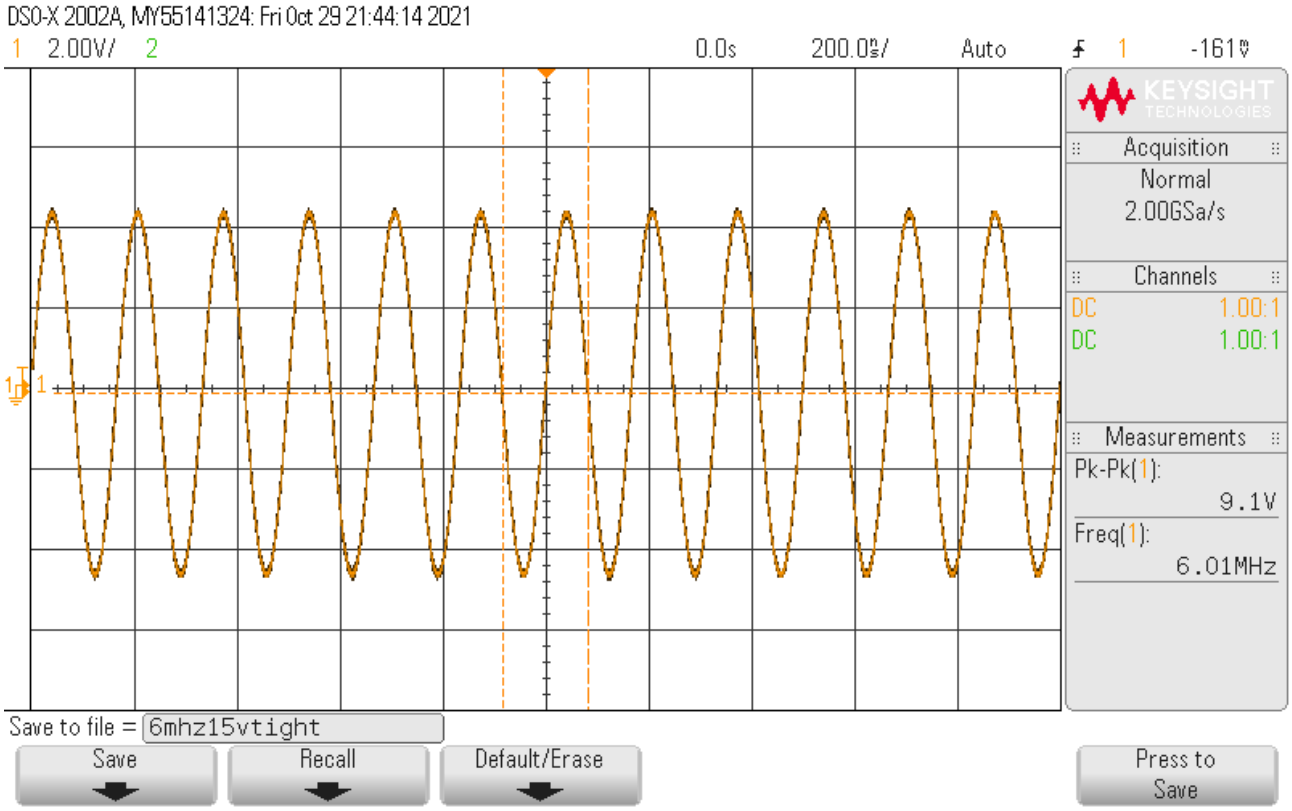

*Figure 5.33 Voltage output at 6Mhz signal on an oscilloscope (coils "**squashed**")*

5.4 Results of the Filter designs

Software Results

All the software results for the filters are achieved in LT Spice. Figure 5.34 depicts the five microwave filters that are simulated. An AC analysis is done to observe the frequency response of each circuit. The output to be shown is when the probes are placed on the respective Vout(frequencies).

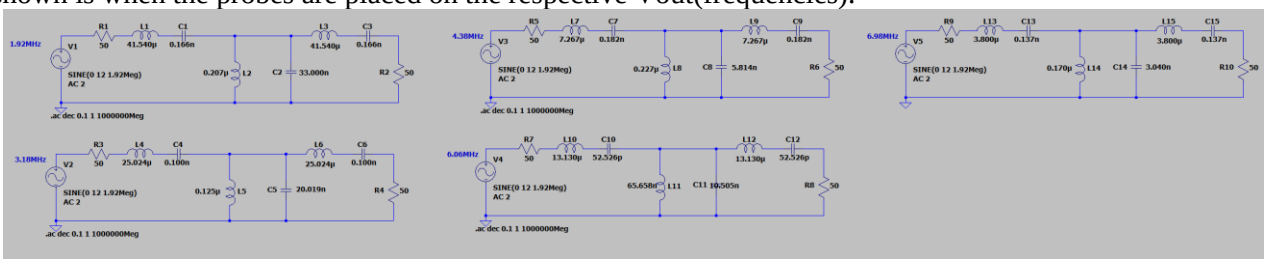

Figure 5.34 Microwave filter circuits which are simulated on LT Spice

Figure 5.35 shows the frequency response of a third-order active Butterworth filter. It can be seen that the output in the high-frequency range is highly distorted as active filters used in high-frequency applications are susceptive to instability and they also amplify high-frequency noise components. Using an active filter was therefore not suitable for this project.

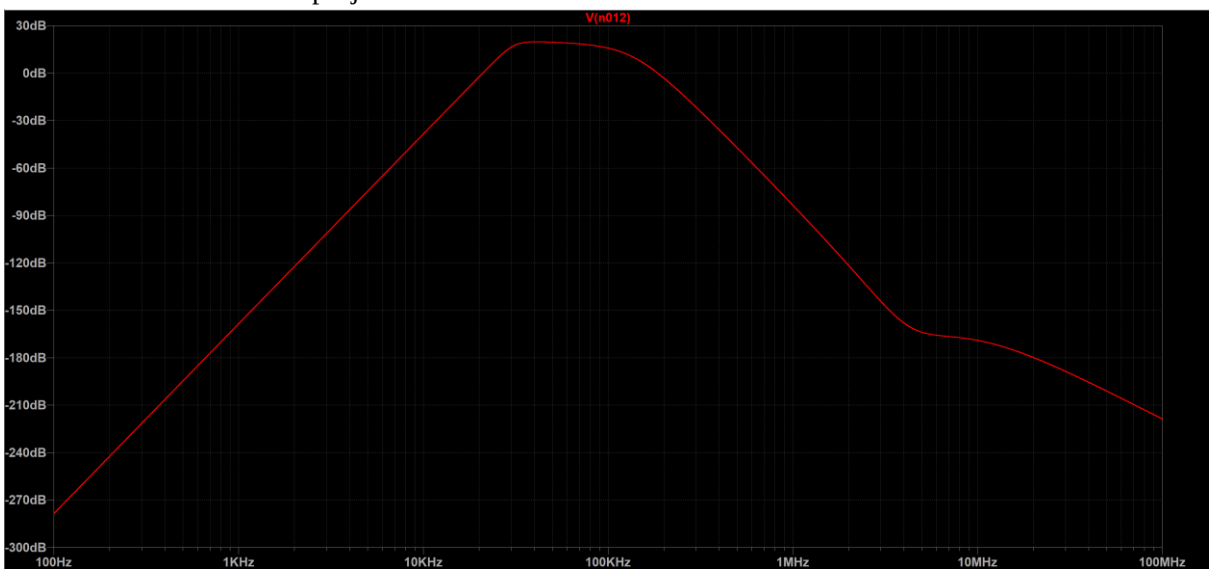

Figure 5.35 Third-order active filter frequency response simulated on LT Spice

Figures 5.36 shows the frequency responses of the passive RC second, third and fourth-order filters. The individual responses can be seen in Appendix A in Figures A.1, A.2, and A3. It can be seen that the roll-off steepness increases proportionally with the order. The greater the steepness, the easier it becomes to isolate desirable frequency in the passband, which makes higher-order filters more desirable. The third-order filter is preferred over the fourth-order because in Figure 5.37 which is a close-up of the fourth-order frequency response, it can be seen that the output is not very smooth and is starting to ripple. A fourth-order filter, or any order higher, is therefore not a suitable option.

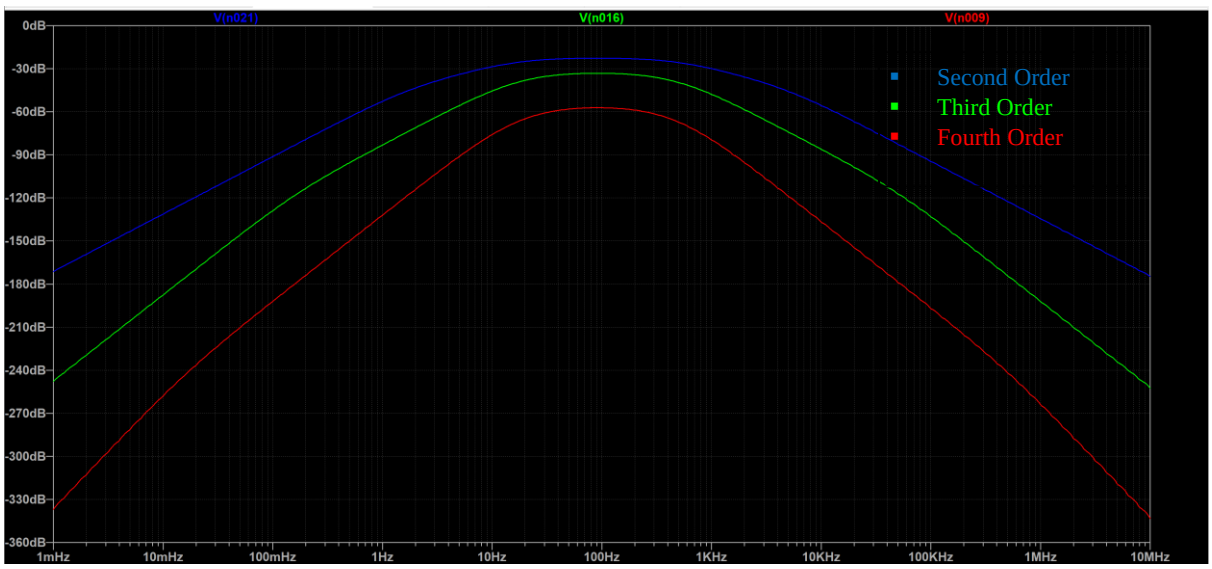

Figure 5.36 Comparison of RC passive higher-order filters simulated on LT Spice

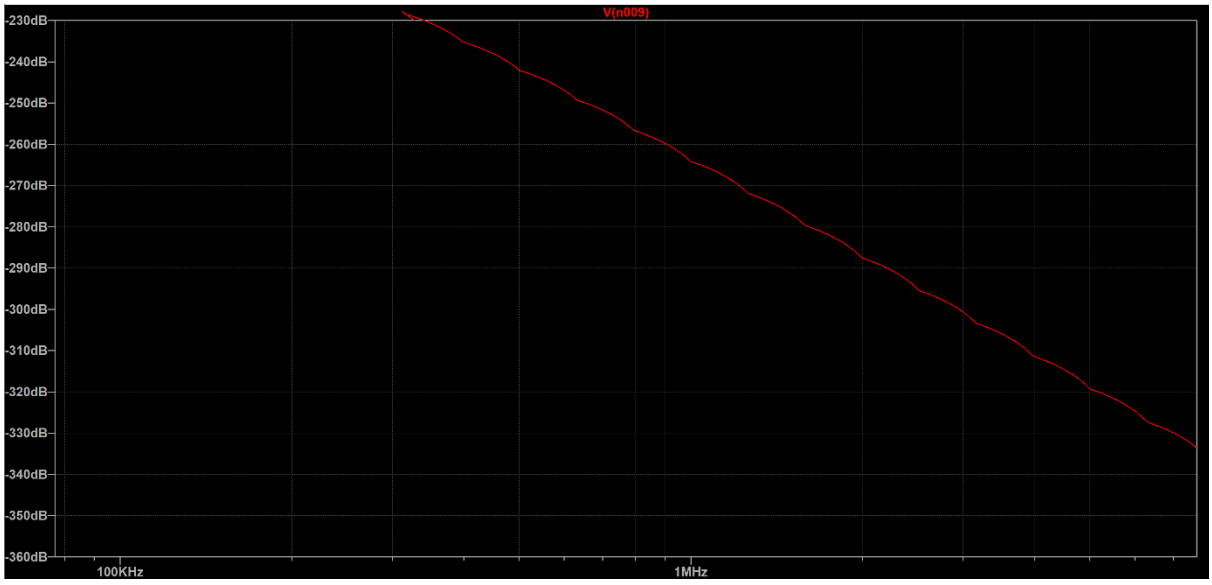

Figure 5.37 Close up of the fourth-order RC passive filter's output simulated on LT Spice

Figure 5.38 shows the frequency response of the Chebyshev microwave filter. The peak frequency, 1.92MHz is isolated and surrounding frequencies are attenuated. However, the frequency response shows that this peak is highly attenuated as well by -30dB and therefore a Chebyshev design is not a viable option.

Figures 5.39 show the frequency responses of the five microwave bandpass filters. Each of the filters effectively isolated their oscillation frequencies and attenuated the surrounding frequencies appropriately. The microwave filters, therefore, proved to be an effective design choice due to their ability to provide steep roll-offs and operate under very high frequencies. The individual responses can be seen in Appendix A in Figures A.4, A.5, A.6, A.7, and A.8.

Figure 5.40 shows the frequency response of the microwave filter that was built to obtain a peak frequency of 1.92MHz with the altered inductor values. The plot shows that the peak frequency is shifted to 2MHz but is attenuated due to changed inductor values. The attenuation is further investigated under the hardware results.

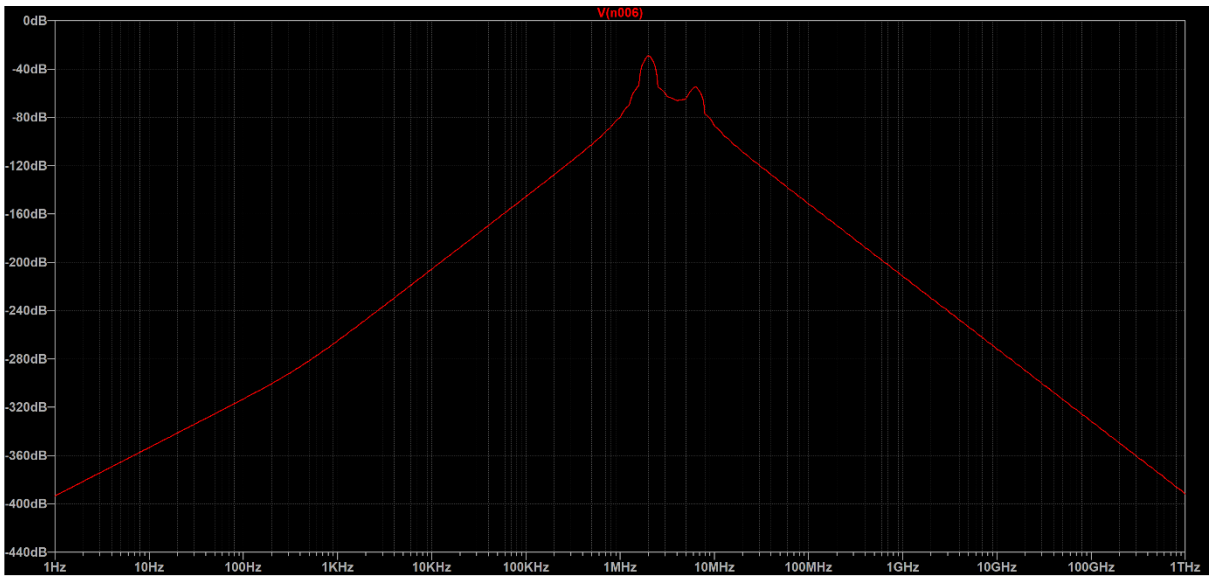

Figure 5.38 Frequency response of the Chebyshev microwave filter simulated on LT Spice

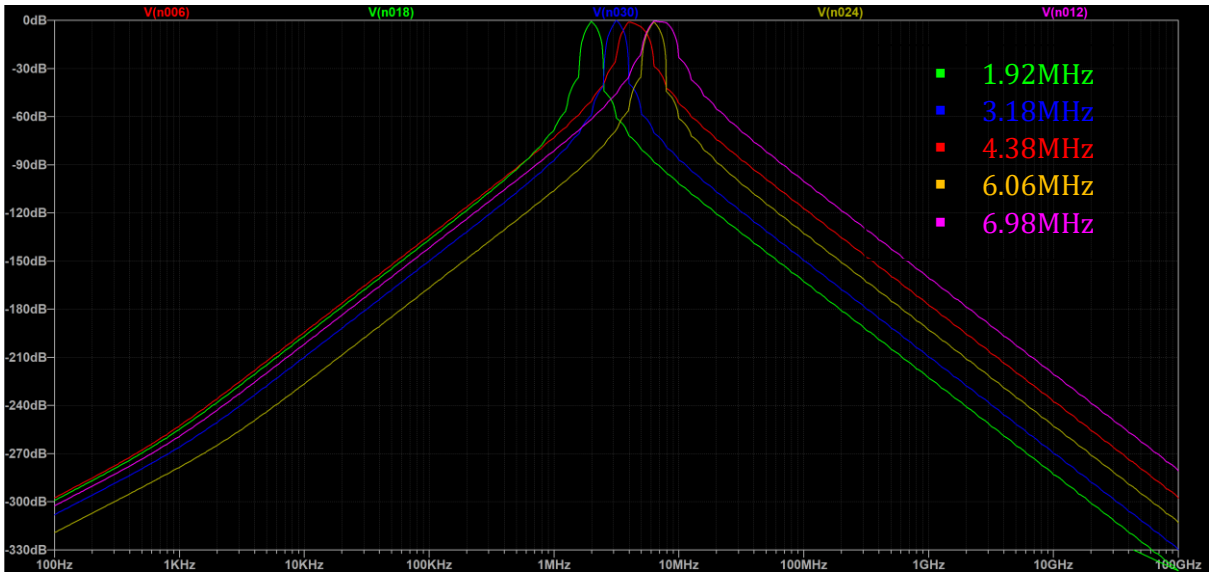

Figure 5.39 Frequency responses of the five microwave bandpass filters simulated on LT Spice

Figure 5.40 Frequency response of microwave filter with altered inductor values simulated on LT Spice

Hardware Results

Figures 5.41, 5.42, 5.43, 5.44, and 5.45 show the voltage output of the filter circuit built to obtain a peak frequency of 2MHz at different frequencies: 2MHz, 3MHz, 4MHz, 5MHz, and 6MHz. The green signal is the input and the orange signal is the output. It can be seen that at 2MHz (Figure 5.41), which is the peak frequency that was obtained after altering the inductor values, the voltage output is at its greatest. When the frequency is varied to 2MHz, 3MHz, 4MHz, 5MHz, and 6MHz, the voltage output decreases, as expected.

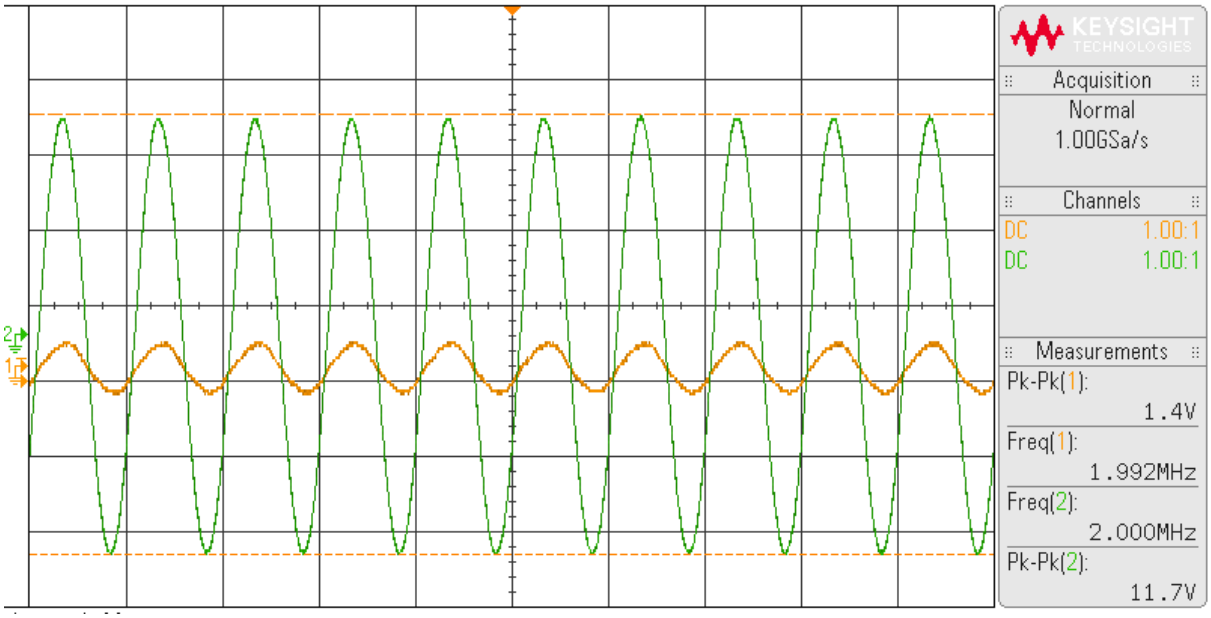

Figure 5.41 Input and output of microwave filter at 2MHz

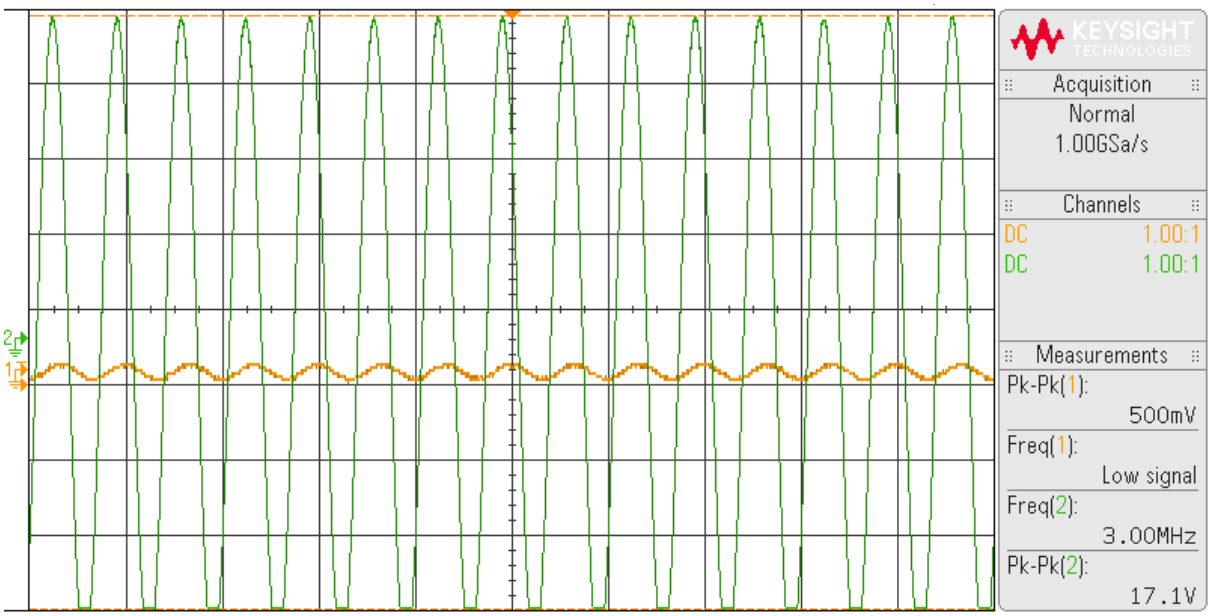

Figure 5.42 Input and output of microwave filter at 3MHz

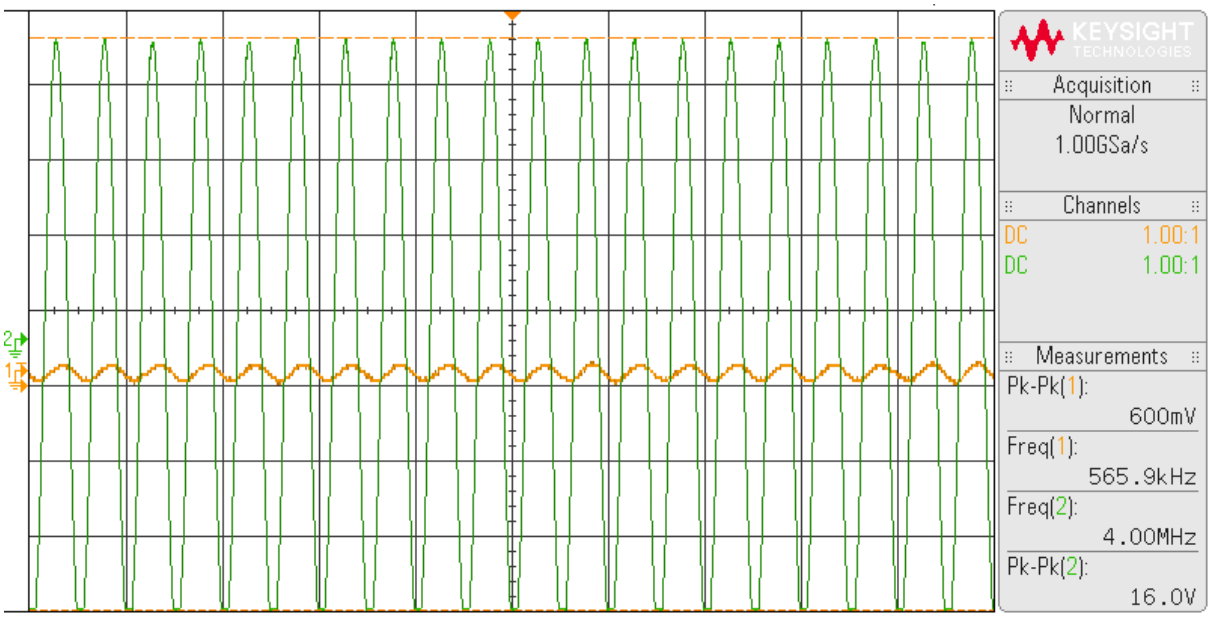

Figure 5.43 Input and output of microwave filter at 4MHz

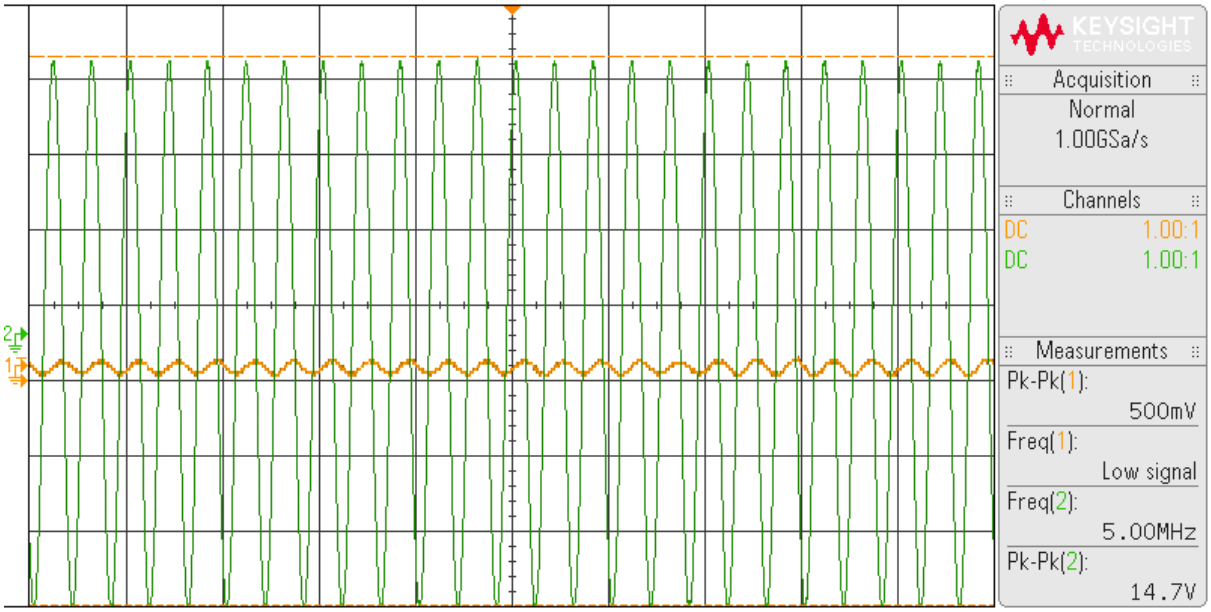

Figure 5.44 Input and output of microwave filter at 5MHz

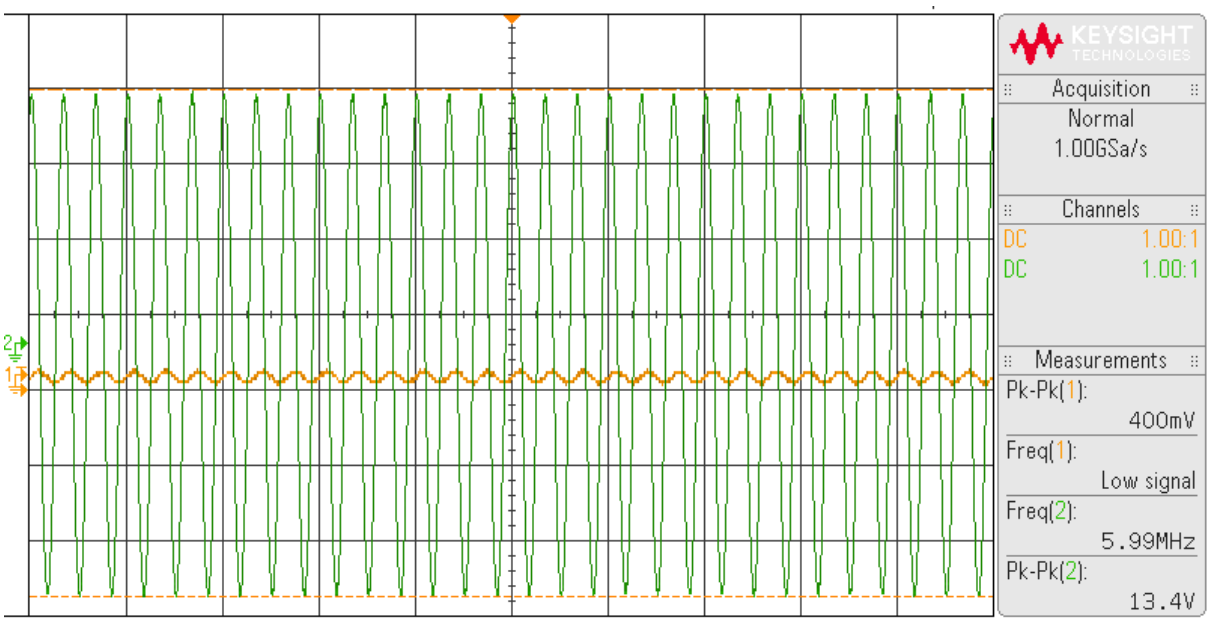

Figure 5.45 Input and output of microwave filter at 6MHz

5.5 Results of the Rectifier designs

Software Results

The software results for the rectifiers are gathered in LT Spice. Figure 5.46 depicts the five rectifiers that are simulated with input signals whose frequencies are changed from 2MHz to 6MHz at increments of roughly 1MHz. A transient analysis to 10ms is done. The output shown is when the probes are placed on the respective Vout. As all these circuits are identical, the same expected result is achieved each time, therefore the result of only one of them is shown.

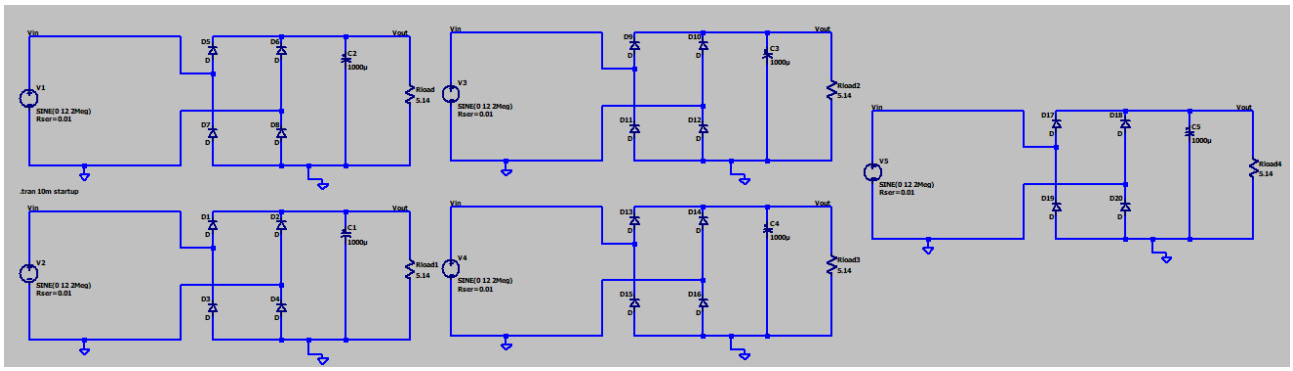

Figure 5.46 Identical rectifier circuits to be simulated

In Figure 5.47 a 12V peak-to-peak AC signal at 2 MHz is fed into the input. Here, ideal diodes are used. As is seen the output is an approximate 10V DC signal smoothened out by the capacitor. The drop is due to the load (5.14Ω resistor imitating a bulb) and the capacitor. In Figure 5.48 where the 1N194 (similar to the physical IN5404 diode) diodes are used, there is a further voltage drop. This is due to the forward voltage drop of 1V of the diodes.

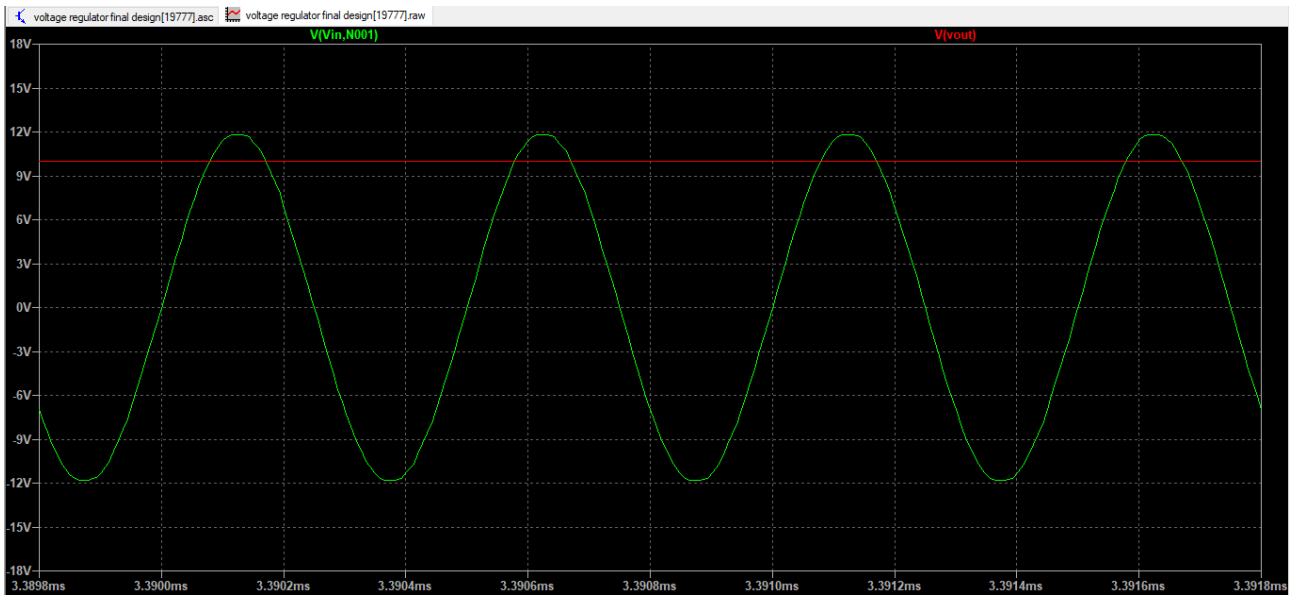

Figure 5.47 Output of the rectifier with ideal diodes

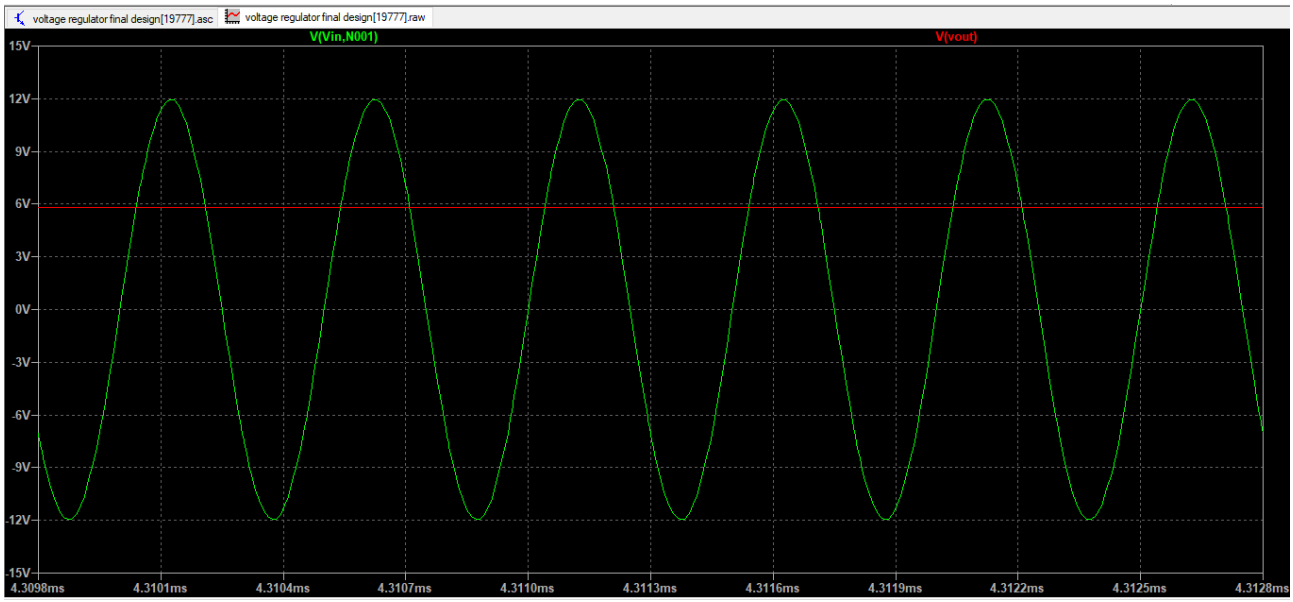

Figure 5.48 Output of the rectifier with 1N194 diodes

Hardware Results

Using the IN5404 diodes the rectifiers are built and simulated. As with the simulation an input voltage of 12V peak-to-peak AC is supplied at different frequencies. The outputs of the 2MHz and 6MHz signals are shown in Figures 5.49 and 5.50 respectively. As expected, the negative half cycle is inverted and made positive. The voltages of the oscilloscope had a bug so the voltage is ignored at this stage.

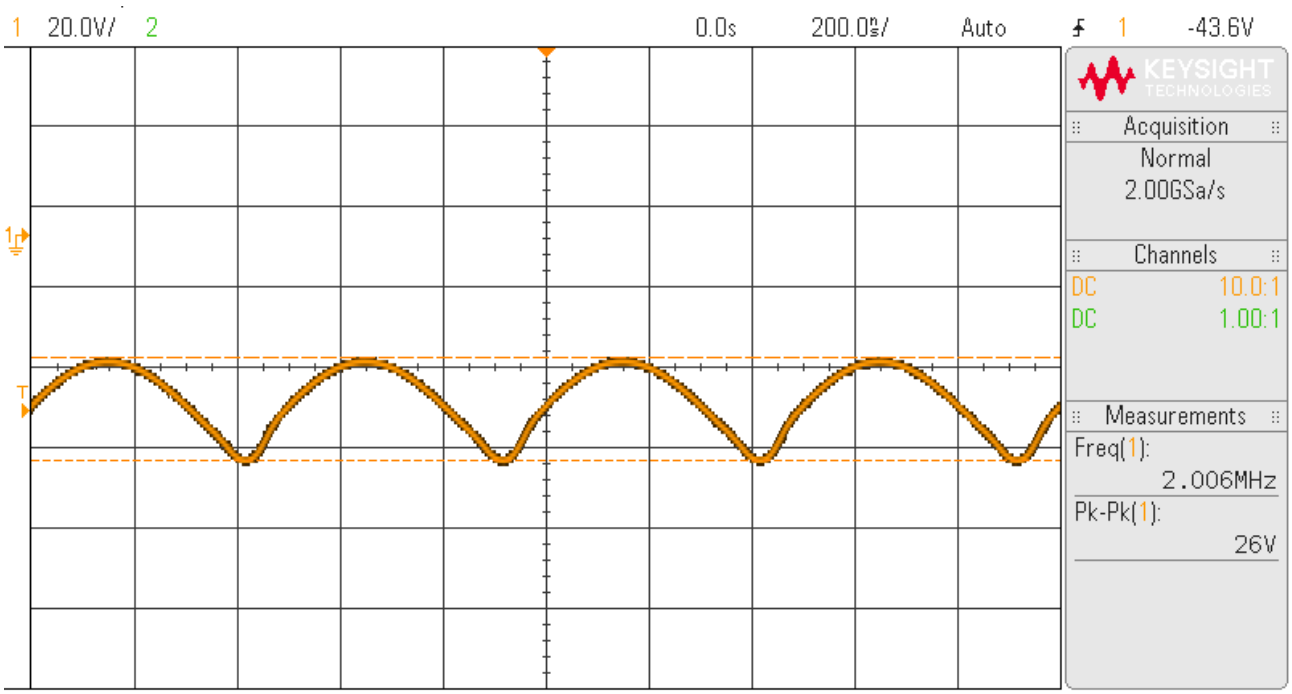

Figure 5.49 Oscilloscope output of the rectifier for the 2MHz signal

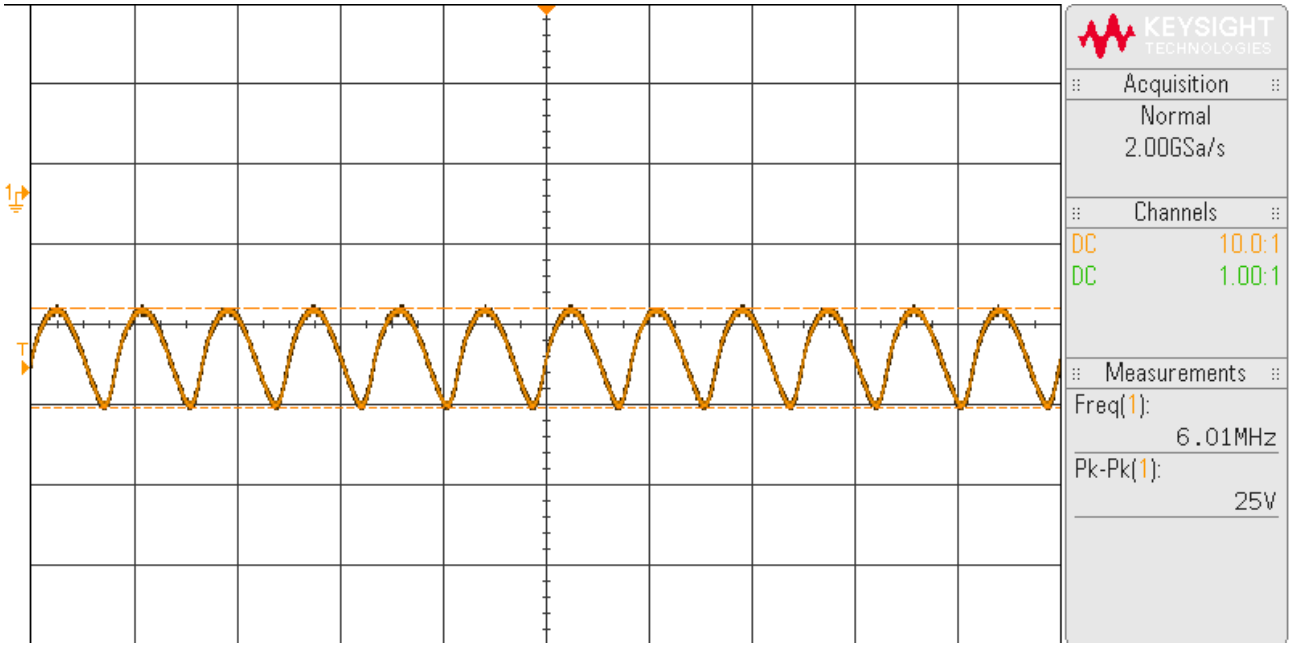

Figure 5.50 Oscilloscope output of the rectifier for the 6MHz signal

Next, the effect of the smoothing capacitors is shown in Figures 5.51 and 5.52. The output is flattened and looks like a DC voltage as is expected.

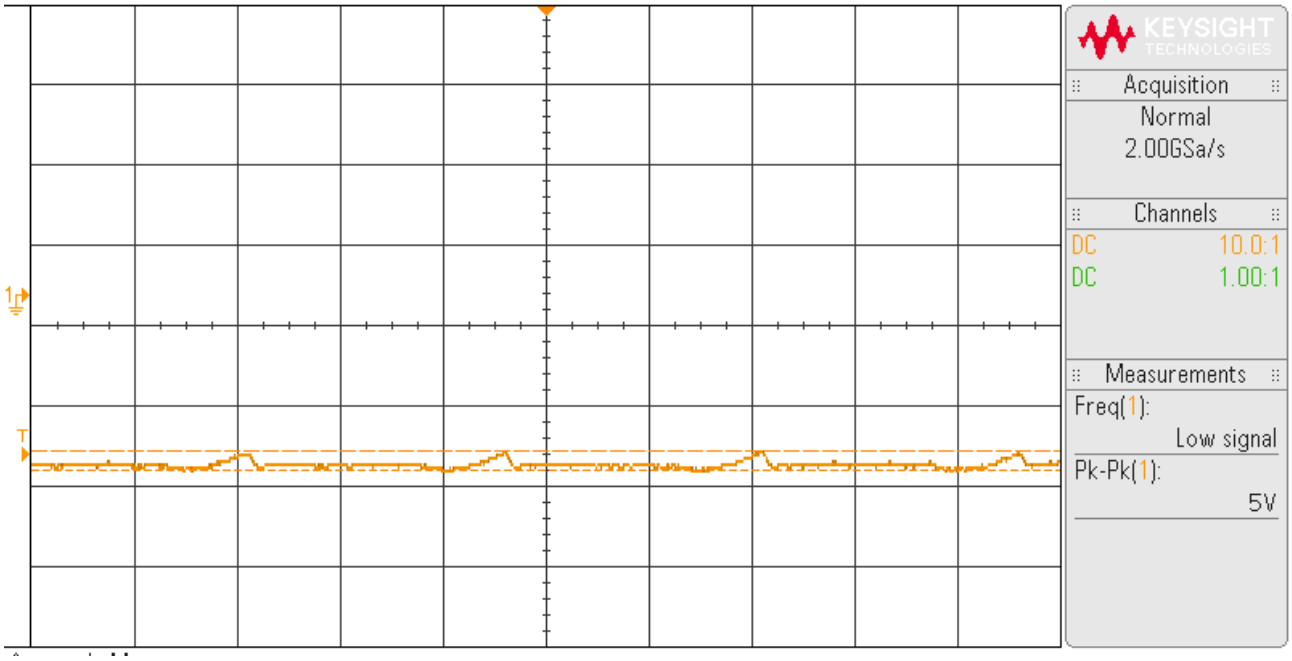

Figure 5.51 Effect of smoothing capacitor on the 2MHz signal

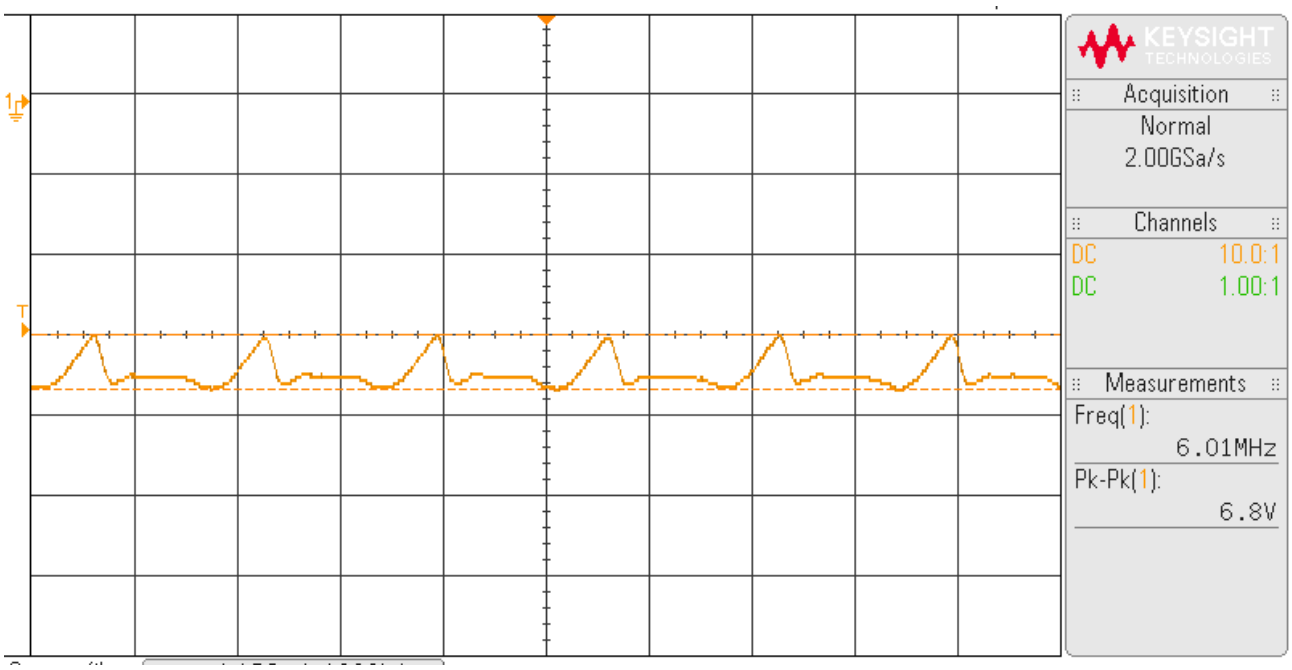

Figure 5.52Effect of smoothing capacitor on the 6MHz signal

5.6 Results of the Combined system

Although individual parts of the system work in simulation and hardware, the building up of errors makes the combined system very difficult to implement. As mentioned in the results, all the errors that are seen need to first be ironed out before complete testing is worthwhile.

One of the biggest problems regarding the combination of the circuits in the simulation is seen when the output of the amplifier is sent through the coupling circuit. This is due to loading and will need to be looked at in future iterations of the project. Another major problem is the gain of the oscillator circuit which did not provide the expected output. The correct transistor for the amplification part of this circuit needs to be found with an appropriate resistor ratio.

With the simulation having undesirable effects, it is obvious that the hardware implementation would have similar problems. Apart from this, sourcing the same components as simulated is not simple. These cause significant error margins, especially for components such as op-amps and transistors.

6. Conclusion

6.1 Conclusions

This project covers an application of wireless energy transfer, namely inductive coupling. The project's aim to design a magnetic coupling system for trailer and caravan signal lights is extensively met. Indicator, brake, foglights, and rear lights for caravans and trailers receive power from the vehicle through a special socket. The socket, which relies on the physical contact of conductors is prone to interruption. This interruption is caused by dust and oil accumulation on the conductors. This project, therefore, contains a design of a contactless alternative using magnetic induction to transfer information and energy.

Various oscillators and filters are designed and implemented, crucial for transferring and distinguishing information. These worked very well in simulation, with a few problems in physical implementation.
Moreover, an efficient coupling is achieved through the design of inductive coils, which are optimised. These coils worked well both in simulation and hardware. A successful housing for these coils is 3-D printed, as well. Lastly, basic circuitry such as amplifiers and rectifiers are designed and built.

Due to a lack of time and finances, some problems cannot be solved and are left for future iterations. Moreover, due to computational limits and software licences, certain desirable experiments are left undone. With the current Covid-19 climate, another challenge is seen, in terms of gathering information and parts.

6.2 Future work

Extensive research into oscillators
As seen in the report the amplifier stage of the oscillator produced inconsistent results. Therefore, more theory needs to be looked and more tests need to be done to acquire better results. Improving this will also remove the need for the operational amplifier, which has problems at high frequencies. Thus the circuitry required would be less and the system would be made smaller.

Implementation of a transformer
Due to the losses seen in wireless power transfer, it is obvious that the 12V from the battery is not enough to wirelessly power the lights. At least not simply this is. Implementing a step-up transformer at the input would make losses insignificant improving the power of the system.

Alternative wireless power transfer
A lot of research has been in resonant coupling. Therefore, this would be easier to implement and it will be optimised already. Therefore, this topic should be looking at a different method of transferring information.

Giving the trailer a separate power source
Although this is moving away from wireless power transfer, it may be more efficient for the end result which the project aims to achieve. Only information would need to be transferred which would simplify the project. However, to reiterate, this moves away from wireless power transfer, which is the essence of the project.

List of References

[1] A.Mishra, “Oscillators” , presented to EEE3090F Electronic Devices and circuits, University of Cape Town, Cape Town, Western Cape, South Africa, May. 17,2021. [*Powerpoint* slides]. Available:https://vula.uct.ac.za/access/content/group/857284fb-4fe8-44be-a19d-e856d479dc8c/Term_2/Oscillators/Slides_with_voice_notes/Oscilators_1.pptx , Accessed on: Oct. 12,2021

[2]T. Floyd, *Electronic devices*, 9th ed. Upper Saddle River, N.J.: Pearson Education, Prentice Hall, 2012, p. 818-822.

[3] Y.Gaffar, “Components-BJT” , presented to EEE3090F Electronic Devices and Circuits, University of Cape Town, Cape Town, Western Cape, South Africa, Feb. 4,2021. [*Powerpoint* slides]. Available:https:https://vula.uct.ac.za/access/content/group/857284fb-4fe8-44be-a19d-e856d479dc8c/02%20%20Slides/08%20%20Components%20-%20BJTs.pdf , Accessed on: Oct. 16,2021

[4] J.Son, “lecture_18_BJT_CC_amp(2)” , presented to EEE2045F ANALOGUE ELECTRONICS, University of Cape Town, Cape Town, Western Cape, South Africa, Mar. 10,2020. [*Powerpoint* slides]. Available:https://vula.uct.ac.za/access/content/group/6890a883-70ce-4a70-9180-0ab59872c951/Lectures/Jarryd_s%20Lectures/lecture_18_BJT_CC_amp_2_.pdf, Accessed on: Oct. 17,2021

[5] Y.Gaffar, “Devices-Operational Amplifiers ” , presented to EEE3090F Electronic Devices and Circuits, University of Cape Town, Cape Town, Western Cape, South Africa, Mar. 8,2021. [*Powerpoint* slides]. Available:https:https://vula.uct.ac.za/access/content/group/857284fb-4fe8-44be-a19d-e856d479dc8c/02%20%20Slides/09%20%20Devices%20-%20Operational%20Amplifiers.pdf , Accessed on: Oct. 16,2021

[6] J.Mwangama, “Pages from Week 7-2” , presented to EEE2045F ANALOGUE ELECTRONICS, University of Cape Town, Cape Town, Western Cape, South Africa, May. 9,2021. [*Powerpoint* slides]. Available:https://vula.uct.ac.za/access/lessonbuilder/item/464142/group/6890a883-70ce-4a70-9180-0ab59872c951/Online%20Learning%20Joyce/Week%207/Slides/Pages%20from%20Week%207%20-2.pdf, Accessed on: Oct. 19,2021

[7] J.Keaveney, “Magnetostatics_Electromagnetic_induction_delivered” , presented to PHY2010S Electromagnetism for Engineers, University of Cape Town, Cape Town, Western Cape, South Africa, Sep. 10,2019. [*Powerpoint* slides]. Available:https://vula.uct.ac.za/access/content/group/f8f01b16-7f04-4b34-9d42-a4d1d260bb34/Magnetism/Lecture_12__Magnetostatics___Electromagnetic_induction_delivered.pdf, Accessed on: Oct. 19,2021

[8] D.Oyedokun, “30-07-19_V1_Intro & Ideal Transformer” , presented to EEE2044S Electromagnetism for Engineers, University of Cape Town, Cape Town, Western Cape, South Africa, Jul. 30,2019. [*Powerpoint* slides]. Available:https://vula.uct.ac.za/access/content/group/07eacacd-15cd-4e5f-b956-cdf9a81b1618/Lecture%20Slides/DTO%20Oyedokun/Transformers/30-07-19_v1_Ideal%20Transformer.pdf, Accessed on: Oct. 20,2021

[9] Y. Cheng and Y. Shu, "A New Analytical Calculation of the Mutual Inductance of the Coaxial Spiral Rectangular Coils," in *IEEE Transactions on Magnetics*, vol. 50, no. 4, pp. 1-6, April 2014, Art no. 7026806, doi: 10.1109/TMAG.2013.2290972.

[10] Liao, S., Li, W., Lin, S., Tang, K., Liou, C. and Tsou, C., 2018. A study of the effect of different coplanar dual-coil geometries on the performance of mutual inductance. *Sensors and Actuators A: Physical*, 269, pp.99-110. https://doi.org/10.1016/j.sna.2017.07.022

[11] Liu, S., Su, J. and Lai, J., 2019. Accurate Expressions of Mutual Inductance and Their Calculation of Archimedean Spiral Coils. *Energies*, 12(10), p.2017. https://doi.org/10.3390/en12102017

[12] S. Santalunai, C. Thongsopa and T. Thosdeekoraphat, "An increasing the power transmission efficiency of flat spiral coils by using ferrite materials for wireless power transfer applications," *2014 11th International Conference on Electrical Engineering/Electronics, Computer, Telecommunications and Information Technology (ECTI-CON)*, 2014, pp. 1-4, doi: 10.1109/ECTICon.2014.6839838.

[13] A. Roc'h, R. Iannarelli and F. Leferink, "New materials for inductors," *2009 International Symposium on Electromagnetic Compatibility - EMC Europe*, 2009, pp. 1-4, doi: 10.1109/EMCEUROPE.2009.5189700.

[14] Ali, A., Yasin, M., Husin, M. and Hambali, N., 2019. Design and analysis of 2-coil wireless power transfer (WPT) using magnetic coupling technique. *International Journal of Power Electronics and Drive Systems (IJPEDS)*, 10(2), p.611. DOI: 10.11591/ijpeds.v10.i2.pp611-616

[15] Tavakkoli, H., Abbaspour-Sani, E., Khalilzadegan, A., Abazari, A. and Rezazadeh, G., 2019. Mutual inductance calculation between two coaxial planar spiral coils with an arbitrary number of sides. *Microelectronics Journal*, 85, pp.98-108. https://doi.org/10.1016/j.mejo.2019.01.012

[16] L. Xie, Y. Shi, Y. T. Hou and A. Lou, "Wireless power transfer and applications to sensor networks," in *IEEE Wireless Communications*, vol. 20, no. 4, pp. 140-145, August 2013, doi: 10.1109/MWC.2013.6590061.

[17] L. Olvitz, D. Vinko and T. Švedek, "Wireless power transfer for mobile phone charging device," *2012 Proceedings of the 35th International Convention MIPRO*, 2012, pp. 141-145.

[18] M. Fareq *et al*., "Solar wireless power transfer using inductive coupling for mobile phone charger," *2014 IEEE 8th International Power Engineering and Optimization Conference (PEOCO2014)*, 2014, pp. 473-476, doi: 10.1109/PEOCO.2014.6814475.

[19] S. Li and C. C. Mi, "Wireless Power Transfer for Electric Vehicle Applications," in *IEEE Journal of Emerging and Selected Topics in Power Electronics*, vol. 3, no. 1, pp. 4-17, March 2015, doi: 10.1109/JESTPE.2014.2319453.

[20] L. Zhao, D. J. Thrimawithana, U. K. Madawala, A. P. Hu and C. C. Mi, "A Misalignment-Tolerant Series-Hybrid Wireless EV Charging System With Integrated Magnetics," in *IEEE Transactions on Power Electronics*, vol. 34, no. 2, pp. 1276-1285, Feb. 2019, doi: 10.1109/TPEL.2018.2828841.

[21] D. Arnitz and M. S. Reynolds, "Wireless power transfer optimization for nonlinear passive backscatter devices," *2013 IEEE International Conference on RFID (RFID)*, 2013, pp. 245-252, doi: 10.1109/RFID.2013.6548161.

[22] Y. Gaffar, “Filters”, presented to EEE3090F Electronic Devices and Circuits, University of Cape Town, Cape Town, Western Cape, South Africa, Feb 04, 2021.

[*PowerPoint*slides]. Available: https://vula.uct.ac.za/access/content/group/857284fb-4fe8-44be-a19d-e856d479dc8c/02%20%20Slides/10%20%20Filters%20-%20first%20order%20response.pdf, Accessed on: Oct 25, 2021.

[23] Amin, A., Islam, M.,2016. Importance of High Order High Pass and Low Pass Filters. *World Applied Sciences Journa*l, 34(9), pp.1261-128.

[24] Z. Chen, F. Blaabjerg and J. K. Pedersen, "A study of parallel operations of active and passive filters," 2002 IEEE 33rd Annual IEEE Power Electronics Specialists Conference. Proceedings (Cat. No.02CH37289), 2002, pp. 1021-1026 vol.2, doi: 10.1109/PSEC.2002.1022589.

[25] Y. Gaffar, "Filters: second order response", presented to EEE3090F Electronic Devices and Circuits, University of Cape Town, Cape Town, Western Cape, South Africa, Feb 04, 2021. [*PowerPoint*slides]. Available: https://vula.uct.ac.za/access/content/group/857284fb-4fe8-44be-a19d-e856d479dc8c/02%20%20Slides/11%20%20Filters%20-%20second%20order%20response.pdf, Accessed on: Oct 26, 2021.

[26] Pozar, D., 1998. *Microwave engineering*. New York, N.Y.: Wiley, 8(3), pp.399-411.

[27] Floyd, T., 2012. *Electronic devices*. 9th ed. Upper Saddle River, N.J.: Pearson Education, Prentice Hall, 2012, pp.764-785.

[28] Y. Gaffar, "Filters: standard filter responses", presented to EEE3090F Electronic Devices and Circuits, University of Cape Town, Cape Town, Western Cape, South Africa, Feb 04, 2021. [*PowerPoint*slides]. Available: https://vula.uct.ac.za/access/content/group/857284fb-4fe8-44be-a19d-e856d479dc8c/02%20%20Slides/12%20%20Filters%20-%20standard%20filter%20responses.pdf , Accessed on: Oct 27, 2021.

[29] J.Son, "lecture_4_rectifiers" , presented to EEE2045F ANALOGUE ELECTRONICS, University of Cape Town, Cape Town, Western Cape, South Africa, Feb. 13,2020. [*Powerpoint* slides]. Available:https://vula.uct.ac.za/access/content/group/6890a883-70ce-4a70-9180-0ab59872c951/Lectures/Jarryd_s%20Lectures/lecture_4_rectifiers.pdf, Accessed on: Oct. 18,2021

[30] Y. Gaffar, "Voltage Regulators: Introduction", presented to EEE3090F Electronic Devices and Circuits, University of Cape Town, Cape Town, Western Cape, South Africa, Feb 04, 2021. [*PowerPoint*slides]. Available: https://vula.uct.ac.za/access/content/group/857284fb-4fe8-44be-a19d-e856d479dc8c/02%20%20Slides/27%20%20Voltage%20regulators%20-%20introduction.pdf, Accessed on: Oct 22, 2021.

[31] Takealot.com. 2021. *Takealot*. [online] Available at: <https://www.takealot.com/moto-quip-globe-type-1034-12v-d-c-tail-light-double/PLID40661038> [Accessed 1 November 2021].

[32] Humood, K., Imran, O. and Taha, A., 2020. Design and simulation of high frequency colpitts oscillator based on BJT amplifier. *International Journal of Electrical and Computer Engineering (IJECE)*, 10(1), p.160. DOI:10.11591/ijece.v10i1.pp160-170

[33] J.Son, "lecture_10_DC_load_line" , presented to EEE2045F ANALOGUE ELECTRONICS, University of Cape Town, Cape Town, Western Cape, South Africa, Feb. 25,2020. [*Powerpoint* slides].Available:https://vula.uct.ac.za/access/content/group/6890a883-70ce-4a70-9180-0ab59872c951/Lectures/Jarryd_s%20Lectures/lecture_10_DC_load_line.pdf, Accessed on: Oct. 18,2021

[34] Pdf1.alldatasheet.com. 2021. *2N2222 pdf, 2N2222 description, 2N2222 datasheets, 2N2222 view ::: ALLDATASHEET :::*. [online] Available at: <https://pdf1.alldatasheet.com/datasheet-pdf/view/15067/PHILIPS/2N2222.html> [Accessed 12 October 2021].

[35] Pdf1.alldatasheet.com. 2021. *OP07CP pdf, OP07CP description, OP07CP datasheets, OP07CP view ::: ALLDATASHEET :::*. [online] Available at: <https://pdf1.alldatasheet.com/datasheet-pdf/view/27256/TI/OP07CP.html> [Accessed 15 October 2021].

[36] Takealot.com. 2021. *Takealot*. [online] Available at: <https://www.takealot.com/moto-quip-metal-trailer-socket-male-7-pin/PLID40661015?gclid=Cj0KCQjw_fiLBhDOARIsAF4khR1FK6SO1LCqlULkMqBpE9Tfml3CkIOwikjKGBdKRyyeMHqDkikeJ48aAkLqEALw_wcB&gclsrc=aw.ds> [Accessed 7 October 2021].

[37] Shi, X., Qi, C., Qu, M., Ye, S., Wang, G., Sun, L. and Yu, Z., 2014. Effects of coil shapes on wireless power transfer via magnetic resonance coupling. *Journal of Electromagnetic Waves and Applications*, 28(11), pp.1316-1324.

[38] Tavakkoli, H., Abbaspour-Sani, E., Khalilzadegan, A., Abazari, A. and Rezazadeh, G., 2019. Mutual inductance calculation between two coaxial planar spiral coils with an arbitrary number of sides. *Microelectronics Journal*, 85, pp.98-108.

[39] "CUL 100/1,00 | Block Single Core 1mm diameter Copper Wire, 11m Long | RS Components", Za.rs-online.com, 2021. [Online]. Available: https://za.rs-online.com/web/p/copper-wire/7790713/. [Accessed 22 October 2021].

[40] Pdf1.alldatasheet.com. 2021. *IN5404 pdf, IN5404 description, IN5404 datasheets, IN5404 view ::: ALLDATASHEET :::*. [online] Available at: <https://pdf1.alldatasheet.com/datasheet-pdf/view/329392/CHENG-YI/IN5404.html> [Accessed 26 October 2021].

[41] Pdf1.alldatasheet.com. 2021. *L7812CT pdf, L7812CT description, L7812CT datasheets, L7812CT view ::: ALLDATASHEET :::*. [online] Available at: <https://pdf1.alldatasheet.com/datasheet-pdf/view/22666/STMICROELECTRONICS/L7812CT.html> [Accessed 1 November 2021].

[42] Wikihow.com. 2021. *How to Hook Up a Trailer: 12 Steps (with Pictures) - wikiHow*. [online] Available at: <https://www.wikihow.com/Hook-Up-a-Trailer> [Accessed 26 October 2021].

Appendices

Appendix A

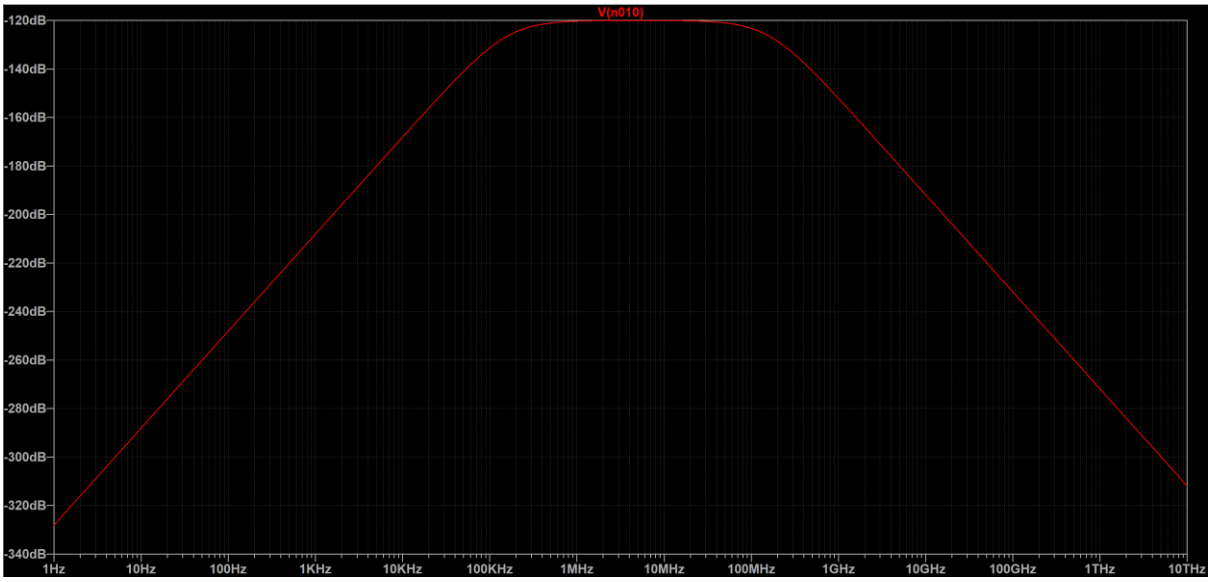

Figure A.1 Second-order RC passive filter frequency response

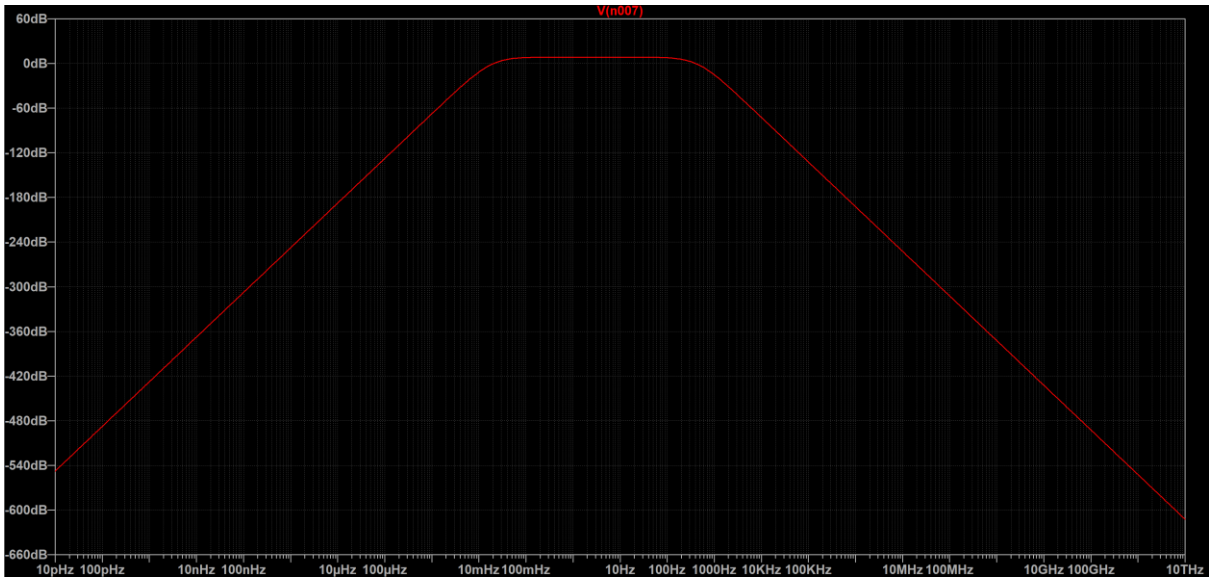

Figure A.2 Third-order RC passive filter frequency response

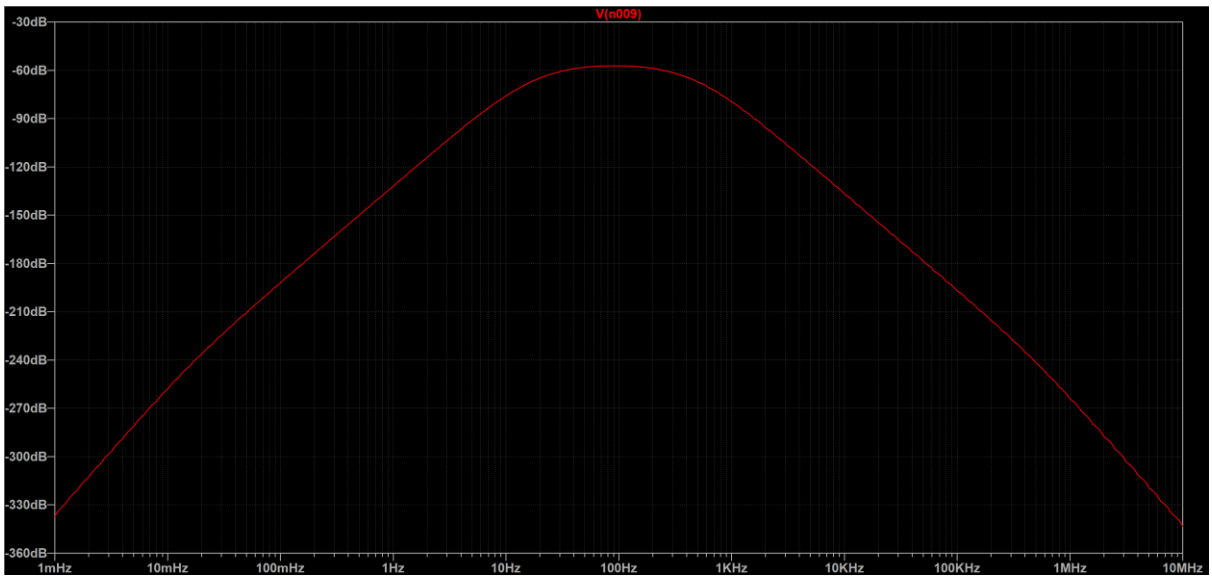

Figure A.3 Fourth-order RC passive filter frequency response

Figure A.4 Microwave filter frequency response with a 1.92MHz peak frequency

Figure A.5 Microwave filter frequency response with a 3.18MHz peak frequency

Figure A.6 Microwave filter frequency response with a 4.38MHz peak frequency

Figure A.7 Microwave filter frequency response with a 6.06MHz peak frequency

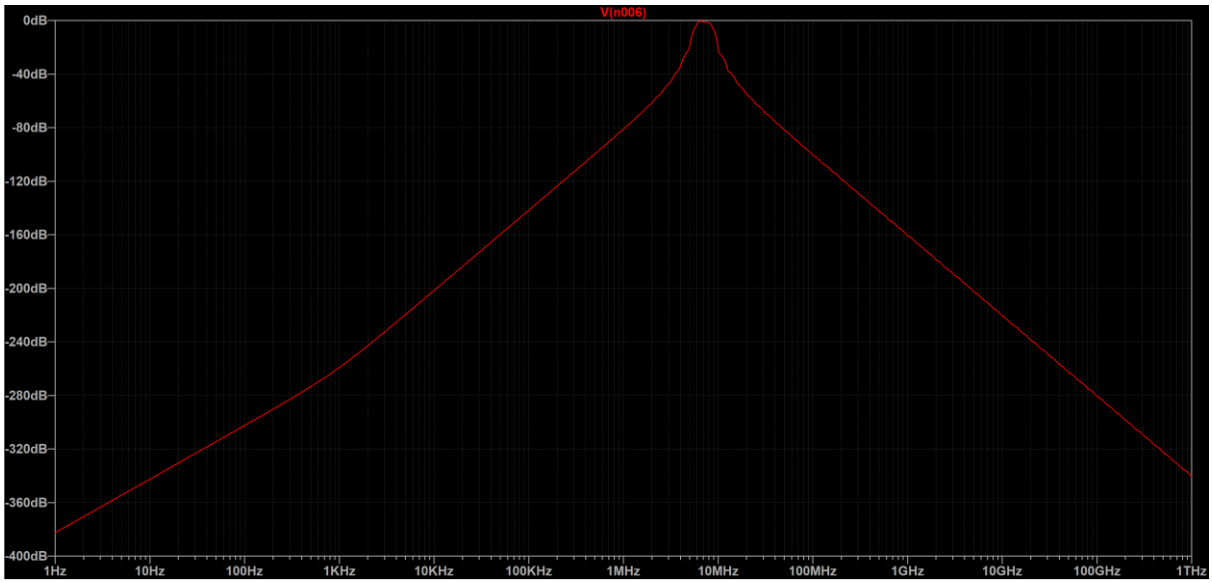

Figure A.8 Microwave filter frequency response with a 6.98MHz peak frequency

EBE Faculty: Assessment of Ethics in Research Projects

Application for Approval of Ethics in Research (EiR) Projects
Faculty of Engineering and the Built Environment, University of Cape Town

ETHICS APPLICATION FORM

Please Note:
Any person planning to undertake research in the Faculty of Engineering and the Built Environment (EBE) at the University of Cape Town is required to complete this form **before** collecting or analysing data. The objective of submitting this application *prior* to embarking on research is to ensure that the highest ethical standards in research, conducted under the auspices of the EBE Faculty, are met. Please ensure that you have read, and understood the **EBE Ethics in Research Handbook** (available from the UCT EBE, Research Ethics website) prior to completing this application form: http://www.ebe.uct.ac.za/ebe/research/ethics1

APPLICANT'S DETAILS		
Name of principal researcher, student or external applicant		Azhar Ebrahim
Department		EBE (Electrical Engineering Department)
Preferred email address of applicant:		EBRAZH001@MYUCT.AC.ZA
If Student	Your Degree: e.g., MSc, PhD, etc.	BSc in Engineering in Mechatronics
	Credit Value of Research: e.g., 60/120/180/360 etc.	40
	Name of Supervisor (if supervised):	DR. Willem SCHONKEN
If this is a researchcontract, indicate the source of funding/sponsorship		None
Project Title		Design of a Magnetic Coupling for Caravan and Trailer Signal

I hereby undertake to carry out my research in such a way that:

- there is no apparent legal objection to the nature or the method of research; and
- the research will not compromise staff or students or the other responsibilities of the University;
- the stated objective will be achieved, and the findings will have a high degree of validity;
- limitations and alternative interpretations will be considered;
- the findings could be subject to peer review and publicly available; and
- I will comply with the conventions of copyright and avoid any practice that would constitute plagiarism.

APPLICATION BY	Full name	Signature	Date
Principal Researcher/ Student/External applicant	Azhar Ebrahim		8/17/2021
SUPPORTED BY	Full name	Signature	Date
Supervisor (where applicable)	Dr. WPF Schonken	WPF Schonken	18 Aug 2021